

**FABRICATION OF LOW COST FLEXIBLE  
CARBON NANOTUBE COATED FABRIC  
FOR SPECIAL APPLICATIONS**

**Thesis**

Submitted in partial fulfillment of the requirements for the degree of

**DOCTOR OF PHILOSOPHY**

**by**

**ARUNKUMAR.D.S**

**(Registration Number: 177054MT002)**



**DEPARTMENT OF METALLURGICAL AND MATERIALS  
ENGINEERING  
NATIONAL INSTITUTE OF TECHNOLOGY KARNATAKA,  
SURATHKAL, MANGALORE – 575 025**

**OCTOBER, 2023**

# **FABRICATION OF LOW COST FLEXIBLE CARBON NANOTUBE COATED FABRIC FOR SPECIAL APPLICATIONS**

**Thesis**

Submitted in partial fulfillment of the requirements for the degree of

**DOCTOR OF PHILOSOPHY**

by

**ARUNKUMAR.D.S**

**(Registration Number: 177054MT002)**

**Under the Guidance of**

**Dr. MOHAMMAD RIZWANUR RAHMAN**

**and**

**Dr. KRISHNAMOORTHY.K**



**DEPARTMENT OF METALLURGICAL AND MATERIALS  
ENGINEERING  
NATIONAL INSTITUTE OF TECHNOLOGY KARNATAKA,  
SURATHKAL, MANGALORE – 575 025**

**OCTOBER, 2023**

## DECLARATION

*By the Ph.D. Research Scholar*

I hereby declare that the Research Thesis entitled "**Fabrication of Low Cost Flexible Carbon Nanotube Coated Fabric for Special Applications**" which is being submitted to the **National Institute of Technology Karnataka, Surathkal** in partial fulfillment of the requirements for the award of the Degree of **Doctor of Philosophy in Metallurgical and Materials Engineering**, is a bonafide report of the research work carried out by me. The material contained in this Research Thesis has not been submitted to any university or Institution for the award of any degree.



ARUNKUMAR.D.S

Reg. NO.: 177054MT002

Department of Metallurgical and Materials Engineering

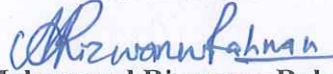
Place: NITK - Surathkal

Date: 12/10/2023

## CERTIFICATE

This is to certify that the Research Thesis entitled “**Fabrication of Low Cost Flexible Carbon Nanotube Coated Fabric for Special Applications**” submitted by Mr. **ARUNKUMAR.D.S (Register Number: 177054MT002)**, as the record of the research work carried out by him, is accepted as the Research Thesis submission in partial fulfillment of the requirements for the award of the **Degree of Doctor of Philosophy in Metallurgical and Materials Engineering.**

**Research Guide**



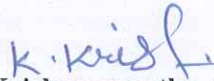
**Dr. Mohammad Rizwanur Rahman**

Associate Professor

Department of Metallurgical and Materials Engineering

NITK, Surathkal

and



**Dr. Krishnamoorthy. K**

Associate Professor

Department of Electronics and Communication Engineering

NITK, Surathkal



**Chairman - DRPC**

Department of Metallurgical and Materials Engineering

NITK, Surathkal

**Chairman - DRPC**  
Dept. of Metallurgical and Materials Engineering  
National Institute of Technology Karnataka, Surathkal  
Post Srinivasnagar, Mangaluru - 575 025  
Karnataka, India

***Dedicated to my beloved parents, and my brother***

***Late Shri. KiranKumar.D.S.***

## ACKNOWLEDGEMENT

The research work, which is presented in this dissertation, is more of teamwork and I would like to thank many who have contributed their time and energy for the study.

First and foremost, I am grateful to my advisor **Dr. Mohammad Rizwanur Rahman**, Department of Metallurgical and Materials Engineering, National Institute of Technology Karnataka, Surathkal (NITK) and co-advisor **Dr. Krishnamoorthy. K**, Department of Electronics and Communication Engineering, NITK, Surathkal as they consistently kept me motivated and instilled good thoughts not only for research but for life as well. His constant and enthusiastic support throughout is the root cause for the research work to see its logical end.

I wish to thank all the members of the Research Program Assessment Committee (RPAC) including **Dr. B. Rajasekaran**, Associate Professor, Department of Metallurgical and Materials Engineering, NITK, Surathkal, and **Dr. A.V. Narasimhadhan**, Associate Professor, Department of Electronics and Communication Engineering, NITK, Surathkal for their unbiased appreciation, support and suggestions provided during the various discussions which have certainly helped in the betterment of this research work.

I am thankful to **Dr. Ravishankar K S**, Head & DRPC Chairman, Department of Metallurgical and Materials Engineering, NITK, Surathkal. I extend my gratitude to the authorities of NITK, Surathkal, Staff and Research Scholars of Department of Metallurgical and Materials Engineering for their help which ensured the satisfactory progress of my research work. My special thanks to Staff, Department of Electronics and Communication Engineering, for their kind support in executing the experiments.

I would like to express my deepest gratitude to my parents, **Shivappa D** and **Lalithamma**, who were always there to support me in my endeavors. Their confidence in my ability to succeed was the impetus I needed to move forward and confront obstacles. I am grateful to my elder sister **Ashwini.D.S** for taking care of my parents during my stay in NITK.

Throughout my Ph.D. studies, I am indebted to my research group members **Mohanraj G T, Aruna M N, K Divya Bharathi, K V Swaroop, V P Singh,** and **Mohammad Muhiuddin** for their continuous support. Without friends, life would not have been as exciting and intriguing, I would like to thank my dearest friends **Vishwanath Bhajantri, Basavaraj Nainegali, Ramesh Sampath, Sharath B O, Umesh Shinde, Mohammed Sohail Bakshi, Rakesh Patil, Suhas A, Yogeeshu Suvama, Akash Gupta, Narendra Babu, Praveen T R** and **Gajula Aravindh** who were always there for me during my Ph.D. work.

I acknowledge with gratitude to all my friends who have helped directly or indirectly in completing my research work successfully. Finally, I am greatly indebted to almighty, all my family members, relatives, and teachers who supported me throughout my life, providing me the opportunity and made me reach this stage.

**ArunKumar.D.S**

## ABSTRACT

A low-cost smart fabric is a need of today's era for different applications such as electromagnetic interference (EMI) shielding, chemical gas sensing, and wearable heaters. Electromagnetic interference (EMI) shielding involves the reflection and/or absorption of electromagnetic (EM) radiation by a material. The presently available EMI shielding materials have poor flexibility, are not economical, and have difficulty achieving good shielding efficiency over the wide bandwidth. It is necessary to develop lightweight, cost-effective, biodegradable EMI shielding material which can be used as an enclosure for electronic devices and systems to reduce EMI. Furthermore, the corrosive gas carbon monoxide (CO) is hazardous to human life since it is odorless and colorless, making it difficult for humans to detect it. Semiconducting metal oxides, a conventional sensing material require a temperature of 150–600°C for operation, resulting in excessive power consumption and safety issues despite having good sensing capabilities on quartz and ceramic substrates. It is essential to develop low-cost, biodegradable, user-friendly, and highly sensitive CO gas sensors operating at room temperature. In addition, recently there has been an increase in the popularity of lightweight, portable, and wearable electronic devices. Traditional heating materials (electrical heating belts, heating mats) require high voltage and localized heating at the resistive wires. It is required to develop flexible, and wearable heating material by a simple processing technique, which can work at a low voltage. Consequently, the present study aimed to address these issues by using carbon nanotubes (CNTs) coated fabric as an EMI shielding material, gas sensor, and wearable heater.

The current study concentrates on fabricating low-cost multi-walled carbon nanotubes coated cotton fabric for reducing electromagnetic interference and detecting carbon monoxide (CO) gas at room temperature. In addition, testing of the electrothermal performance of fabricated multi-walled carbon nanotubes coated cotton fabric in terms of applied voltage and heating rate to evaluate their ability as a wearable heater and overcome the limitations of conventional heating materials.

A dip and drying method is used to fabricate a lightweight, inexpensive, and



biodegradable cotton fabric with multi-walled carbon nanotube coating. The cotton fabric with multi-walled carbon nanotube coating (CMC) samples are fabricated by varying the concentration of multiwalled carbon nanotubes (MWCNTs). The merits of MWCNTs coating on the cotton fabric were evaluated using field emission scanning electron microscopy (FESEM), thermogravimetric analysis (TGA), and surface resistivity. The Fourier transform infrared (FTIR) spectroscopy result supports the bonding between MWCNTs and cotton fabric. Surface resistivity decreases as increasing the weight percentage (wt%) of MWCNTs in the CMC sample. Moreover, the influence of multi-walled carbon nanotubes (MWCNTs) wt% on transmission, reflection, and absorption properties, which leads to an estimation of electromagnetic interference (EMI) shielding was studied. The significant increase of 98.9% of EMI shielding for the highest MWCNTs weight percentage (22.23 wt%) was attributed due to the well-interconnected network of MWCNTs. The shielding mechanism in the high wt% MWCNTs samples is dominated by both reflection and absorption properties.

Furthermore, the fabricated cotton fabric with multi-walled carbon nanotube coating (CMC) sensors are tested for a range of CO concentrations from 25 to 100 ppm at room temperature, and they exhibited good gas response with superior uniformity and repeatability. The fabricated CMC sensors are suitable for low-cost smart textile applications. Also, the electrothermal performance of CMC samples are investigated based on the applied voltage and the rate of heating to evaluate their ability as a heater. The fabricated samples can operate at 10-40 V and generate temperature from 30-80°C for the optimum weight percentage (22.23 wt%) of MWCNTs in the cotton fabric. The heating rate and steady-state temperature were found to be similar, a linear connection between current and voltage values was seen throughout the CMC sample with considerable variance in resistance values. The fabricated CMC samples give the latest design option for applications like wearable electronics.

*key words:* Biodegradable, Cotton fabric, Carbon monoxide, Electromagnetic interference (EMI) shielding, Multi-walled carbon nanotubes, Room-temperature sensors, Wearable heater

## TABLE OF CONTENTS

<b>CONTENTS</b>	<b>PAGE NO.</b>
<b>TABLE OF CONTENTS</b>	<b>i</b>
<b>LIST OF FIGURES</b>	<b>iv</b>
<b>LIST OF TABLES</b>	<b>x</b>
<b>CHAPTER 1</b>	<b>1</b>
<b>INTRODUCTION</b>	<b>1</b>
1.1 Carbon Nanotube	1
1.2 Electromagnetic interference (EMI) shielding and microwave effects on human	4
1.3 Effects of carbon monoxide (CO) gas on human	8
1.4 Electrothermal heating materials	10
1.5 Characterization studies	12
1.5.1 Electromagnetic interference (EMI) shielding mechanism and characterization methods	12
1.5.1.1 Characterization methods	14
1.5.2 Testing of cotton fabric with multi-walled carbon nanotube coating (CMC) sensors with CO gas	17
1.5.3 Testing of electro-thermal heating behavior of CMC samples	18
1.6 Outline of the thesis	19

<b>CHAPTER 2</b>	<b>21</b>
<b>LITERATURE REVIEW</b>	<b>21</b>
2.1 Electromagnetic interference shielding materials	21
2.2 CO gas sensing materials	29
2.3 Electrothermal heating materials	36
2.4 Research gap from the literature survey	41
2.5 Objectives of the research work	42
<b>CHAPTER 3</b>	<b>43</b>
<b>METHODOLOGY</b>	<b>43</b>
3.1 Flow chart of the work	43
3.2 Overview of the materials, surface treatment of cotton fabric, and fabrication of CMC samples	44
3.2.1 Materials	44
3.2.2 Fabric surface treatment	44
3.2.3 Fabrication of MWCNTs coated cotton fabric	44
3.3 Characterization of the multi-walled carbon nanotube coated cotton fabric	47
3.3.1 FESEM study	47
3.3.2 FTIR study	47
3.3.3 Thermogravimetric analysis (TGA)	48
3.3.4 Resistivity measurement	49
3.3.5 Microwave properties measurement	49
3.3.6 Sensing setup and testing of MWCNTs coated cotton fabric gas sensors	50
3.3.7 Testing of electro-thermal heating behavior of CMC wearable heaters	52

<b>CHAPTER 4</b>	<b>53</b>
<b>RESULTS AND DISCUSSION</b>	<b>53</b>
4.1 FESEM and FTIR analysis of fabricated CMC samples	53
4.2 Thermogravimetric analysis	57
4.3. Bulk and surface resistivity of CMC samples	58
4.4. Properties measured at the microwave frequency range	61
4.4.1 Permittivity	61
4.4.2 Reflection, transmission, and absorption properties	64
4.4.3 EMI shielding property	66
4.5 Detection of CO gas by CMC sensors	70
4.6 Electrothermal heating behavior of CMC samples	76
<b>CHAPTER 5</b>	<b>80</b>
<b>CONCLUSIONS AND SCOPE OF FUTURE WORK</b>	<b>80</b>
5.1 Conclusions	80
5.2 Scope of future work	81
<b>LIST OF PUBLICATIONS</b>	<b>82</b>
<b>REFERENCES</b>	<b>83</b>
<b>BIO-DATA</b>	<b>99</b>

## LIST OF FIGURES

<b>Figure No.</b>	<b>Description</b>	<b>Page No.</b>
1.1	High-resolution TEM images of multi-wall and single-wall CNTs observed by Sumio Iijima in 1991 and 1993 respectively: (a) Multi-wall, (b) double-wall, and (c) single-wall CNT. The first two images are adapted from Iijima, and the latter image is from Iijima and Ichihashi (Iijima, S 1991; Ichihashi, T 1993).	2
1.2	Schematic illustration of nanotube morphologies: (a) Armchair, (b) Zig-zag, and, (c) Chiral ( Terrones, M 2003).	3
1.3	Ionizing and non-ionizing radiation spectrum.	6
1.4	Variation of scaling exponent (Ahamed et al. 2008).	7
1.5	Sources of CO gas using pie chart (Sandilands and Bateman 2016).	9
1.6	(a) Commercially available heating mat, (b) Electrical heating blanket, and (c) Electrical heating belt.	11
1.7	Attenuation of an electromagnetic wave by a shield.	13
1.8	Schematic of open Field method (Geetha et al. 2009).	15
1.9	Schematic of shielded box technique (Geetha et al. 2009).	15
1.10	Schematic of shielded room technique (Geetha et al. 2009).	16
1.11	Schematic of coaxial transmission technique (Geetha et al. 2009).	17
2.1	Real ( $\epsilon'$ ) (a) and imaginary ( $\epsilon''$ ) (b) parts of the relative complex permittivity of SWCNTs/SCPU composites with different loadings (Zunfeng Liu et al. 2007).	23

2.2	Dielectric loss (a) and Reflection loss (b) of SWCNTs/SCPU composites of different loadings v/s frequency (Zunfeng Liu et al. 2007).	23
2.3	(a) CNT dispersion in epoxy resin by a three roll-milling machine, and (b) Schematic of a three roll-milling process (Nam et al. 2011).	24
2.4	Reflection loss (a), absorption loss (b), SE of the CNT films bonded on the mortar composite in the unit of dB (c), and EMI SE of the CNT films bonded on the mortar composite in the unit of percentage (d) (Nam et al. 2011).	25
2.5	Schematic diagram for the formation of TiO <sub>2</sub> -coated MWCNT nanocomposite (Bhattacharya et al. 2012).	26
2.6	(a) Reflection loss vs frequency plot of (a) RAM-MW and RAM-Ti, and (b) RAM-Ti@MW and RAM-Ti@MW/Fe (Bhattacharya et al. 2012).	27
2.7	(a) Effect of frequency on EMI SE of the nanocomposites, and (b) Effect of MWCNT content on the EMI SE of the nanocomposites (Dinesh et al. 2012).	29
2.8	(a) Time response of the polyaniline thin film with CNT dispersion to CO gas, and (b) Sensitivity of polyaniline thin film with and without CNT to carbon monoxide gas (Wanna et al. 2006).	30
2.9	(a) Real-time electrical resistance response of CNT-Pd sensor for 20 to 80 ppm concentration of CO gas, and (b) Sensitivity and response of CNT-Pd sensor for 20 to 80 ppm concentration of CO gas (Choi et al. 2011).	31
2.10	(a) Response of sensors for different concentration of CO, and (b)	32

	The sensor calibration curve (Hannon et al. 2014).	
2.11	Response of acid treated SCNP sensor when exposed to variation of concentration of CO gas at room temperature (Kim et al. 2011).	33
2.12	SEM/TEM Images and pictures : (a) Spin-capable CNT forest, (b) and (c), CNT sheets pulled from the CNT forest, and (d) Pt nanoparticles on CNT sheet (Han et al. 2019).	34
2.13	(a) Sensitivity of the gas sensor with respect to CO concentrations, and (b) Sensitivity of the Pt-CNT gas sensor as a function of time with respect to CO concentrations (Han et al. 2019).	35
2.14	Sensitivity of Pt-CNT sensors for different CO gas concentrations with respect to Pt- thicknesses (Han et al. 2019).	36
2.15	Electro thermal heating performance of MWCNT sheet films on the glass; temperature profiles v/s time with respect to different applied voltages for (a) one layer, (b) double layers, (c) acid treated one layer, and (d) decorated with Ni (Jung et al. 2014).	37
2.16	The temperature profiles of Graphene-based heaters with two different doping agents and an ITO-based heater, measured by (a) an infrared camera, and (b) a thermocouple (K-type) (Kang et al. 2011).	39
2.17	(a) The steady-state temperature of graphene film treated with the infrared laser of varying powers, and (b) The temperature profile of graphene film with 180mW laser power (Zhang et al. 2017).	40
2.18	Graphene thin film ON/OFF temperature response at 100, 180, and 240mW (Zhang et al. 2017).	41

3.1	Fabrication of CMC sample using a dip and dry process: (a) Dispersed MWCNTs in DI water, (b) NaOH treated plain woven cotton fabric, (c) Cotton fabric dipped inside the MWCNTs dispersed solution (during 1 <sup>st</sup> cycle of dipping), and (d) Dried cotton fabric with multi-walled carbon nanotube coating (CMC) sample (after 50 cycles of dip and dry process).	45
3.2	FESEM interfaced with a computer.	47
3.3	Fourier transform infrared (FTIR) spectroscopy.	48
3.4	TGA instrument.	48
3.5	Four-probe measurement setup.	49
3.6	(a) PNA-x flexible network analyzer system (Model No: N5224B), and (b) Waveguide along with the sample holder.	50
3.7	Gas sensing setup.	51
3.8	Schematic diagram of gas sensing measurement system and a photograph of CMC sensor placed inside the glass chamber.	51
3.9	(a) Schematic diagram of the two-terminal side contact setup for testing the electrothermal heating behavior of CMC samples, and (b) image of the heater.	52
4.1	FESEM images: (a) Cotton fabric, (b) Cotton fabric with multi-walled carbon nanotube coating (CMC6 sample), (c) FESEM at low magnification of the MWCNTs coated cotton fabric, (d) FESEM at high magnification of the MWCNTs coated cotton fabric, and (e) EDS spectrum of CMC sample.	54
4.2	The FESEM images of cotton fabric coated with multi-walled carbon	55



nanotubes: (a) CMC 1 (1 mg/ml), (b) CMC 2 (1.25 mg/ml), (c) CMC 3 (1.5 mg/ml), (d) CMC 4 (1.75 mg/ml), (e) CMC 5 (2 mg/ml), (f) CMC 6 (2.25 mg/ml), and (g) CMC 7 (2.5 mg/ml).

4.3	FTIR spectra of cotton fabric and MWCNTs coated cotton fabric.	56
4.4	(a) TGA curve of plain-woven cotton fabric and MWCNTs coated cotton fabric (CMC 6 sample), and (b) TGA of MWCNTs coated cotton fabric.	58
4.5	Changes in the resistivity of CMC 3 (7.97 wt%) sample with respect to the number of dips: (a) Bulk resistivity, and (b) Surface resistivity.	59
4.6	The resistivity of CMC 1 (5.96 wt%) to CMC 7 (22.23 wt%): (a) Bulk resistivity, and (b) Surface resistivity.	60
4.7	The current(I)-voltage(V) characteristics of CMC samples.	60
4.8	The permittivity v/s frequency for real (a) and imaginary part (b) of CMC samples in the X band, and for real (c) and imaginary part (d) in the Ku band.	63
4.9	Tan $\delta$ of CMC samples in the X band (a) and Ku band (b).	63
4.10	Scattering parameters for CMC fabrics (a) S21 parameter, (b) S11 parameter, (c) Transmission, (d) Reflection, and (e) Absorption in X band.	65
4.11	Scattering parameters for CMC fabrics (a) S21 parameter, (b) S11 parameter, (c) Transmission, (d) Reflection, and (e) Absorption in Ku band.	65
4.12	The shielding effectiveness v/s frequency of CMC fabrics (a), (b) in	68

the X band, and (c), (d) in the Ku band.

- |      |   |    |
|------|---|----|
| 4.13 | The shielding effectiveness of CMC 1 (5.96 wt%) to CMC 7 (22.23 wt%).   | 68 |
| 4.14 | CMC sensor response to a series of carbon monoxide (CO) exposures ranging from 25 to 100 ppm at room temperature: (a) Sensor CMC 3, (b) Sensor CMC 4, (c) Sensor CMC 5, (d) Sensor CMC 6, and (e) Sensor CMC 7.   | 71 |
| 4.15 | (a) Response time of CMC sensors towards different concentration of CO, and (b) Recovery time of CMC sensors towards different concentration of CO.   | 73 |
| 4.16 | Response comparison of CMC sensors towards different concentrations of carbon monoxide at room temperature.   | 74 |
| 4.17 | Comparison of the present work and published research on carbon monoxide sensor response.   | 75 |
| 4.18 | (a) Heating behavior of CMC 7 samples using a thermocouple and DC power supply (turn on and turn off), temperature as a function of time with varying applying voltage, and (b) Steady-state temperature comparison of CMC samples for the different applied voltage. | 77 |
| 4.19 | (a) Heating behavior of CMC 5 sample at 40V, and (b) TGA graph of plain-woven cotton fabric and MWCNTs coated cotton fabric (CMC 5 sample).   | 78 |
| 4.20 | Temperature response of the wearable heater (CMC 7 sample) under a heat cycle.  | 79 |

## LIST OF TABLES

<b>Table No.</b>	<b>Description</b>	<b>Page No.</b>
1.1	The frequency range of ionizing and non-ionizing radiation emitting electromagnetic waves.	6
1.2	Health problems based on carbon monoxide (CO) concentration and inhalation time.	10
2.1	Composition used for RAMs preparation.	27
2.2	Samples designation.	28
3.1	Details of the cotton fabric with different concentration of MWCNTs coating.	46
4.1	MWCNTs wt% in CMC samples.	58
4.2	Electrical conductivity of MWCNT and CMC samples.	61
4.3	Comparison between microwave properties of carbon composites in the literature and CMC samples of this work.	69

## **CHAPTER 1**

### **INTRODUCTION**

The present dissertation aims to study the development of cotton fabric with multi-walled carbon nanotube coating (CMC) for EMI shielding, detecting carbon monoxide (CO) gas, and wearable heater. So, this chapter provides an overview of carbon nanotube (CNT) properties, electromagnetic interference (EMI) shielding and microwave effects on human, effects of carbon monoxide (CO) gas on human. Further, this chapter presents a review of electrothermal heating materials and their limitations. Finally, characterization studies.

#### **1.1 Carbon Nanotube**

Carbon nanotube (CNT) was considered to be one of the most interesting new materials in the last 30 years. It has gotten a lot of attention since Japanese electron microscopist Sumio Iijima found a CNT in 1991 as tubular shapes in amorphous soot on electrodes from an arc-discharge process (Iijima, S 1991). They are characterized as hexagonal arrangements of carbon (graphene) rolled up into a tube (Fig. 1.1). A graphene sheet can be rolled up in various lattice directions, which determines the final properties of the CNT whether it's semiconducting or metallic. A single graphene sheet roll is termed a single-wall carbon nanotube (SWCNT) and when multiple sheets are rolled, a multi-wall carbon nanotube (MWCNT) is formed. In addition, a comprehension of chirality is necessary because it helps to categorize CNTs by their physical and electronic structure. Carbon nanotubes that can be superimposed on their own mirror images are called achiral nanotubes, while those that can't are called chiral nanotubes. Based on the geometry of the circular cross-section of CNTs, achiral carbon nanotubes are further subdivided into armchair or zigzag carbon nanotubes. Briefly, single-wall CNT is classified into three types: chiral, armchair, and zigzag, whereas the last two are achiral as shown in Fig. 1.2 (Terrones, M 2003). Carbon nanotubes are good electrical conductors and CNT has an electrical conductivity of  $10^2$  to  $10^6$  S/m. In addition, carbon nanotubes have a thermal conductivity about double that of diamond and are thermally stable in a vacuum up to 2800°C, making them better thermal conductors (Lewandowski et al. 2015).

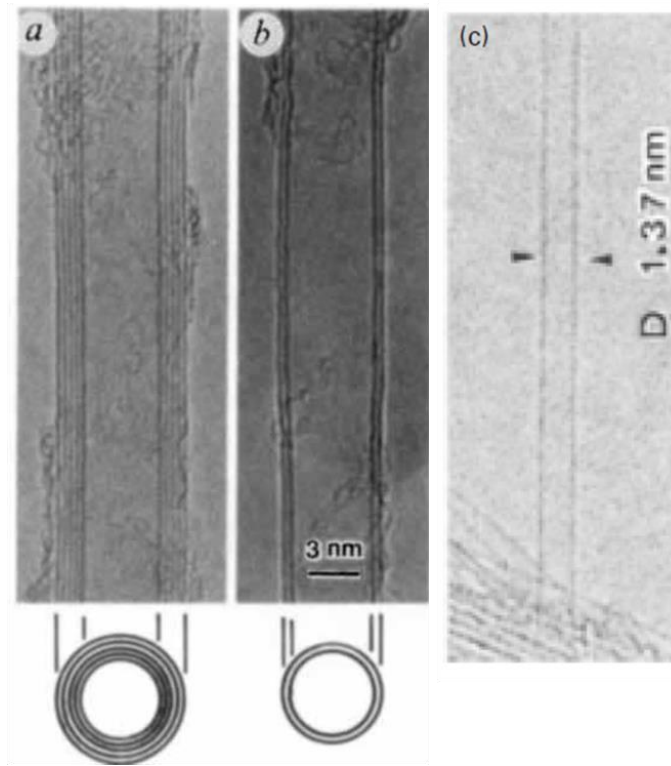


Figure. 1.1: High-resolution TEM images of multi-wall and single-wall CNTs observed by Sumio Iijima in 1991 and 1993 respectively: (a) Multi-wall, (b) double-wall, and (c) single-wall CNT. The first two images are adapted from Iijima, and the latter image is from Iijima and Ichihashi (Iijima, S 1991; Ichihashi, T 1993).

The two most common methods of CNT production are arc discharge and chemical vapor deposition (CVD) (Ichihashi, T 1993). Usually, arc discharge is the easiest method of producing CNTs. By using this technique, a complex mixture is generated, that isolates the carbon nanotubes from the soot and the catalytic metals. For the production of CNTs, two carbon rods are positioned end-to-end in an inert gas-filled enclosure and subjected to arc vaporization. A direct current of 50 to 100 A is used to produce a high-temperature discharge between two electrodes. High-temperature discharge vaporizes the carbon electrode surfaces, resulting in a thin rod-shaped electrode. The homogeneity of the plasma arc is crucial to the optimal synthesis of CNTs. Also, SWCNTs can be produced using the arc discharge technique with liquid nitrogen (Journet et al. 1997). In

contrast to the arc discharge method, the CVD is a more practicable technique for the mass production of CNT. In the CVD process, at high temperature, a gaseous or volatile carbon compound is decomposed onto a substrate in a tube reactor. Usually, transition metal films are employed as the substrate and the precursor gas is methane (Kumar et al. 2010). When the substrate gets colder, carbon becomes less soluble on the substrate, which results in the formation of CNTs on the substrate by the carbon nucleus. One of the main benefits of CVD growth methods is that they work well with the current complementary metal–oxide–semiconductor (CMOS) technology.

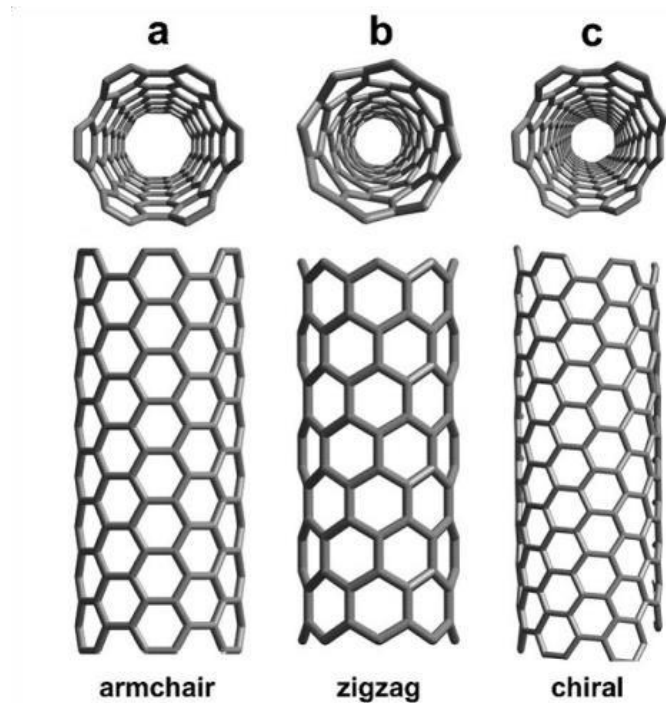


Figure. 1.2: Schematic illustration of nanotube morphologies: (a) Armchair, (b) Zig-zag, and, (c) Chiral ( Terrones, M 2003).

The carbon-based materials with carbon nanofillers (e.g., carbon black (CB), carbon nanotubes (CNTs), carbon nanocoils (CNCs), and graphite nanosheets (GNs)) showed excellent EM wave attenuation because of their thermally activated carrier hopping coupled with defect states. Among the carbon nanomaterials, the CNTs have a high electrical conductivity. Therefore, it may be the best candidate to use in carbon-based

materials for obtaining better electrical conductivity, higher  $\tan \delta$ , and high EMI shielding efficiency (Wen et al. 2014; Chen et al. 2013). In addition to achieving enhanced gas sensing capability (Kong et al. 2000) and excellent electrothermal performance (Chu et al. 2013).

## **1.2 Electromagnetic interference (EMI) shielding and microwave effects on human**

Electromagnetic interference (EMI) shielding involves reflection and/or absorption of electromagnetic radiation by a material. A highly efficient flexible EMI shielding material is a need of today's era (Kumar and Kumar 2009; Yang et al. 2005). Flexible electromagnetic shielding material is used for protecting implanted electronic devices (pacemakers (PM) and cardiovascular implantable devices (CIEDs)) (Shenthar et al. 2016). It is also used as a radome in defense applications (Santini et al. 2013). It is difficult to imagine a socially active man in the 21st century who doesn't use a phone with Wi-Fi. Cell phone use has grown a lot in the last 20 years all over the world. Cell phone use is going up without people thinking about the drawbacks. People all over the world have been debating the health hazards associated with the electromagnetic radiation of cell phones. Recent problems with radio-frequency interference or electromagnetic wave interference (EMI), such as information leakage, cross talk, noise production, etc., have been caused by the overuse of digital devices and circuits in electronic and electrical equipment in the industry, the military, personal electronics and scientific research (Nam et al. 2011). EMI occurs when a system or equipment component sends out unwanted electromagnetic noise or signals that interfere with its performance. In the past few decades, there has been a lot more electronic equipment and wireless system, which has made it easier for electromagnetic interference to occur (Håkansson et al. 2006). There are two main kinds of electromagnetic interference: continuous interference and impulse interference.

**Continuous interference:** Continuous EMI describes EMIs that are emitted constantly by a source. As long as a coupling mechanism exists between the EMI source and the receiver (Mathur and Raman 2020), interference will persist regardless of whether the source is manmade or natural. Continuous interference refers to interferences such as

oscillation or radio waves that persist over time. This interference may be caused by an oscillator without a screen or by wideband noise.

**Impulse interference:** Impulse EMI refers to electromagnetic interference that occurs suddenly or for a very short period of time. Natural or artificial, impulse EMIs are possible (Mathur and Raman 2020). Interference from a short impulse, such as that caused by an electrostatic discharge, lightning, or the switching off a circuit, is known as impulse interference. Aside from identifying the specific interference type, understanding how it moves from source to target is essential. Unfortunately, it is not simple to determine because it is difficult to define the paths. However, these issues can be avoided with the well preliminary design.

In Fig. 1.3, the electromagnetic spectrum shows how both ionizing and non-ionizing radiation behave. Low-frequency electromagnetic fields (EMF) are non-ionizing waves with lower frequencies than visible light. Examples include embedded sensors, microwave ovens, mobile phones, Bluetooth, Wi-Fi, Magnetic resonance imaging (MRI), and electrical lines. High-frequency electromagnetic radiation is ionizing radiation with frequencies greater than those of visible light. These include X-rays, Gamma rays, and ultraviolet light (Yong et al. 2015) and Table 1.1 shows the frequency range of ionizing and non-ionizing radiation emitting electromagnetic waves. These electromagnetic waves have the potential to disrupt radio frequency spectrum use, harm communications networks and safety operations, set fire to combustible materials, and even directly affect human tissue, leading to health complications like leukemia, neurological disorders, Stroke, respiratory problems, anxiety, and sleep issues, etc (Geetha et al. 2009). Since the human body is composed of 70% water, it absorbs electromagnetic radiation when exposed to it. The effect of microwave absorption is significantly more pronounced in those areas of the body that contain a greater amount of fluid (water, blood, etc). Recent studies have shown that the radiation emitted from cell phones can have a considerable effect on both the heart rate and the fertility of men (Kumar and Kumar 2009). The signals that are produced by the operating functions of a cell phone, such as turning it on, ringing, talking on the phone, and turning it off, contain low-frequency sounds



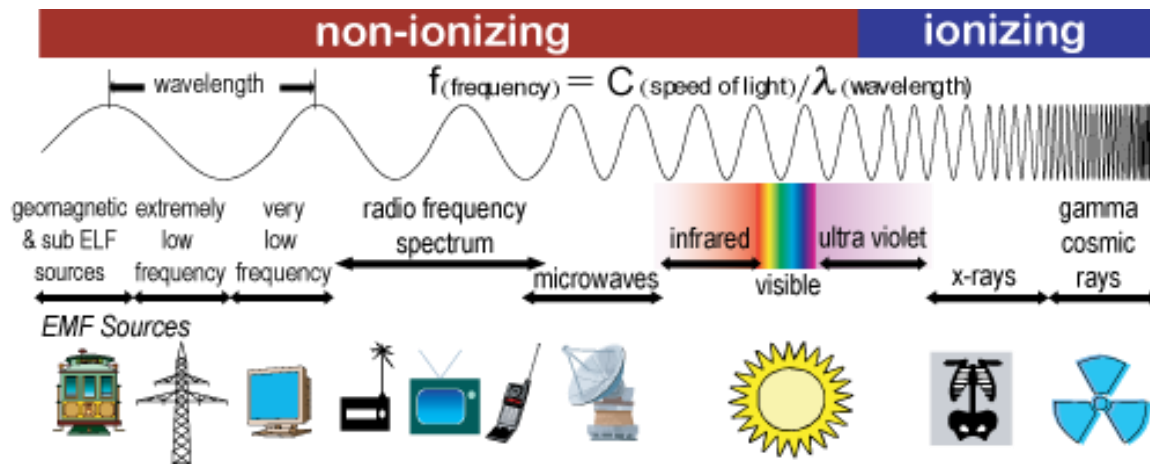


Figure. 1.3: Ionizing and non-ionizing radiation spectrum.

Table 1.1: The frequency range of ionizing and non-ionizing radiation emitting electromagnetic waves.

<b>Extremely low frequency (ELF)</b>	<b>(<math>0 &lt; f \leq 300\text{Hz}</math>)</b>
<b>Intermediate frequency (IF)</b>	<b>(<math>300\text{Hz} &lt; f \leq 100\text{kHz}</math>)</b>
<b>Radio frequency (RF) and Microwaves</b>	<b>(<math>30\text{kHz} &lt; f \leq 300\text{GHz}</math>)</b>
<b>Infrared, visible light, ultraviolet</b>	<b>above 300GHz</b>
<b>X-rays and gamma rays</b>	<b>above 30PHz</b>
<b>Mobile phones operating frequency range</b>	<b>450MHz -3800MHz</b>

that can mess with the way implanted pacemakers work, leading to arrhythmia. This can result in the patient passing away in extreme circumstances. Ahamed et al. 2008 studied the scaling exponent experimental conditions to analyze the heart rate change and the variation of scaling exponent is shown in Fig. 1.4. Heart rate variability analysis in ten participants showed a decrease in scaling exponent without using a mobile phone (Normal) in comparison to scaling exponent with a mobile phone on the head. In addition, 10 of the 14 participants had a greater scaling exponent with a mobile phone on the chest compared to the scaling exponent without using a mobile phone.

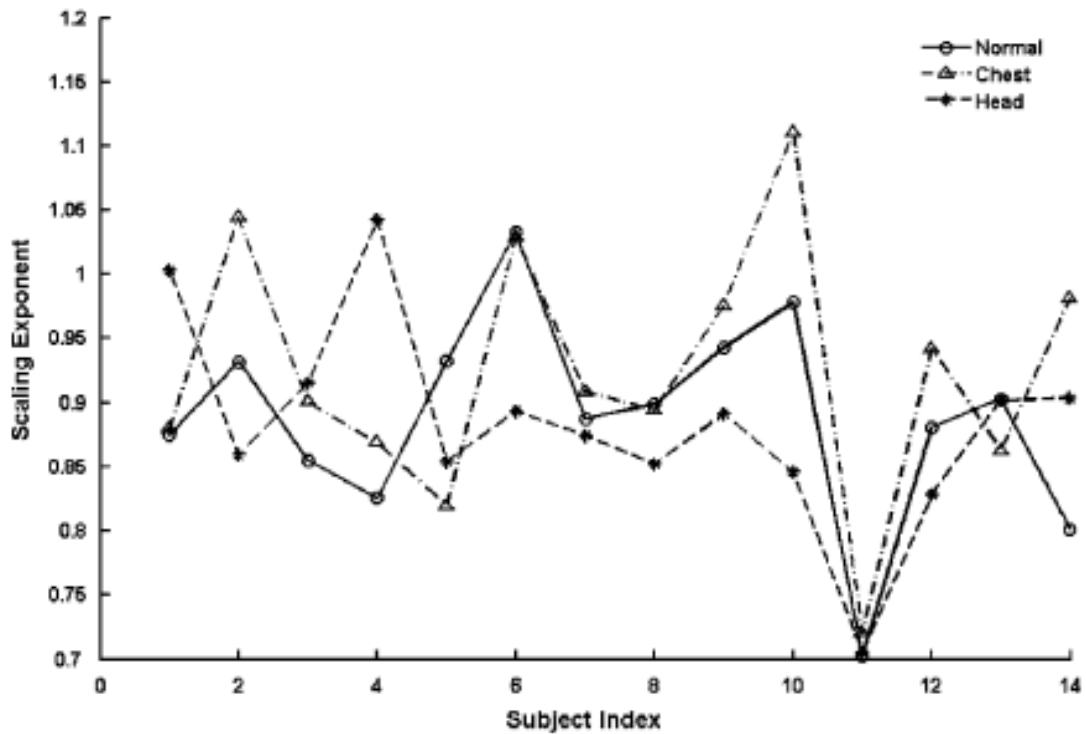


Figure. 1.4: Variation of scaling exponent (Ahamed et al. 2008).

The effects of direct mobile phone radiation on sperm quality were investigated by Gorpinchenko et al. (2014). They found that cell phone use by men is correlated with decreased semen quality, sperm count, motility, viability, and normal morphology. Extensive mobile phone users have been shown to have damaged sperm and a 30% drop in sperm count. The average number of sperm per milliliter of seminal fluid was found to be 59 million, down from 83 million for men who were not constantly exposed to cell phone radiation. Long-distance call-taking was associated with a decrease in quickly motile sperm, from 51.3% to 36.3% in men. Meanwhile, long-term exposure to mobile phones' electromagnetic radiation can disrupt spermatogenesis and increase the risk of other diseases, such as cancer, via the development of oxidative stress and DNA fragmentation. Additionally, sperm DNA may become fragmented when there is an increase in the number of people who have non-progressive movement and when there is extended direct contact with mobile phones. Recent research and interest have been focused on determining the impact that radiation from mobile phones has on male

fertility as well as on patients who wear pacemakers. This study aims to overcome the effect of mobile radiation on the human body by using a wearable mobile radiation reflector. More specifically introducing CNTs into the cotton fabric, which can reflect mobile radiation. CNTs can be incorporated into clothing to protect against electromagnetic radiation, and CNT-coated cotton fabric can be used as an enclosure for electronic devices and systems to reduce electromagnetic interference.

### **1.3 Effects of carbon monoxide (CO) gas on human**

Carbon monoxide (CO) has become one of the leading causes of death since its concentration in the air has risen over the past decade. Since carbon monoxide is odorless, colorless, and tasteless, its presence can kill humans before even realize its presence (Guzman 2012). Carbon monoxide is an essential industrial gas that is utilized as fuel and is widely employed as a reducing agent in the chemical industry. Various fossil fuels such as charcoal, coal, petroleum, natural gas, and wood are incompletely burned to produce it (Ogunkunle and Ahmed 2021). Carbon monoxide is a highly toxic gas that is a lot more dangerous to humans than carbon dioxide because the incomplete combustion of hydrocarbon fuels, due to a lack of sufficient oxygen ( $\text{CH}_4 + \text{O}_2 \rightarrow \text{CO} + \text{H}_2\text{O}$ ) results in the formation of one carbon and one oxygen atom. The difference in one O molecule makes a significant difference in the chemical composition and lethality of the compound. The environmental protection agency (EPA) reported that CO levels in the environment are rising as a result of industrial emissions, fire grills, gas heaters, and any other source of combustion (Ogunkunle and Ahmed 2021). The smoke from fires and exhaust gases from uncatalyzed automobile engines are two common sources of CO gas. Fig. 1.5 shows the sources of CO gas using a pie chart, in which carbon monoxide pollution has been caused mainly by motor vehicles, which release about 45% of all CO pollution into the air. In addition, 40% of CO pollution is from other transportation, and the remaining is from smelters, residential and other industrial processes (Sandilands and Bateman 2016).

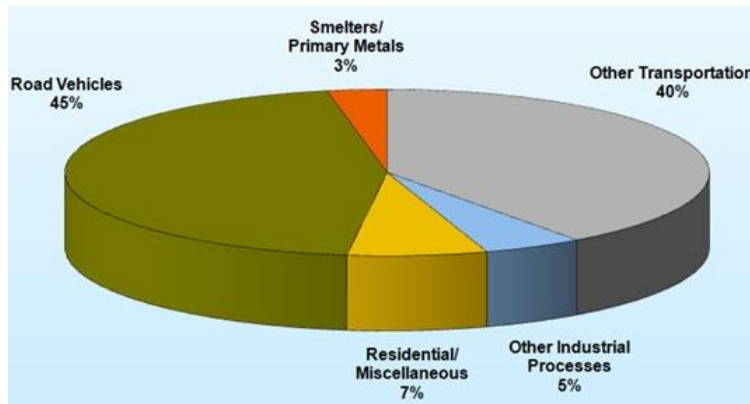


Figure. 1.5: Sources of CO gas using pie chart (Sandilands and Bateman 2016).

On average, about 500 people die every year in the United States because of CO (Guzman 2012). Carbon monoxide (CO) poisonings are common in the United States due to the inappropriate utilization of portable gasoline-powered generators (Damon et al. 2013). In the power outage, gasoline-powered generators lead to the most accidental CO-poisoning deaths that are not caused by fire. These poisonings usually happen after harsh summer and winter storms like hurricanes, tornadoes, floods, and ice storms (CDC 2006). The Centers for Disease Control and Prevention say that CO poisoning sends a few thousand people to hospital emergency rooms each year. Most of these deaths were caused by a lack of ventilation in small spaces, which allowed carbon monoxide to build up and poison people (CDC 2007). The symptoms of CO poisoning depend on how much of the gas was breathed in. Table 1.2 lists the health problems based on the amount of carbon monoxide (CO) and how long it was breathed in. Low and moderate CO poisoning have early signs that are similar to the flu. Headaches, tiredness, dizziness, shortness of breath, and feeling sick are some of the signs. As a person's exposure to CO gets worse, they may become confused, vomit, lose muscle control, lose consciousness, and eventually die. The amount of gas inhaled and how long it is inhaled are directly related. The more gas and how long it is inhaled, the more dangerous the symptoms and the worse the result (Nandy et al. 2018).

Table 1.2: Health problems based on carbon monoxide (CO) concentration and inhalation time.

<b>Concentration of CO in air (ppm)</b>	<b>Inhalation time</b>	<b>Toxic symptoms</b>
<b>9</b>	Short time exposure	The American Society of Heating, Refrigerating and Air-Conditioning Engineers ( <a href="#">ASHRAE</a> ) recommended maximum allowable concentration in the living area.
<b>35</b>	8 hours	The maximum exposure allowed by Occupational Safety and Health Administration ( <a href="#">OSHA</a> ) in the workplace is over eight hours.
<b>200</b>	2-3 hours	Slight headache, tiredness, and dizziness.
<b>400</b>	1-2 hours	Serious headache-other symptoms intensify.
<b>800</b>	45 minutes	Unconscious within 2 hours. Death after 2-3 hours.
<b>1600</b>	20 minutes	Headache, dizziness. Death within 1 hour.
<b>3200</b>	5-10 minutes	Headache, dizziness. Death within 1 hour.
<b>6400</b>	1-2 minutes	Dizziness. Death within 25-30 minutes.
<b>12800</b>	1-3 minutes	Death within 1-3 minutes.

#### **1.4 Electrothermal heating materials**

In places like north India or European countries or any other colder places, heating mats and electrical heating blankets are the most used products in the winter season. The heating mat shown in Fig. 1.6(a) is made up of a copper coil, which requires high energy to operate and is not flexible. An electrical heating blanket shown in Fig. 1.6(b) is minimally unsafe, incorrectly used one can cause burns and fires and use excessive amounts of electricity. Electric blankets can cause pregnant women to get too hot, So several medical groups advise against the use of electric blankets while pregnancy. The

electric heating belt is shown in Fig. 1.6(c) and is a commonly used heating element and is also prescribed in orthopedic practice. For instance, an electric cervical collar is utilized to reduce muscle pain as well as provide heat therapy to injured joints.



Figure. 1.6: (a) Commercially available heating mat, (b) Electrical heating blanket, and (c) Electrical heating belt.

In addition, it is also used as a heat source for the effective treatment of Cervical Spondylosis. But, this electrical heating belt is equipped with a dual thermostat and an imported heavy-duty heating coil. These dual thermostats and heating coils require high vitality to work and the quality of the inbuilt temperature controller is not great. Furthermore, maintenance of this heating belt is very difficult and causes uncomfortable for the users. Such as, persons can't sleep with an electrical cervical collar when it has worn, requires disconnection of the main cord from power when not being used, and also usage of

this belt is limited. Apart from these disadvantages, traditional heating materials have certain limitations such as

1. Poor flexibility (compact ability)
2. Required high voltage
3. Localized heating at the resistive wires
4. Weight of the heating device is more

To meet the technical requirements of modern society, there has recently been a significant interest in electronics that are wearable, portable, and light. Cotton fabric continues to be the most widely chosen textile substrate for electronic applications, owing to potential advantages such as economical, easy processing, mechanical, and wearable properties (Ilanchezhiyan et al. 2015). CNTs, which have remarkable physical, chemical, and electrical properties, tend to be the important nanomaterial in fabric-based wearable devices (Baughman et al. 2002). CNTs-based cotton fabric has created considerable interest in textile-based wearable devices. Instead of using traditional heating materials, the use of CNTs coated cotton fabric as an electrothermal heating element would provide a variety of benefits (Negru et al. 2012; Liu et al. 2008). Moreover, it is lightweight and can be used as a wearable heater. This wearable heater can operate at low voltage and it gives possibilities for innovation in wearable electronics design (Iqbal et al. 2019).

## **1.5 Characterization studies**

### **1.5.1 Electromagnetic interference (EMI) shielding mechanism and characterization methods**

Generally, shielding capacity is measured by shielding effectiveness (SE). The degree of transparency to an electromagnetic wave within a specific frequency bandwidth is measured in output decibels (dB). Absorption, reflection, and multiple internal reflections are three mechanisms that lead to total attenuation of EMI in the complete shielding process as shown in Fig. 1.7 (Shahapurkar et al. 2022; Barathi Dassan et al. 2020). The reflected wave is a combination of surface reflection and several internal reflections.

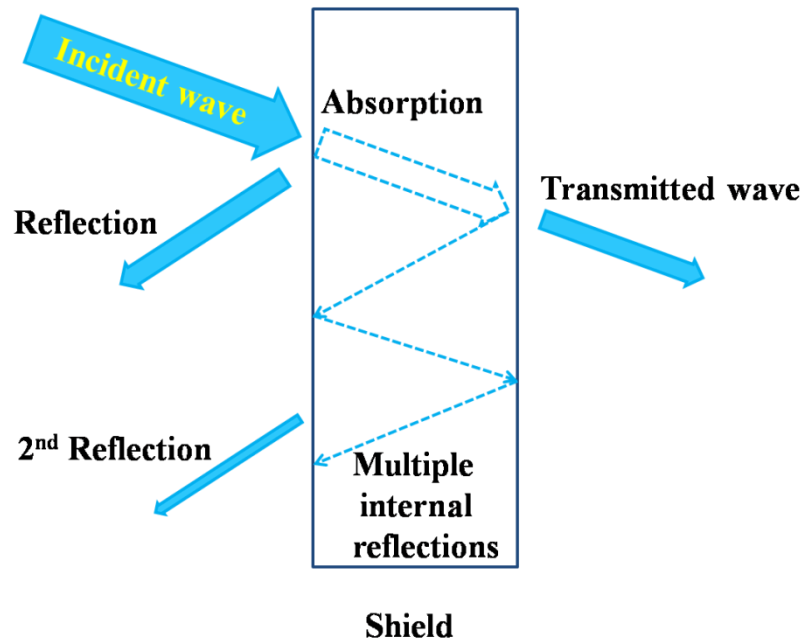


Figure. 1.7: Attenuation of an electromagnetic wave by a shield.

Total  $SE = SE_R + SE_A + SE_M$ , where  $R$  represents reflection,  $A$  represents absorption, and  $M$  represents multiple internal reflection (MIR). Reflection is the principal method for electromagnetic radiation shielding in highly conductive materials like metals. This is because of the presence of free charge carriers (electrons) in the shielding material that can interact with incoming electromagnetic radiation. Because of the impedance mismatch caused by these free charge carriers, a significant portion of the incident wave is reflected. Absorption is induced by electromagnetic radiation interacting with the electric dipoles, electrons, and phonons in the material, and it can also be caused by resistive losses, which involve the Joule effects conversion of electromagnetic energy into heat. Absorption can enhance by increasing the electrical or magnetic dipoles of the shielding material. The multireflection mechanism is challenging to understand and typically insignificant because the shielding material outer conductive surface has high mobile charge carriers that reflect most incident electromagnetic waves. However, a limited portion of the electromagnetic waves that are able to penetrate can be kept for multiple reflections. Likewise,  $SE_M$  is insignificant when  $SE_A$  is more than 10 dB.



The impact of  $SE_M$  is greater when utilizing thin shielding materials at low frequencies (i.e., below 20 kHz).

### **1.5.1.1 Characterization methods**

The most common ways to test EMI shielding are

- Open field or free space method
- Shielded box technique
- Shielded room technique
- Co-axial transmission line technique

The effectiveness of the products EMI shielding in its intended use is evaluated using an open field method as shown in Fig. 1.8 (Shahapurkar et al. 2022). Rather than emphasizing the performance of a particular material, this approach concentrates on shielding the system. In order to measure the radiated emissions, the product under test is put 30 meters away from a receiving antenna. This technique is not recommended for samples constructed from various shielding materials. Fig. 1.9 shows the shielded box method in use for comparing the measured values of test specimens constructed from various shielding materials. The test specimen is affixed to the metallic box edge, and a receiver antenna is positioned in the interior to capture the EM waves. A transmitter antenna is attached externally to the metallic box to monitor the electromagnetic waves emitted by the shielding material. However, this approach has certain drawbacks:

- The electrical connection between the shielding box and the test sample is difficult.
- The electromagnetic wave operational frequency is restricted to 500 MHz.
- Estimating electromagnetic interference shielding efficiency by absorption, reflection, and transmission independently is not possible.

Fig. 1.10 shows the shielded room technique and it is the most modern way to determine EMI shielding. It was made to fix the problems with the shielded box method. The basic principle is similar to the shielded box method.

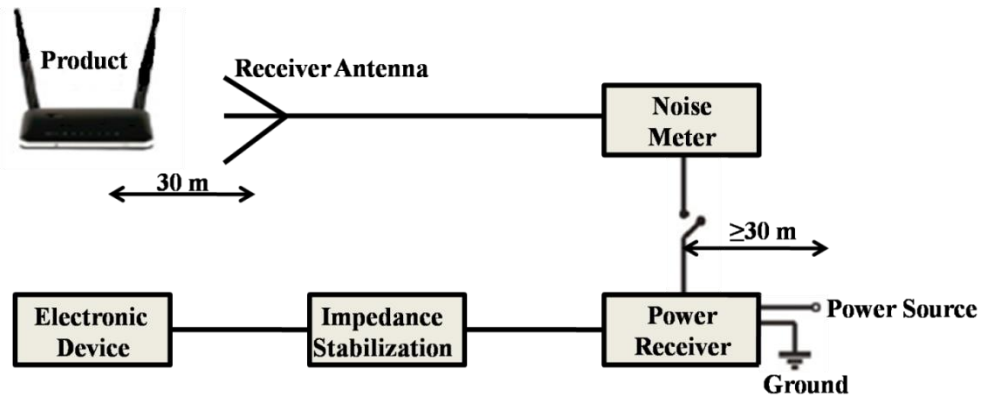


Figure. 1.8: Schematic of open field method (Geetha et al. 2009).

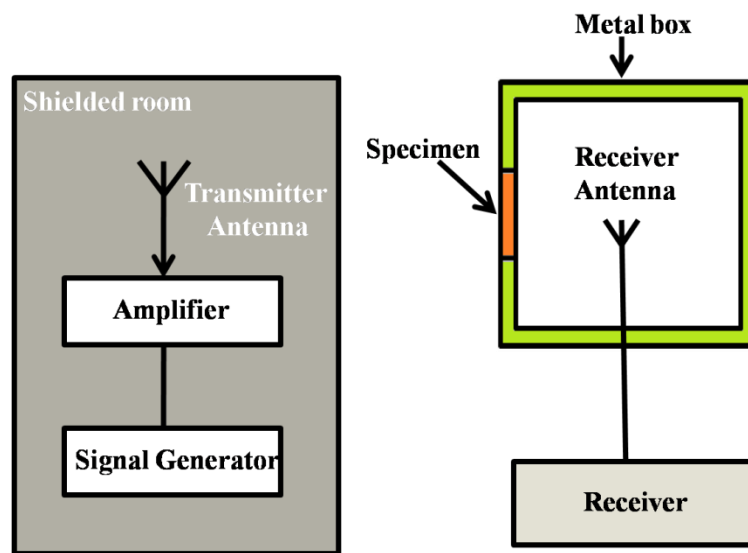


Figure. 1.9: Schematic of shielded box technique (Geetha et al. 2009).

To prevent interference, the measuring apparatus, recorder, transmitter antenna, signal generator, and receiver antenna are kept in distinct shielded rooms. Also, the test sample size is massively improved, usually to about 2.5 m<sup>2</sup>, and the antennas are placed in chambers that are the size of a room that absorbs sound. The EM wave has a much wider range of frequencies, and the data can be reproduced much more accurately.

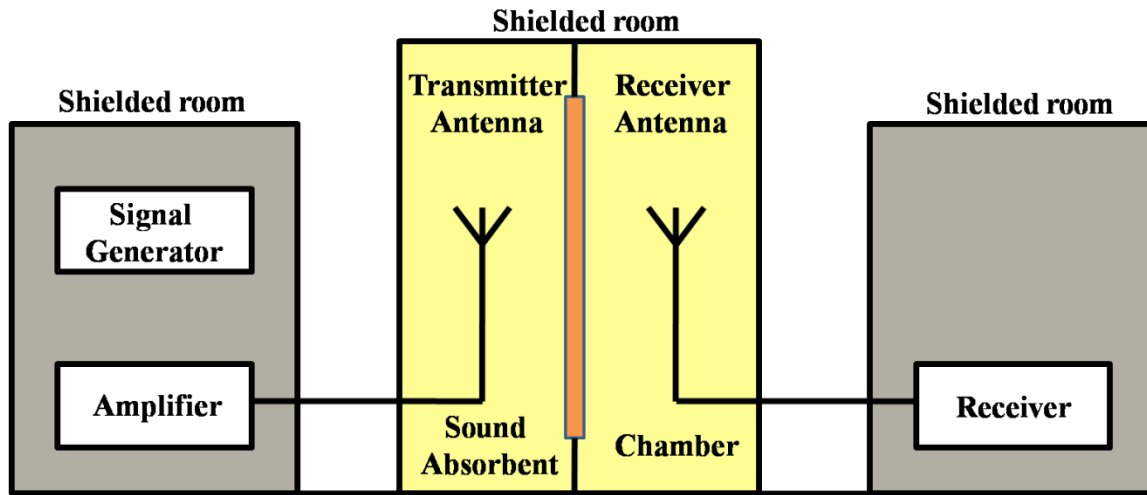


Figure. 1.10: Schematic of shielded room technique (Geetha et al. 2009).

The coaxial transmission line approach is the mainly popular method for determining electromagnetic interference (EMI) shielding due to its many benefits. In this manner, the shielding effectiveness (SE) based on absorption, transmission, and reflection can be determined separately. The schematic diagram of the measurement technique is shown in Fig. 1.11. Also, the outcomes from various test centers can be compared. This method is advantageous for nano-reinforced materials because it only needs a small test sample. Coaxial transmission cables have a lower loss and may produce electromagnetic waves over a wider frequency range than antennas. Based on waveguide approaches (dimension and shape), the scalar network analyzer (SNA) and the vector network analyzer (VNA) are used to measure EMI shielding. VNA can measure the magnitude and phases in addition to their signal amplitude, whereas SNA can only determine the signal amplitude. Due to its ability to monitor complex signals, such as complex permittivity, despite being more expensive, the VNA is a better instrument. In this study, a VNA was utilized to determine the permittivity, transmission, reflection, absorption, and EMI shielding of fabricated CMC samples in the microwave frequency range of X- and Ku-band. The testing of CMC samples using a PNA-x flexible network analyzer is shown in Fig. 3.6.

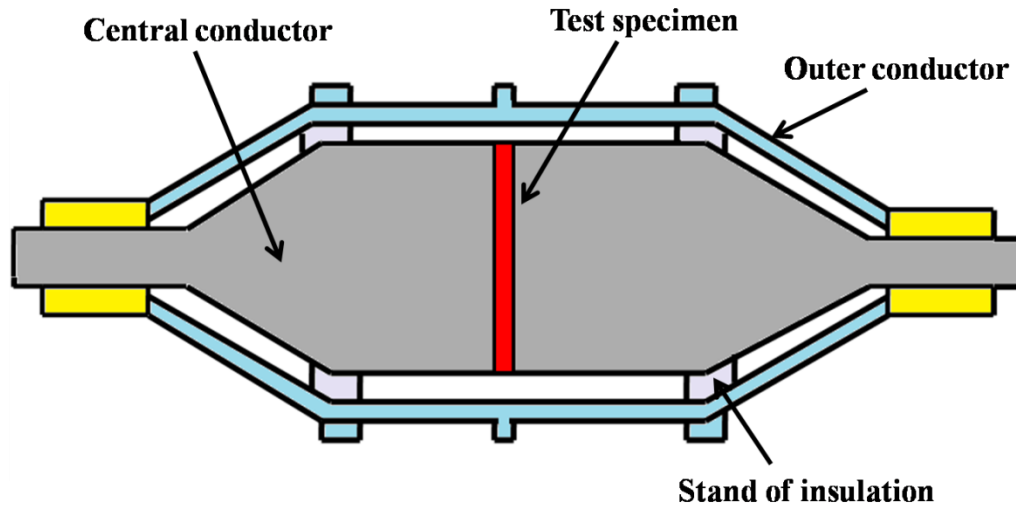


Figure. 1.11: Schematic of coaxial transmission technique (Geetha et al. 2009).

### 1.5.2 Testing of cotton fabric with multi-walled carbon nanotube coating (CMC) sensors with CO gas

CNT-based gas sensors have attracted a lot of interest due to their properties, including their small size, low working temperature, large surface area, high response, and quick response. Experiments have shown that when CNTs are exposed to toxic gases like  $\text{NO}_2$ ,  $\text{NH}_3$ , and  $\text{CO}$ , their ability to conduct electricity changes, even when they are used at room temperature (Kim et al. 2011). When p-type semiconducting CNTs interact with electron acceptors like  $\text{NO}_2$  or electron donors like  $\text{NH}_3$ , they alter the number of holes, which are the primary charge carriers in the nanotube. This alters the conductivity of CNTs (Zhang et al. 2008). Because of this feature, carbon nanotubes can be used as the basis for electrical chemical gas sensors. Some CNTs are p-type semiconductors and a process whereby electrons are transferred from carbon nanotubes to gas molecules that have been adsorbed on their surface changes the electrical conductance of the CNTs; this is how CNTs gas sensors work (Zhao et al. 2002; Peng et al. 2004). The CNTs electric resistance decreases as more oxidizing molecules adsorb on p-type semiconducting CNT. In this study, the sensitivity of CMC samples to different concentrations of  $\text{CO}$  gas was tested at room temperature (ranging from 25 to 100 ppm). The absorption of  $\text{CO}$

molecules changes the electrical conductivity of CNTs. The variation in electrical resistance of carbon nanotubes could be associated with the amount of CO gas absorbed. A Keithley source measuring unit was used to measure the resistance as a function of time. The response (%) of the fabricated CMC sensors is calculated using the change in the resistance of the CMC sensors. A detailed description of the testing of CMC sensors using a gas sensing measurement system is depicted in Fig. 3.8.

### **1.5.3 Testing of electro-thermal heating behavior of CMC samples**

The thermal and electrical properties of CNTs coated cotton fabric enables the development of flexible, lightweight heaters with low operating voltage. Although many studies have looked at the electrical heating behavior of CNT and CNT composite devices when heated or cooled for transparent and conducting heating applications (Chu et al. 2013; Liu et al. 2010; Markevicius et al. 2014), few studies have been done on the electrical heating behavior of CNTs coated cotton fabric.

Herein, the cotton fabric has a low thermal conductivity (0.026–0.065 W/mK, which is better than other synthetic and natural fabrics) and a strong ability to absorb moisture. It also has an open texture pattern, which helps convection in this application (Stanković et al. 2008; Majumdar et al. 2010). The CNTs rapid temperature response could be useful in effectively heating surfaces of any size because of their better electrical conductivity properties. The importance of our heaters resides in their engineering, which enables them to be developed in a variety of sizes. The entire study of the CNT-based cotton fabrics revealed that the materials retain the inherent conductivity and mechanical stability of CNT for specified wearable heating requirements. In this work, the electrothermal performance of CMC samples was investigated in terms of applied voltage and heating rate to evaluate their ability as a heater. The steady-state temperature, as well as better heating and cooling response of the wearable heater CMC samples were evaluated using thermocouple and DC power supply (The performance of the electrothermal system was investigated at various applied voltages). The testing of CMC samples for wearable heating applications using the two-terminal side contact setup is schematically depicted in Fig. 3.9.

## 1.6 Outline of the thesis

In the present work, initially, the received cotton fabric is subjected to surface treatment. Then, the dispersion of MWCNTs. Using the MWCNTs dispersed solution, CMC samples are fabricated by a dip and dry process. The morphology of each CMC sample is characterized using the FESEM technique. However, based on the uniform coating of MWCNTs on the cotton fabric, the characterizations such as FTIR, TGA, and resistivity measurements were carried out. In addition, the properties such as permittivity, transmission, reflection, absorption, and EMI shielding were measured for all CMC samples at the microwave frequency range (X- and Ku- band). Further, the responsive behavior of fabricated cotton fabric with multi-walled carbon nanotube coating (CMC) sensors are tested for different concentrations of CO ranging from 25 to 100 ppm. Finally, the heating behavior of the wearable heater CMC samples were evaluated at various applied voltages.

The thesis has been presented in five chapters

**Chapter 1** introduces an overview of carbon nanotubes (CNTs) structure and its properties with respect to electrical and thermal conductivity. Also, it introduces the need of electromagnetic interference (EMI) shielding, the effects of microwaves and CO gas on human. Further, it introduces conventional electrothermal heating materials and their disadvantages followed by characterization studies.

**Chapter 2** gives a detailed review of the published literature relevant to the present study. The literature review presented mainly includes earlier research work carried out on the characterization studies, the concentration of carbon nanomaterials, and improvement in the EMI shielding effectiveness with respect to the thickness of the material under different frequency range. In addition, earlier work related to the wide application of CO gas sensors using carbon nanomaterials at room temperature was also reviewed. Further, past studies on the electrothermal performance of carbon nanomaterials-based electrothermal heating materials. Finally, the broad objectives of the present research work are drawn based on the gaps observed in the available literature.

**Chapter 3** describes the methodology which includes material selection, surface treatment of material, dispersion of MWCNTs, and experimental procedure for the fabrication of CMC samples. Further, characterization techniques for fabricated CMC samples are discussed.

**Chapter 4** comprises the results and discussion of characterization studies of fabricated cotton fabric with multi-walled carbon nanotube coating (CMC) samples through FESEM, FTIR, TGA, and resistivity measurement. Then, the evaluation of microwave interactive properties of fabricated CMC samples in the frequency range of X- and Ku-band. Further, testing of CMC sensors for different concentrations of CO gas ranging from 25 to 100 ppm, and evaluation of the electrothermal response of CMC wearable heaters based on response time and input voltage.

**Chapter 5** presents the conclusions drawn based on the results obtained in this research work and the future scope of work is also enlisted. The list of references are shown at the end of the dissertation.

## **CHAPTER 2**

### **LITERATURE REVIEW**

A detailed literature review of published research articles related to characterization studies of EMI shielding materials, CO gas sensors at room temperature, and electrothermal heating materials using carbon nanomaterials was reported. In addition, this chapter presents the impact of carbon nanomaterials on the performance of EMI shielding materials, CO gas sensors, and electrothermal heating materials studied by various investigators.

#### **2.1 Electromagnetic interference shielding materials**

Conductive polymer materials are desirable for usage in electronic and electrical equipment casings because of their flexibility, low cost, light weight, and processability in order to meet electromagnetic compatibility criteria. A device is considered electromagnetically compatible for a particular frequency range with its surroundings if it does not interfere with other devices or itself, and it does not affect by electromagnetic wave emissions from other devices. Consequently, an effective shielding material must inhibit both incoming and outgoing electromagnetic interference (EMI). The effectiveness of electromagnetic interference (EMI) shielding (SE) is measured in decibels (dB). It is generally agreed that a 20 dB shielding effectiveness, which corresponds to a 99.9% reduction in EMI radiation is an appropriate level of shielding for the majority of applications (Yang et al. 2005).

Polymers offer various advantages over traditional EMI shielding materials such as metals and ceramics. They can be easily formed, and a lot of different combinations, and formulations can be made that are much lighter. However, the metal and ceramic EMI shielding materials can withstand higher temperature for special applications. For general application, a higher shielding efficiency with lighter weight and better flexibility is also required. Therefore, polymer materials in combination with carbon nanostructure are preferred.

Previously, carbon materials such as carbon fibers, graphite, and carbon black



were mixed into polymers to achieve good EMI shielding (Chung 2001). The focus rapidly switched to carbon nanomaterials like carbon nanofibers, graphene, and CNTs in order to increase the electrical conductivity of conductive polymer materials and accomplish high EMI shielding. Carbon nanomaterials are adequate to shield electromagnetic radiation in the GHz frequency range (Harris 2004). In this case, graphene, nanotubes, and carbon nanofibres are good candidates for the production of effective electromagnetic interference shielding material since they have a larger specific surface area, and better conductivity (Geetha et al. 2009). Even though carbon nanofillers coated polymers have been studied extensively in the past few years, several factors that influence their effectiveness as high-frequency electromagnetic shields remain unexplored or only partially covered. Indeed, few published studies on this application of carbon nanomaterials prove the importance of collecting and analyzing fresh experimental results for use in developing more accurate models and enhancing our knowledge.

Dielectric loss is a potential cause of microwave attenuation which is responsible for the absorption of the microwave within the material. According to transmission line theory, several variables influence the reflectivity of an electromagnetic wave as it travels through a medium. These variables include the frequency of the wave, the sample thickness, and permittivity (Michielssen et al. 1993). Zunfeng Liu et al. (2007) fabricated the processable composites of single-walled carbon nanotubes (SWCNTs) and soluble cross-linked polyurethane (SCPU) with increasing loadings of SWCNTs (from 0% to 25% by weight). The authors used the compression moulding method to fabricate the samples. To study the effects of the absorption and look into the primary causes of the absorption, investigations of microwave-absorbing properties in the 2–18 GHz range have been done. Utilizing the transmission/reflection (T/R) coaxial line approach, the authors independently tested SWCNT/SCPU composites relative complex permittivity, dielectric loss, and reflection loss as shown in Fig. 2.1 and 2.2. Consistent with previous research on SWCNT (Kim et al. 2003; Li et al. 2006), and MWCNT (Grimes et al. 2001; Watts et al. 2003) composites, it has been shown that an increase in the SWCNT loading

causes a significant increase in the real and imaginary parts of the permittivity (Fig. 2.1(a) and (b)). The dielectric tangent loss ( $\tan \delta_E = \epsilon''/\epsilon'$ ) has been determined by the authors using the composites permittivity values. At a 25 wt% SWCNT loading, the composite can achieve dielectric loss tangent values up to 0.9 (Fig. 2.2(a)).

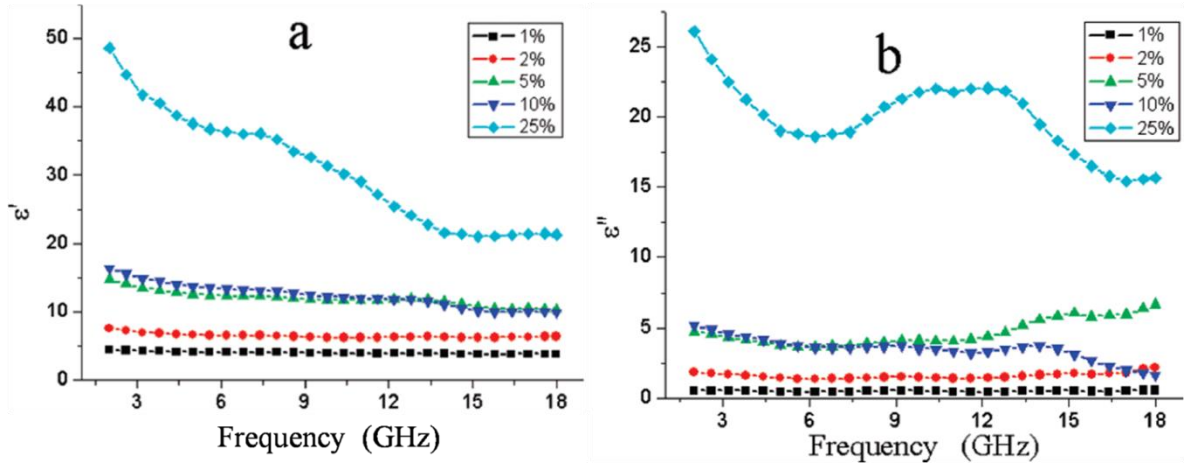


Figure. 2.1: Real ( $\epsilon'$ ) (a) and imaginary ( $\epsilon''$ ) (b) parts of the relative complex permittivity of SWCNTs/SCPU composites with different loadings (Zunfeng Liu et al. 2007).

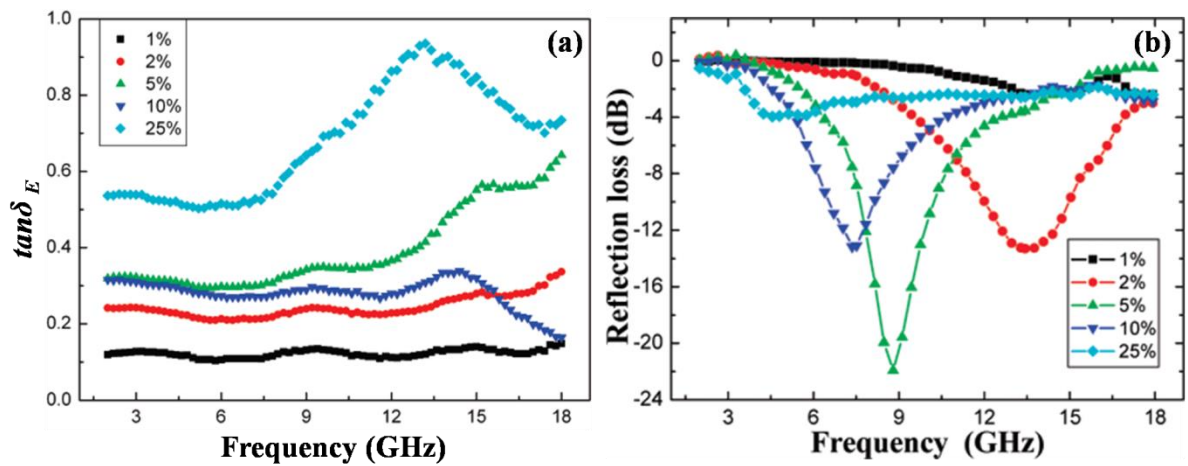


Figure. 2.2: Dielectric loss (a) and Reflection loss (b) of SWCNTs/SCPU composites of different loadings v/s frequency (Zunfeng Liu et al. 2007).

Reflection loss for SWCNTs/SCPU composites against frequency is shown in Fig. 2.2(b) for frequency from 2 to 18 GHz, with SWCNTs loading ranging from 1 to 25 wt%.

The absorption peak of the composite film increases from 1 dB for 1 wt% to 21.9 dB for 5 wt%. The ability to absorb waves reduces when the SWCNT loading is further increased to 10 wt% and 25 wt%. As the concentration of SWCNTs is increased, it can be seen that the maximum absorption peak shift towards the lower frequency.

Nam et al. (2011) used three-roll milling and lamination techniques to fabricate carbon nanotube-epoxy films (also called CNT films) as seen in Fig. 2.3. In order to improve the electrical characteristics of the composites, by layering CNT films, multilayered CNT-epoxy composites (CNT plates) were fabricated. Different thicknesses of composites were tested for EMI shielding efficiency. A network analyzer was used to take readings of S11 and S21 through the coaxial transmission line technique, which are related to the energy that was reflected and the energy that was transmitted. In Fig. 2.4, the composites reflection loss, absorption loss, electromagnetic interference (EMI) SE in dB, and EMI SE in percentage against frequency are shown. In a study comparing the electromagnetic properties of carbon nanotube (CNT) films and CNT plates, the CNT plates provided superior shielding performance for frequencies between 1 and 5 GHz.

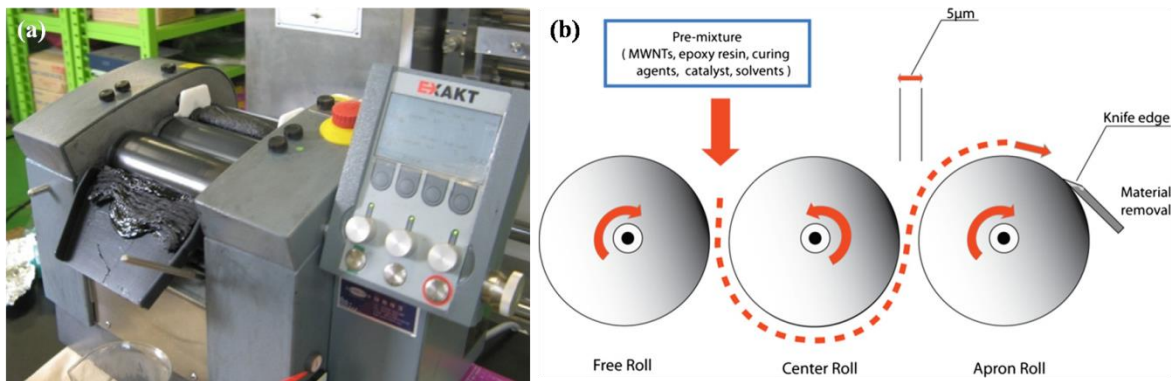


Figure. 2.3: (a) CNT dispersion in epoxy resin by a three roll-milling machine, and (b) Schematic of a three roll-milling process (Nam et al. 2011).

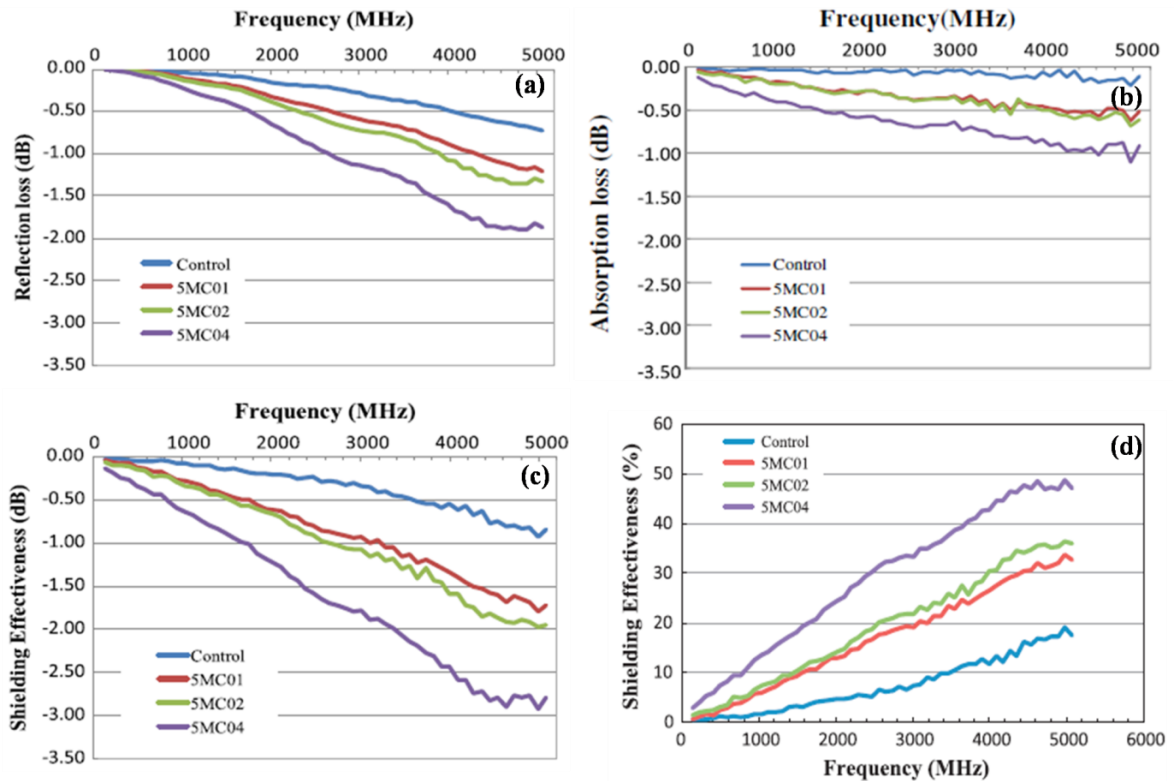


Figure. 2.4: Reflection loss (a), absorption loss (b), SE of the CNT films bonded on the mortar composite in the unit of dB (c), and EMI SE of the CNT films bonded on the mortar composite in the unit of percentage (d) (Nam et al. 2011).

Both reflection loss and absorption loss increase as increasing the thickness of the composite in the frequency range of 1 to 5 GHz shown in Fig. 2.4(a) and (b) respectively. Reflection loss averaged 60.8% of the EMI SE value, while absorption loss averaged 39.2% for 5MC04 composite. The reflection loss of 5MC04 composite is 1.55 times higher than its absorption loss. Consequently, EMI SE increases as increasing the CNT film thickness. When exposed to electromagnetic waves at 5 GHz, the highest EMI shielding effectiveness value of approximately -2.92dB (49.0%) was observed in the 5MC04 composite (Fig 2.4(d)). Consequently, the shielding effectiveness of 5MC04 was 3.97 times higher than the EMI SE of the control (without CNT).

Bhattacharya et al. (2012) fabricated nanocomposites using multiwall carbon nanotube (MWCNT) through the sol-gel method and solution blending process. The authors have made four different types of nanocomposites using a wide variety of filler combinations. Fig. 2.5 illustrates the formation of  $\text{TiO}_2$ -coated MWCNT nanocomposite.  $\text{TiO}_2$ -coated MWCNT and  $\text{Fe}_3\text{O}_4$  were mixed with a ball milling method to make RAM-Ti@MW/Fe. In Table 2.1, the compositions of all radar-absorbing materials (RAMs) are listed. The reflection loss vs frequency plot for all four RAMs in the X band region is shown in Fig. 2.6(a) & (b). As seen in Fig. 2.6(a), compared to a nanocomposite based on  $\text{TiO}_2$ , the MWCNT-based one had better microwave absorbing properties. The addition of magnetite ( $\text{Fe}_3\text{O}_4$ ) increased the microwave absorption capabilities of MWCNT composites coated with  $\text{TiO}_2$  shown in Fig. 2.6(b). The RAM-Ti@MW/Fe shows the maximum reflection loss of  $-42.53$  dB at 10.98 GHz.

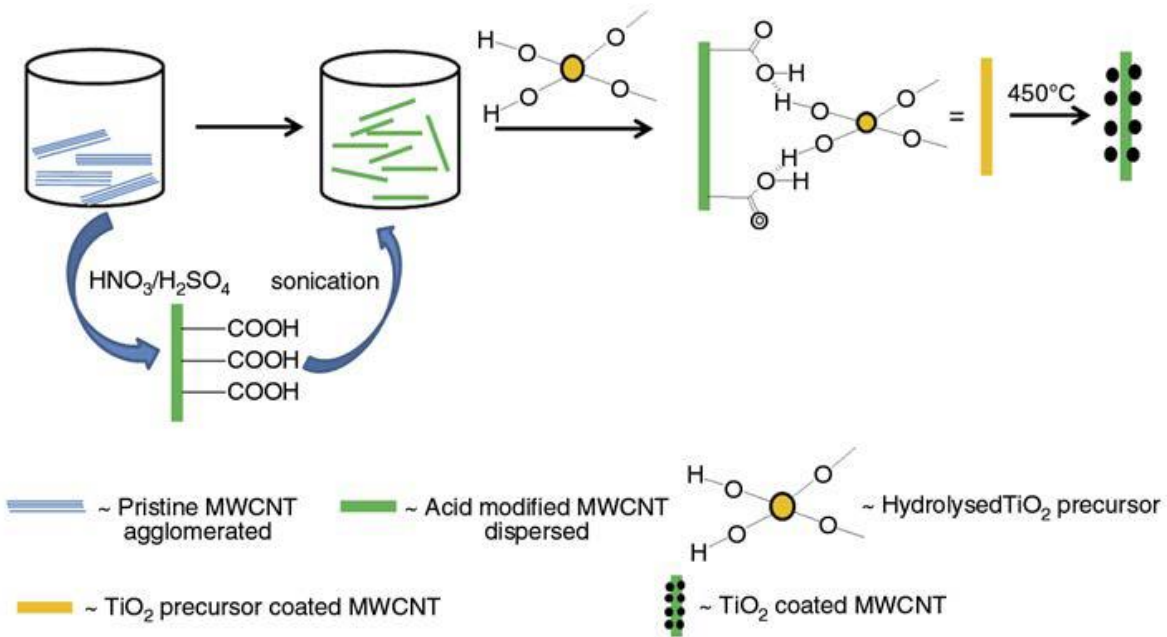


Figure. 2.5: Schematic diagram for the formation of  $\text{TiO}_2$ -coated MWCNT nanocomposite (Bhattacharya et al. 2012).

Table 2.1: Composition used for RAMs preparation.

Sample code	Components
RAM-MW	MWCNT (30%)
RAM-Ti	TiO <sub>2</sub> (30%)
RAM-Ti@MW	TiO <sub>2</sub> coated MWCNT (30%)
RAM-Ti@MW/Fe	TiO <sub>2</sub> coated MWCNT (15%) + Fe <sub>3</sub> O <sub>4</sub> (15%)

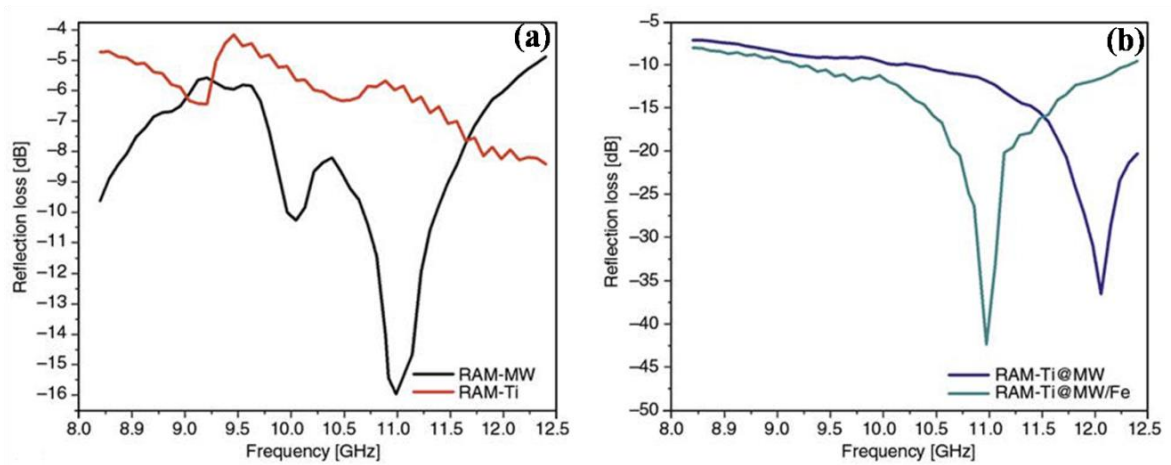


Figure. 2.6: Reflection loss vs frequency plot of (a) RAM-MW and RAM-Ti, and (b) RAM-Ti@MW and RAM-Ti@MW/Fe (Bhattacharya et al. 2012).

RAM-MW and RAM-Ti both absorb microwaves can be explained by the way they conduct electricity. For effective microwave absorption, a material must have good conductivity. The complete absorption of microwaves is possible in strongly conducting materials and partial absorption possible in moderate conductivity materials (Li et al. 2012). Since the MWCNTs skeleton has electrons, making it is capable of absorbing energy (Wu and Kong 2004). TiO<sub>2</sub> is a semiconductor with a band gap energy of only 3.23 eV, it can also help absorb microwaves (Xiao et al. 2006). Currently, when MWCNT and titanium dioxide were combined to form a composite, the result was significantly superior to that of either component alone. Fe<sub>3</sub>O<sub>4</sub> is added to TiO<sub>2</sub>-coated

MWCNT composites to enhance absorption and boost the reflection loss caused by a magnetic element. Thus, out of all materials, RAM-Ti@MW/Fe is the best material that effectively absorbs microwaves. The dielectric and magnetic losses in RAM-Ti@MW/Fe make it more efficient at absorbing microwave energy than RAM-Ti@MW, which only accounts for the dielectric loss.

Dinesh et al. (2012) fabricated nanocomposites of high-density polyethylene (HDPE) embedded with carbon black (CB) and multiwalled carbon nanotubes (MWCNTs). They used a melt mixing procedure to fabricate the electrically conducting nanocomposites, and they used HDPE together with 20 wt% of CB and 0 to 1 wt% of multiwalled carbon nanotubes. The prepared samples are labeled as shown in Table 2.2. These composites have been tested using the co-axial transmission line method for their ability to shield electromagnetic interference (EMI) in the X band (8.2-12.4 GHz). Fig. 2.7(a) depicts the EMI SE of HDPE-CB-MWCNT nanocomposites with various MWCNT loadings at 8.2 to 12.4 GHz frequency range. The SE of composites is discovered to be frequency dependent. At 8.2 GHz, the shielding effectiveness rises from 9.5 to 16 decibels for samples a to e respectively. The X-band measurements of the composite including 1 wt.% MWCNTs showed an EMI SE of 16 dB.

Table 2.2: Samples designation.

<b>Samples</b>	<b>Designation</b>
<b>HDPE + 20 wt.% CB</b>	a
<b>HDPE + 20 wt.% CB + 0.25 wt.% MWCNTs</b>	b
<b>HDPE + 20 wt.% CB + 0.5 wt.% MWCNTs</b>	c
<b>HDPE + 20 wt.% CB + 0.75 wt.% MWCNTs</b>	d
<b>HDPE + 20 wt.% CB + 1 wt.% MWCNTs</b>	e

The impact of filler loading on the EMI shielding effectiveness of nanocomposites is depicted in Fig. 2.7(b). When more MWCNTs are added, the SE improves across the whole frequency range. This is because of the formation of CB and MWCNT conducting networks in the matrix of insulating HDPE. Around 20 dB of EMI SE is ideal for



commercial uses. As shown in the graph, for MWCNT loadings of 1 wt.% in HDPE-CB-MWCNT nanocomposites the SE was 16 dB at 8.2 GHz and falls slightly short of the specifications.

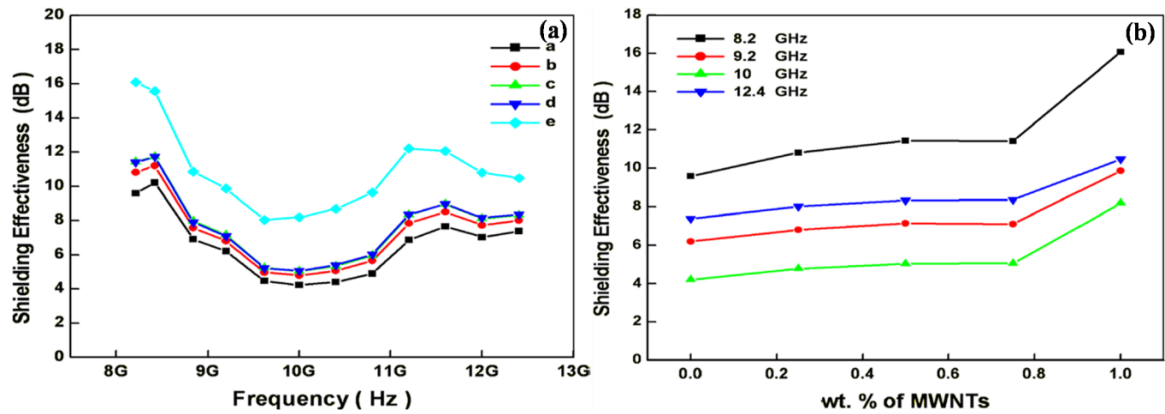


Figure. 2.7: (a) Effect of frequency on EMI SE of the nanocomposites, and (b) Effect of MWCNT content on the EMI SE of the nanocomposites (Dinesh et al. 2012).

## 2.2 CO gas sensing materials

Conductive polymer materials are desirable for detecting gases at room temperature due to their low cost, versatility, and ease of fabrication. Somewhat recently, the concept of CO gas detection by means of adsorption processes in conductive polymer materials was presented. Polymers with carbon nanofillers are better at detecting gases like ammonia ( $\text{NH}_3$ ) (Han et al. 2014), carbon monoxide (CO) (Wanna et al. 2006), hydrogen ( $\text{H}_2$ ) (Kauffman et al. 2008), and nitrogen dioxide ( $\text{NO}_2$ ) (Chauhan et al. 2019) than traditional metals and ceramics. They are significantly lighter and can be formed easily. In the early stages of the fabrication of gas sensing devices, graphite, carbon black, and carbon fibers were the first components to be mixed with polymers (Chung 2001). Soon, researchers shifted their focus to carbon nanomaterials because they could make more conductive composites with smaller amounts of carbon. Furthermore, a filler can be active in sensing throughout its entire cross-section (Harris 2004). In this perspective, carbon nanotubes and graphene are good options for the detection of various corrosive and noncorrosive gases since they have a larger specific surface area and aspect ratio than their micro-scale



analogues (Yin et al. 2021).

Wanna et al. (2006) fabricated a polyaniline thin film with CNT dispersion and without CNT dispersion on an interdigitated Al electrode glass substrate via the solvent casting method. The fabricated sensors were evaluated for carbon monoxide (CO) detection at room temperature with concentrations of CO ranging from 167 to 500 ppm. The time response and sensitivity of polyaniline thin film with CNT dispersion for CO gas is shown in Fig. 2.8(a) and (b). The sensor resistance of polyaniline thin film with CNT dispersion is lower than that of the thin film without CNT dispersion by more than three orders of magnitude (Fig. 2.8(a)). The polyaniline thin film with CNT dispersion is more responsive to CO gas exposure shown in Fig. 2.8(b) and it is noted that two curves of sensitivity for each case in Fig. 2.8(b) are the average sensitivity obtained from two groups of samples that were prepared separately. The sensitivity of polyaniline thin film with CNT dispersion is 6 times greater than polyaniline thin film without CNT dispersion. This is because the CNT has better electrical conductivity and a high surface to volume ratio. These properties should be attributable to increased active gas adsorption.

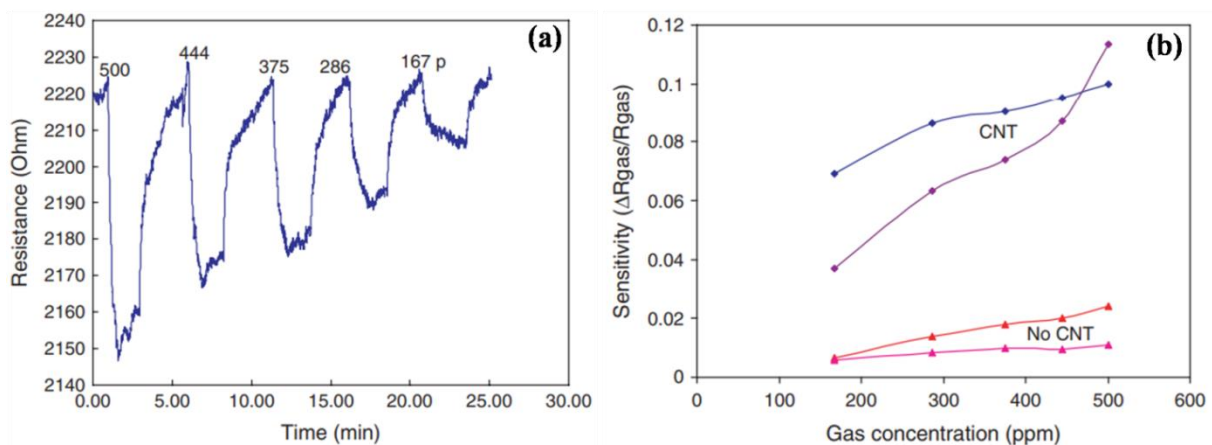


Figure. 2.8: (a) Time response of the polyaniline thin film with CNT dispersion to CO gas, and (b) Sensitivity of polyaniline thin film with and without CNT to carbon monoxide gas (Wanna et al. 2006).

Choi et al. (2011) used carbon nanotubes (CNTs) and reduced palladium nanoparticles (Pd NPs) for the fabrication of noxious gas sensors that could detect carbon monoxide (CO) gases at ambient temperature. They synthesized the reduced CNT-Pd using the melt-mixing technique. Fig. 2.9 depicts the real-time electrical resistance response, sensitivity and response of the CNT-Pd sensor for 20 to 80 ppm CO gas concentration. The CNT-Pd sensors have better sensitivity for different concentrations and can detect CO concentrations as low as 20 ppm with a response time of less than 16s. The fast response is carried on by molecule adsorption onto low-energy binding sites, such  $sp^2$ -bonded carbon, whereas the slower response is carried on by interactions between molecules and higher-energy binding sites, including vacancies, structural flaws, and functional groups. Weak dispersive forces are responsible for adsorption onto a  $sp^2$ -bonded carbon. Nevertheless, single and double hydrogen bonds, as well as defects like carboxylic acid groups, permit binding energies of at least a few hundred millielectron volts per molecule or more. This is the most significant distinction between fast and slow responses. In the end, they concluded that CNT-Pd sensors could be utilized as an easy and efficient noxious gas sensor at room temperature due to their rapid response, constant sensitivity, a low limit of detection, and excellent repeatability across a wide range of concentrations.

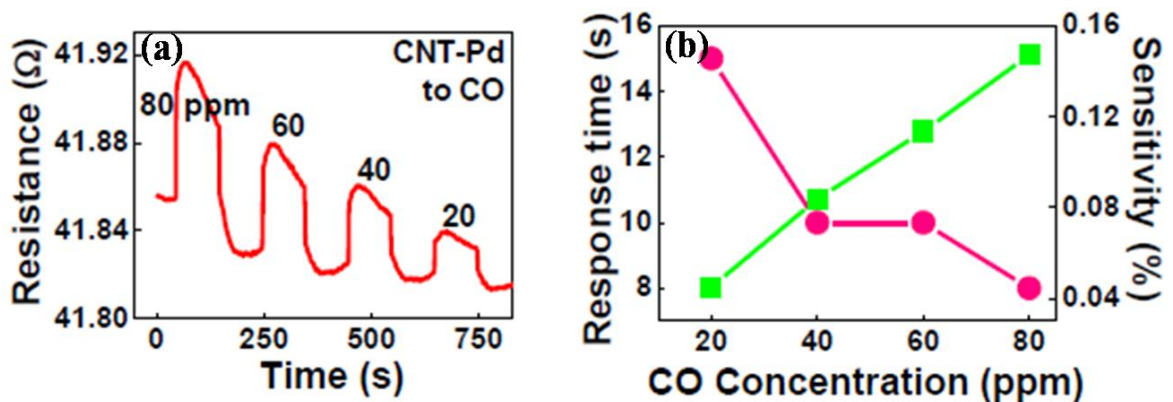


Figure. 2.9: (a) Real-time electrical resistance response of CNT-Pd sensor for 20 to 80 ppm concentration of CO gas, and (b) Sensitivity and response of CNT-Pd sensor for 20 to 80 ppm concentration of CO gas (Choi et al. 2011).

At room temperature, Hannon et al. (2014) detected carbon monoxide using an integrated electrode structure based on sulfonated single-walled carbon nanotubes. To fabricate sensor chips, researchers have employed a printed circuit board (PCB) as the substrate, etching away the gold (Au) coating using a photolithography procedure. They manually deposited Sulfonated SWCNTs (0.3  $\mu$ L solution) on the eight interdigitated electrodes surface of the chips using a pipette. The sensor chip was subjected to concentrations of CO at 0.5, 2, 10, 25, 50, 60, 75, and 100 ppm, as seen in Fig. 2.10(a). This material was found to have a very stable baseline. All eight sensors have responses that are very close to each other. The sensor-to-sensor variation is a consequence of the hand deposition procedure used to add nanotubes to the chip, which results in varying nanomaterial densities inside each sensor element. The response of the sensor is dependent upon CO gas concentration and it increases with the increase of CO concentration.

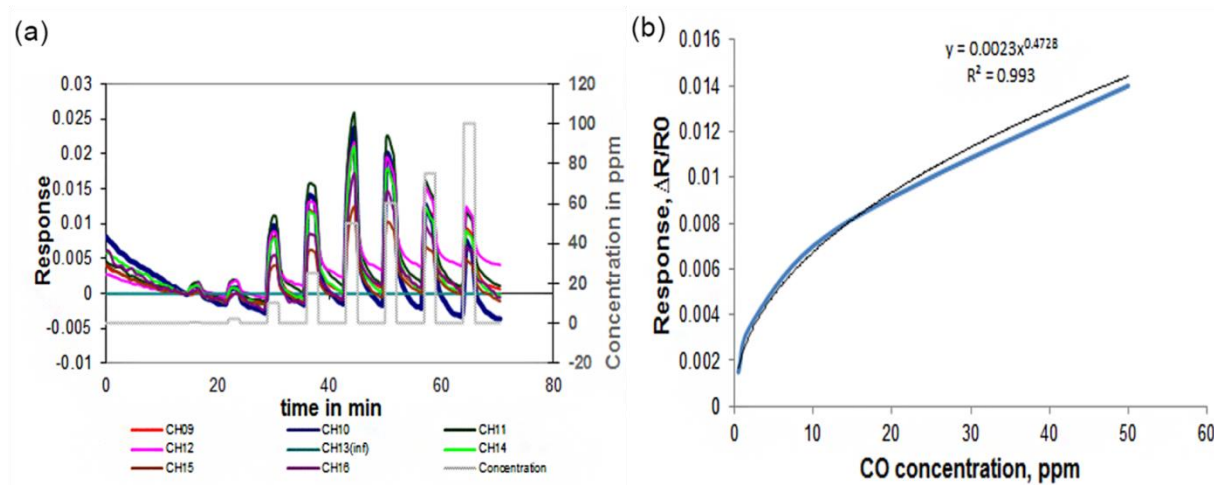


Figure. 2.10: (a) Response of sensors for different concentration of CO, and (b) The sensor calibration curve (Hannon et al. 2014).

Sulfonated SWCNTs sensors shows better response to CO concentrations at room temperature. This behavior is to be anticipated because oxygenated and sulfonated functional groups are present at the ends of the SWCNTs and these functional groups make electron transmission easier. Possible explanations for the enhanced response seen with sulfonated sensors include the inclusion of regulated carboxylic and sulfonic acid

defects, which provide minimal energy adsorption sites and make it easy for the charge to move at defect sites. Like the  $-\text{COOH}$  group,  $-\text{SO}_3\text{H}$  is an electron-withdrawing group, therefore, the sulfonic acid groups applied to the surface of the SWCNTs may result in an increase in charge density. This can boost the hole current of p-type sulfonated SWCNT by increasing the quantity of transfer of electrons between sulfonated single-walled carbon nanotubes and carbon monoxide molecules (Dong et al. 2013).

Kim et al. (2011) made a gas sensor based on shell-shaped carbon nanoparticles (SCNP) that can detect CO and  $\text{H}_2$  gas at room temperature. Laser-assisted reactions in a stream of pure acetylene gas were used to synthesize crystalline SCNPs, then synthesize crystalline SCNPs were treated chemically (with acid) to get well-dispersed SCNPs, and the ion-induced focusing method was used to deposit dispersed SCNPs on a glass substrate. Fig. 2.11 illustrates the response of acid-treated SCNPs sensor for different concentrations of CO gas at room temperature. The sensor shows the highest response of 2% for 100 ppm concentration of CO gas.

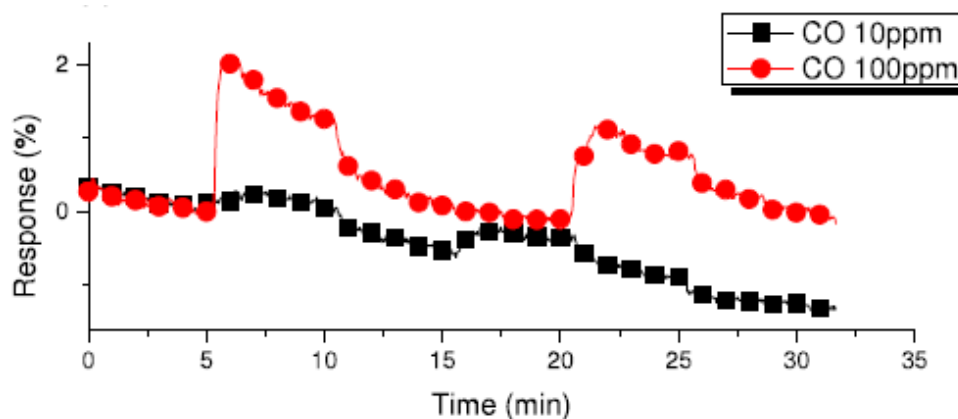


Figure. 2.11: Response of acid treated SCNP sensor when exposed to variation of concentration of CO gas at room temperature (Kim et al. 2011).

Importantly, the acid-treated SCNPs exhibited CO sensing capabilities, indicating that the ability to sense CO may be due to the oxidized material from the outermost layer which is identical to graphene oxide (Lu et al. 2009). The treatment with acid breaks apart the carbon shells continuously, leading to the formation of oxidized graphene platelets and an

elongated component that covers the surface of SCNPs. By evaluating the sensing ability of unmodified and functionalized carbon nanoparticles, they demonstrated that functional groups like OH (hydroxyl) and C=O (carbonyl) produced on the SCNPs surface were responsible for the room-temperature sensing of carbon monoxide molecules.

Han et al. (2019) investigated a CO gas sensor with a platinum coated carbon nanotube (CNT) sheet. They fabricated a nanocomposite by coating a layer of platinum (Pt) on a sheet of carbon nanotube (CNT), and they tested it for the detection of carbon monoxide (CO) gas at room temperature. As illustrated in Fig. 2.12, the authors extracted carbon nanotube yarns directly from a CNT forest and transferred them onto a glass substrate. The CNT sheet was coated with a thin layer of Pt nanomaterial by e-beam evaporation. Based on the TEM picture displayed in Fig. 2.12(d), the authors hypothesize that a substantial CNT surface area is exposed, leading to an increase in sensitivity. The carbon nanotube sheet was built from individual CNTs and provided an enormous surface area for carbon monoxide gas reaction.

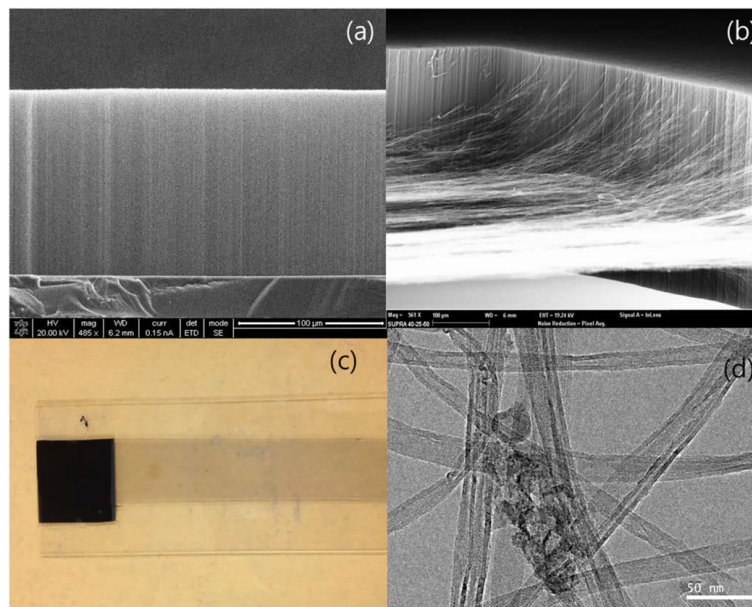


Figure. 2.12: SEM/TEM Images and pictures : (a) Spin-capable CNT forest, (b) and (c), CNT sheets pulled from the CNT forest, and (d) Pt nanoparticles on CNT sheet (Han et al. 2019).

To study the effect of the Pt layer on the CNT sheet, the authors measured the sensitivity of the carbon nanotube sensor with a 5 nm-thick Pt layer and a CNT sensor without the Pt layer for CO gas. The sensitivity of the platinum-carbon nanotube sensor and the CNT sensor for different concentration of CO gas ranging from 20 ppm to 200 ppm is depicted in Fig. 2.13(a). In contrast to the CNT sensor, the Pt-CNT sensor exhibits better sensitivity. The authors hypothesized that the chemical sensitization induced by the overflow effect of gas molecules breaking down into gas atoms on the platinum surface increased the sensitivity of the Pt-carbon nanotube sensor to carbon monoxide gas. As depicted in Fig. 2.13(b), the Pt-CNT sensors maximum response time to CO was less than 30 seconds, and the recovery time is around 40 seconds. Fast response and recovery of the platinum-CNT sensor are likely the result of the catalytic impact of the Pt layers and the CNT sheet conductivity is utilized as the primary sensor template.

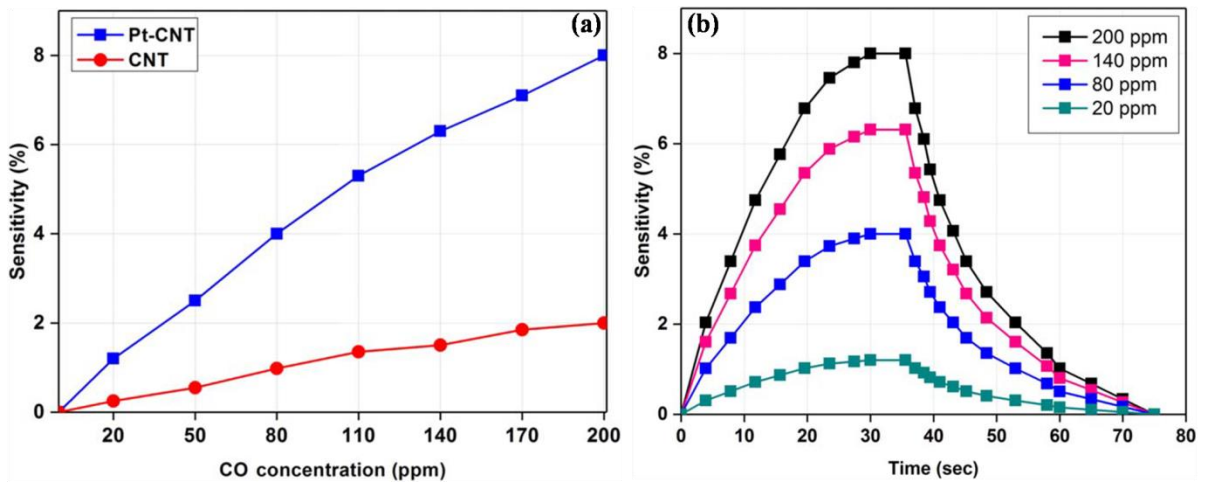


Figure. 2.13: (a) Sensitivity of the gas sensor with respect to CO concentrations, and (b) Sensitivity of the Pt-CNT gas sensor as a function of time with respect to CO concentrations (Han et al. 2019).

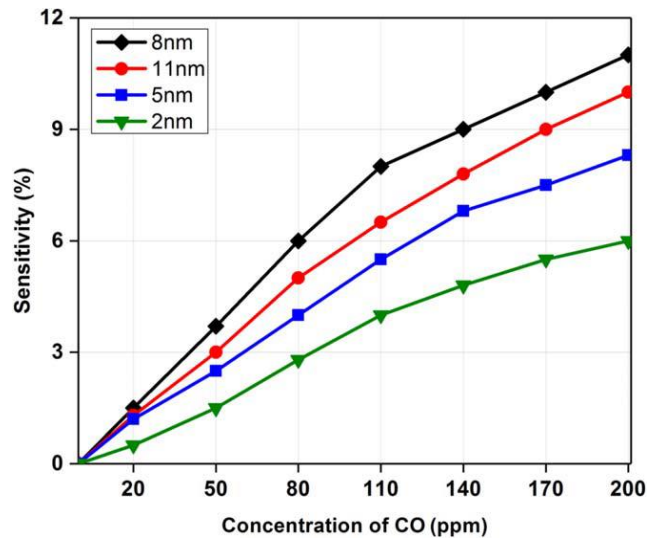


Figure. 2.14: Sensitivity of Pt-CNT sensors for different CO gas concentrations with respect to Pt- thicknesses (Han et al. 2019).

To better understand how sensor sensitivity and Pt layer thicknesses relate to one another, a further experiment was conducted. The authors fabricated four samples of Pt-CNT with different platinum layer thicknesses of 2, 5, 8, and 11 nm. The sensitivity of the sensor for different Pt layer thickness with respect to CO gas concentration is shown in Fig. 2.14. Specifically, the sensitivity increased linearly with thickness from 2 nm to 8 nm. Sensitivity decreased as Pt layers became thicker (11 nm). The sensitivity of the sensor increases as the Pt layer is thicker (up to 8 nm), which can be explained by structural and catalytic effects. To enhance the sensitivity, the interaction between Pt-CNT and CO required more surface area, which led to a greater rate of charge transfer. The authors concluded that the Pt-CNT sensors sensitivity improved with the loading of Pt up to a certain thickness after that it decreased.

### 2.3 Electrothermal heating materials

Electronics that are lightweight, portable, and wearable have recently gained popularity to meet the technical requirements of modern society. The nanomaterials based on carbon offer new design options for wearable electronics. Various authors have investigated the electrothermal heating behavior of carbon nanomaterials-based conductive polymers. The



heating performance of nanomaterials significantly depended on their surface area and the number of contact points. Many techniques, including acid treatment, sheet layer overlap, and the addition of metal nanoparticles, were used to increase the surface area and contact point

Jung et al. (2014) examined the electrothermal performance of the MWCNT sheet-based heaters. The lab grown MWCNT was used to fabricate one-layer, double-layer, acid-treated MWCNT sheet film, and MWCNT/Ni sheet film. Fig. 2.15 depicts the steady-state temperature of all fabricated MWCNT sheet films and in all cases surface temperature of the sheet raised linearly with input power until a steady-state temperature was attained. At 40V of applied voltage, the authors achieved the highest heating rate.

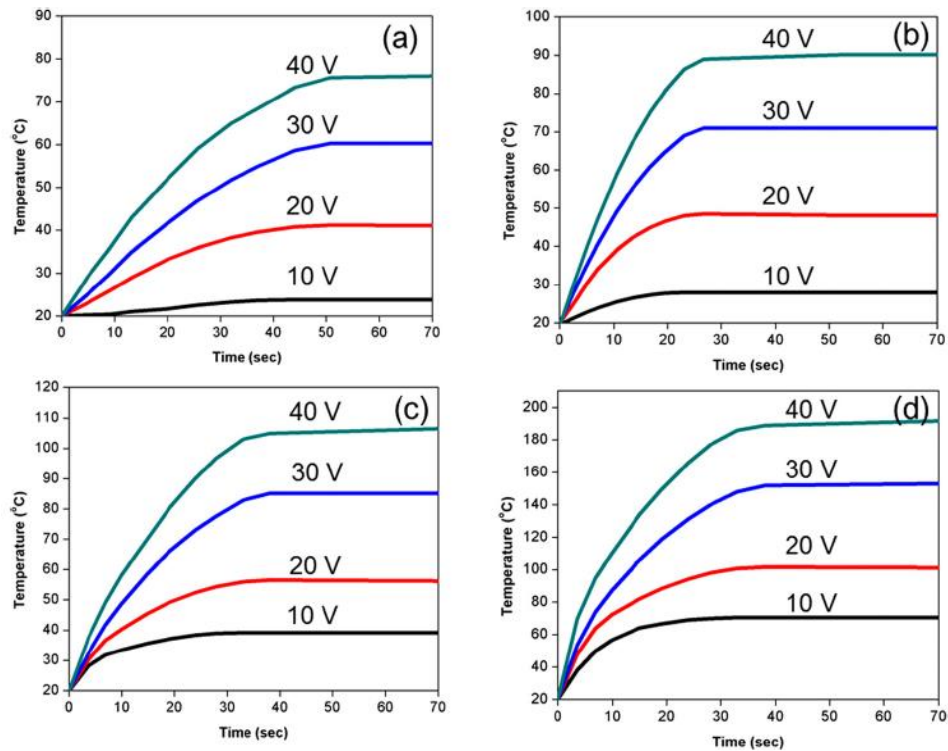


Figure. 2.15: Electro thermal heating performance of MWCNT sheet films on the glass; temperature profiles v/s time with respect to different applied voltages for (a) one layer, (b) double layers, (c) acid treated one layer, and (d) decorated with Ni (Jung et al. 2014).



In Fig. 2.15(c) acid treated sheet showed a higher steady-state temperature than a single-layer and double-layer MWCNT sheet film at a given voltage. The CNT/Ni sheet outperforms both pure CNT sheet and acid treated CNT sheet in terms of heating performance, as shown in Fig. 2.15(d). Heat can be dissipated more effectively by adding metal nanoparticles to MWCNT sheets because metal nanoparticles can produce heat on their surfaces and the individual CNTs become more interconnected as metal nanoparticles are introduced to the MWCNT sheet.

Kang et al. (2011) studied transparent, flexible, high-performance graphene heaters. They fabricated layers of graphene on Cu foils using chemical vapour deposition. The two types of heaters such as graphene treated with various dopants, as well as an ITO-based heater are fabricated and their temperature profile is shown in Fig. 2.16. The heaters were  $4\text{cm} \times 4\text{cm}$  in size. An infrared camera was used to observe the thermal responses of the heaters (Fig. 2.16(a)). They have used a DC power supply to apply 12V to both the graphene heater and the ITO heater, allowing them to monitor the current through the heaters and record their temperatures at regular intervals of three seconds. The time it took for the heater to attain its steady state temperature from the ambient temperature was independent of the heater type. The response time is due to the excess thermal mass, which in this instance is a polyethylene terephthalate (PET) layer enclosing the film heater. Both the ITO- and graphene-based heaters are protected by a PET layer, which serves as a thermal barrier against external conditions. In this experiment, the result shows that graphene heaters doped with  $\text{AuCl}_3$  performed better and reached a steady-state temperature of  $100^\circ\text{C}$  at 12V, while graphene heaters doped with  $\text{HNO}_3$  and ITO heaters only reached  $65^\circ\text{C}$  and  $31.4^\circ\text{C}$  respectively. Based on this comparison, graphene heater performance is significantly influenced by the electrical conductivity of graphene films (Fig. 2.16). Graphene-based heaters outperform traditional transparent ITO heaters, as shown by analyses of temperature profiles and heat distribution as a function of time.

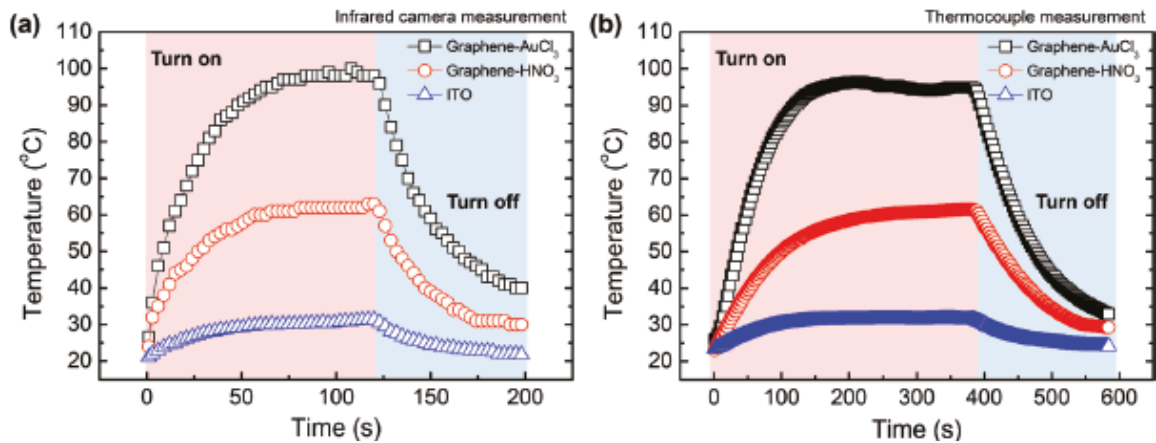


Figure. 2.16: The temperature profiles of Graphene-based heaters with two different doping agents and an ITO-based heater, measured by (a) an infrared camera, and (b) a thermocouple (K-type) (Kang et al. 2011).

In the application fields of photo electricity, where precise temperature control is essential, especially for the integration of microelectronics, the non-contact graphene thin film heater may be an attractive heating material. The non-contact graphene thin film heater has a wide range of applications in the field of optoelectronics. Zhang et al. (2017) fabricated an optically controlled flexible graphene thin film heater using the non-destructive rubbing method. The authors demonstrated the photothermal conversion ability of the heater and stated that the heater not only can preserve high steady-state temperature under low applied laser power, but also fastly change temperature from low to high (or from high to low) by tuning the incident laser power.

Initially, the authors performed the rubbing process with a moderate amount of pressure to get a thin, uniform layer of graphene on the leather. Then the graphene-coated leather was then adhered to the PDMS block by applying pressure. Later the PDMS/graphene/PVA was formed by spin-coating a PVA solution onto the surface and allowing it to dry at 60°C in the air. Finally, PDMS/graphene/PVA was lightly pressed onto the PET substrate for a few minutes. Afterwards, the graphene/PVA/PET flexible sheet was delicately pulled away from the PDMS block. Here the steady-state

temperature of the film is precisely controlled by tuning the laser power. A handheld temperature detector was used to measure the temperature.

Fig. 2.17(a) shows a graph of the steady-state temperature vs time as a function of the laser power applied varied from 50 to 240mW. As can be seen, the steady-state temperature rises with increasing laser power and attains 47.4°C at 240mW laser light illumination, proving that the graphene film heater has an effective capacity for photothermal conversion. In evaluating the ability of film heaters, response time is one of the most important factors. As shown in Fig. 2.17(b), the steady-state temperature is reached after the 70s of laser irradiation at 180mW. In less than the 80s, the temperature of the graphene heaters increased significantly from ambient temperature to steady-state. Due to the increased heat transfer at high temperature, the response time can increase slightly with increasing laser power.

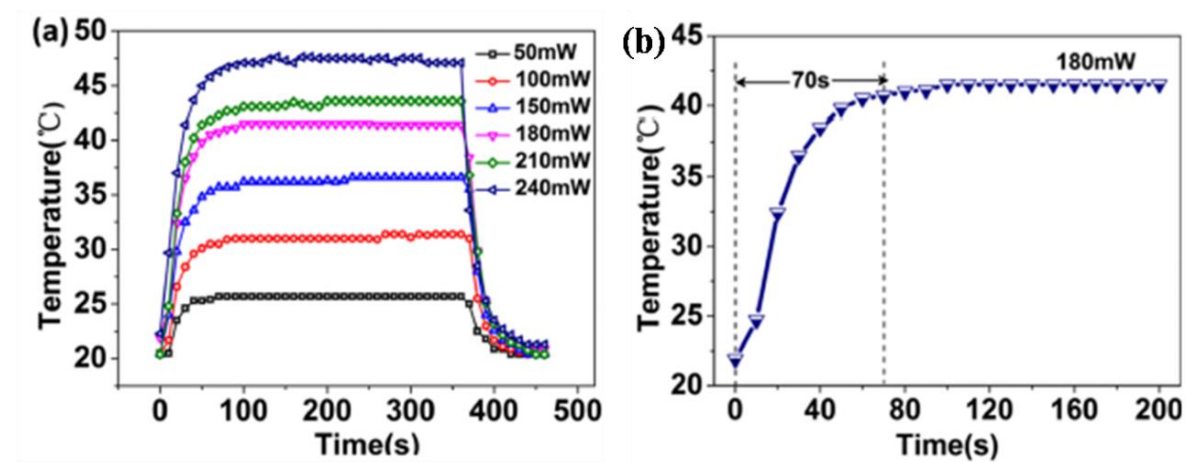


Figure. 2.17: (a) The steady-state temperature of graphene film treated with the infrared laser of varying powers, and (b) The temperature profile of graphene film with 180mW laser power (Zhang et al. 2017).

For a high-performance heater, repeatability is a fundamental need. The authors used ON/OFF cycle testing to evaluate the repeatability of the heater. Fig. 2.18 illustrates the graphene sheet heater stability over a prolonged period. After 10 cycles of turning on and off, the steady-state temperature doesn't change much whether the incident laser power is

100, 180, or 240mW. It was found that a mean temperature of 47.4°C can be maintained for 75 minutes in the presence of a 240mW incident laser power.

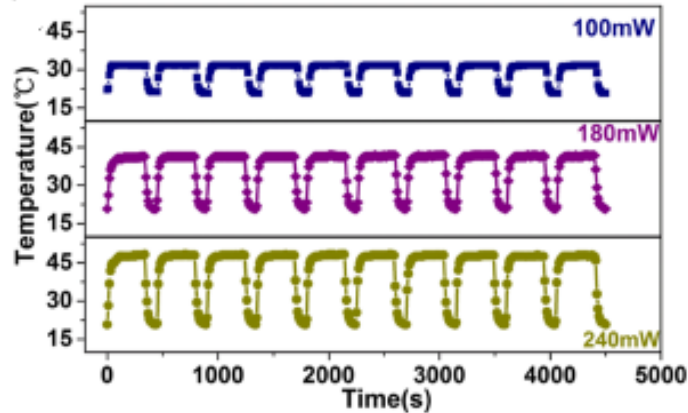


Figure. 2.18: Graphene thin film ON/OFF temperature response at 100, 180, and 240mW (Zhang et al. 2017).

#### 2.4 Research gap from the literature survey

The presently available nanomaterials-based EMI shielding materials, gas sensing materials, and electrothermal heating materials were fabricated with complex and expensive techniques, and also have certain limitations like poor flexibility, costly, and not biodegradable.

In the current existing EMI shielding materials, it is difficult to achieve good shielding efficiency over a wide bandwidth and also present EMI shielding materials having a high thickness. To achieve better EMI shielding efficiency the material should be very thin. In addition, gas sensing materials have less response and it is difficult to accomplish high response for even lower concentration of gas at room temperature. Furthermore, electrothermal heating materials require a high power or voltage to function and it is difficult to attain significant steady-state temperature, as well as better heating and cooling response at low input voltage.

The use of cotton fabric as a substrate would offer a spectrum of advantages. Cotton fabric has become a preferred substrate for electromagnetic interference shielding, gas sensors, and wearable electronic devices. Among the various textile materials studied

thus far, the nanomaterial coated cotton fabric appears to be the most generally preferred material for electronic applications, owing to potential benefits such as lightweight, versatility, low cost, biodegradable, economic processability, and good mechanical and wearable properties, which are currently unavailable in conventional electronic devices. The nanomaterial coated cotton fabric gives good shielding ability over the wide bandwidth, a good response for CO gas at room temperature, and a better electrothermal response at low input voltage.

### **2.5 Objectives of the research work**

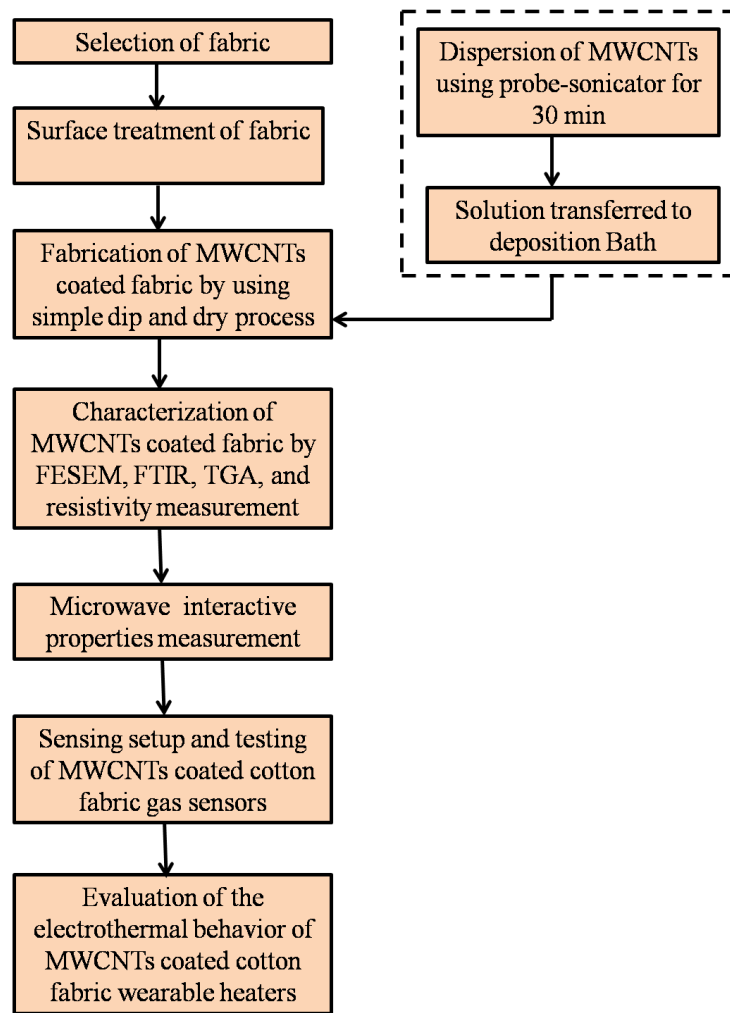
- Fabrication of Cotton fabric with Multi-walled carbon nanotube Coating (CMC).
- Evaluation of microwave interactive properties of fabricated CMC samples.
- Study of Chemical gas sensing behavior of MWCNTs coated cotton fabric.
- Evaluation of electrothermal performances of the CMC samples in terms of applied voltage and heating rate.

## CHAPTER 3

### METHODOLOGY

This chapter summarizes the overview of materials and surface treatment of cotton fabric. In addition, this chapter presents the experimental procedure for the fabrication of CMC samples. Furthermore, details of CMC samples fabricated with different concentration of MWCNTs, and also a detailed description of characterization techniques for fabricated CMC samples.

#### 3.1 Flow chart of the work



## **3.2 Overview of the materials, surface treatment of cotton fabric, and fabrication of CMC samples**

### **3.2.1 Materials**

Plain woven cotton fabric (Thread count 160, areal density 111.00 g/m<sup>2</sup>, and bulk density 0.411 g/cm<sup>3</sup>) was received from the Hi-media Laboratory in Bengaluru, India, and was used as a substrate. Multi-walled carbon nanotubes (length 5-9 μm, diameter 110–200 nm, and purity 90+%) was procured from Sigma Aldrich and used as a coating material. Sodium dodecyl sulfate (SDS) of Sigma Aldrich was used as a surfactant.

### **3.2.2 Fabric surface treatment**

The cotton fabric of 14 cm × 9 cm was soaked for 10 hours in a 10 wt % NaOH solution. The soaked fabric was washed several times to remove any excess amount of NaOH. The cotton fabric is comprised of 88%–97% of cellulose. The remaining constituents are cementing elements such as waxes, proteins, and pectin (Budtova and Navard 2016; Cao et al. 2021; Venkatesha Gupta et al. 2016; Akash et al. 2016). The treatment of cotton fabric with NaOH removes the cementing substances from the cotton fabric surface, resulting in less functional groups and dangling bonds. The treated fabric is dried in the sunlight for one day before being used in the fabrication of MWCNTs coated cotton fabric (Akash et al. 2016; Arun Kumar et al. 2022) and dried treated plain woven cotton fabric is shown in (Fig. 3.1(b)).

### **3.2.3 Fabrication of MWCNTs coated cotton fabric**

The colloidal solution is prepared by mixing MWCNTs and surfactant in 200 ml of deionized water at a ratio of 1:5, respectively. The use of surfactant sodium dodecyl sulfate (SDS) facilitates the improvement of dispersion and deagglomeration of MWCNTs in colloidal solutions, resulting in the formation of suspensions containing MWCNTs. The ability of MWCNTs to interact with water through hydrogen bonding is facilitated by the hydrophilic properties of sodium dodecyl sulfate. SDS decreases the surface tension of water, resulting in a decrease in the energy difference between the interface of MWCNTs and water. This energy reduction facilitates the penetration of

water into the aggregated MWCNT particles, thereby aiding the dispersion process (Orlando et al. 2023). The probe-sonication (30% power of 250 W, on for 10 seconds and off for 10 seconds) is carried out for an hour to properly disperse the MWCNTs in the prepared colloidal solution to achieve homogeneous dispersion and deagglomeration of MWCNTs. The MWCNTs dispersed solution is shown in (Fig. 3.1(a)). Seven CMC samples were developed using the dip and dry process with different concentration of MWCNTs. The samples were marked as CMC 1 to CMC 7 (shown in Table 3.1) corresponding to MWCNTs concentration in the DI water solution as 1, 1.25, 1.5, 1.75, 2, 2.25, and 2.5 mg/ml, respectively. The treated fabric was dip-coated for 10 min in the MWCNTs dispersed solution shown in (Fig. 3.1(c)), followed by drying in a hot air oven for 30 min at 120°C. The dried cotton fabric with multi-walled carbon nanotubes coating (CMC) sample is shown in (Fig. 3.1(d)). The MWCNTs wt% in the cotton fabric was increased by repeated dip and dry process. Similarly, fifty cycles were carried out to improve the continuous network of MWCNTs over the cotton fabric, and the fabrication process was similar for all CMC samples.

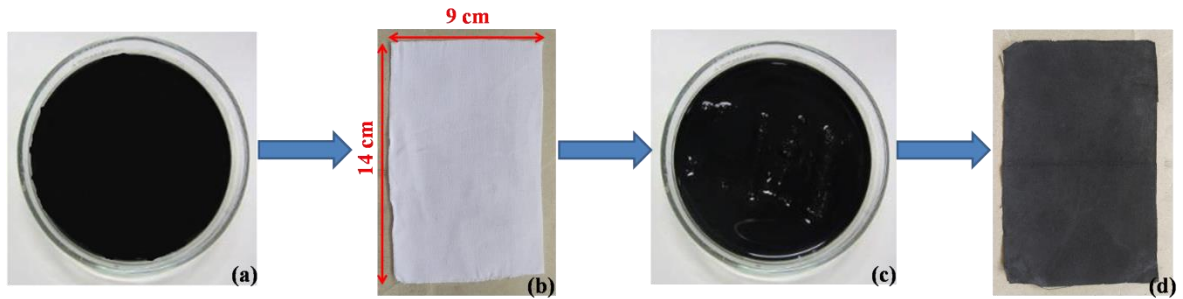


Figure. 3.1: Fabrication of CMC sample using a dip and dry process: (a) Dispersed MWCNTs in DI water, (b) NaOH treated plain woven cotton fabric, (c) Cotton fabric dipped inside the MWCNTs dispersed solution (during 1<sup>st</sup> cycle of dipping), and (d) Dried cotton fabric with multi-walled carbon nanotube coating (CMC) sample (after 50 cycles of dip and dry process).

The thickness of samples were measured by a digital micrometer (Mitutoyo, Model No. MDC-25SX) with an accuracy of 1  $\mu$ m. We have taken 30 measurements at different



areas of the fabric and the average value is considered for the study. The areal and bulk density of the cotton fabric and CMC samples has been calculated to determine the porosity. According to the ASTM D3776/D3776M-20 specification (American Society for Testing & Mater 1985), we have determined the areal density (weight of sample divided by unit area of the sample) and bulk density (weight of sample divided by unit volume of sample) of cotton fabric and CMC samples. Porosity provides the presence of micropores in the structure and is defined as the ratio of the voids volume to the volume of the sample (Mao and Russell 2015). The porosity is calculated as follows using the fabric bulk density and the fiber density (Hsieh 1995; Stankovic et al. 2009).

$$P (\%) = \left(1 - \frac{\rho_{\text{fabric}}}{\rho_{\text{fiber}}}\right) \times 100 \quad (3.1)$$

where P is the fabric porosity (%),  $\rho_{\text{fabric}}$  ( $\text{g}/\text{cm}^3$ ) is the fabric bulk density, and  $\rho_{\text{fiber}}$  ( $\text{g}/\text{cm}^3$ ) is the fiber density. Porosity decreases as increasing the MWCNTs concentration in the cotton fabric (shown in Table 3.1).

Table 3.1: Details of the cotton fabric with different concentration of MWCNTs coating.

<b>Sample name</b>	<b>Cotton fabric dipped in MWCNTs concentration (mg/ml)</b>	<b>Weight of the sample (g)</b>	<b>Thickness of the sample (mm)</b>	<b>Standard deviation: Thickness</b>	<b>Areal Density (<math>\text{g}/\text{m}^2</math>)</b>	<b>Bulk Density (<math>\text{g}/\text{cm}^3</math>)</b>	<b>Porosity (%)</b>
Cotton fabric	NA	1.40	0.270	0.008	111.00	0.411	73.3
CMC 1	1	1.732	0.283	0.01	137.53	0.485	68.5
CMC 2	1.25	1.803	0.284	0.007	140.12	0.493	67.9
CMC 3	1.5	1.843	0.294	0.007	146.27	0.497	67.7
CMC 4	1.75	2.047	0.300	0.009	162.53	0.541	64.8
CMC 5	2	2.094	0.302	0.009	166.26	0.550	64.2
CMC 6	2.25	2.298	0.335	0.018	185.00	0.552	64.1
CMC 7	2.5	2.670	0.382	0.019	211.90	0.554	64.0

### 3.3 Characterization of the multi-walled carbon nanotube coated cotton fabric

#### 3.3.1 FESEM study

The morphology of the CMC marked samples was studied using the field emission scanning electron microscopy (FESEM) (Carl Zeiss AG, Model No. Gemini SEM 300, GERMANY) as shown in Fig. 3.2, and energy dispersive X-ray spectroscopy (EDS) was used to determine the elemental composition of CMC samples.

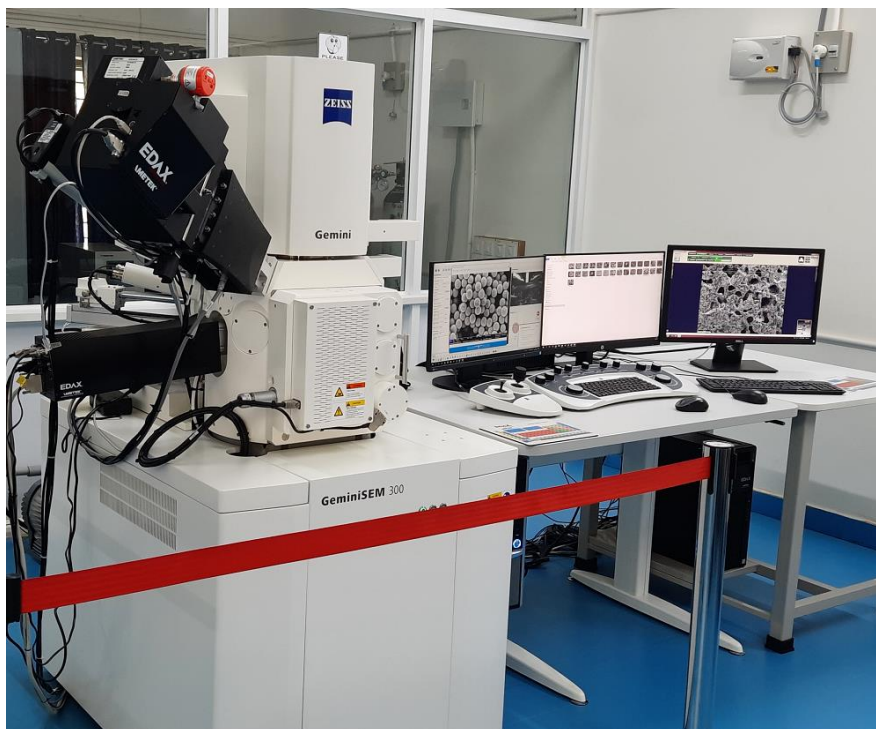


Figure. 3.2: FESEM interfaced with a computer.

#### 3.3.2 FTIR study

The Fourier transform infrared (FTIR) spectroscopy (FTIR-4200, JASCO, Japan) shown in Fig. 3.3 was carried out in the wave number range of  $600\text{ cm}^{-1}$  to  $4000\text{ cm}^{-1}$  (ATR mode), with a resolution of  $4\text{ cm}^{-1}$ . It provides information about the functional groups present in the CMC sample and confirms the adhesion of MWCNTs to the cotton fabric surface.



Figure. 3.3: Fourier transform infrared (FTIR) spectroscopy.

### 3.3.3 Thermogravimetric analysis (TGA)

The TGA (Seiko Exstar, TG-DTA 6300) as shown in Fig. 3.4 was used to determine the MWCNTs wt% in the CMC samples and it shows the thermal degradation of materials that occurs at a particular temperature range.



Figure. 3.4: TGA instrument.

### 3.3.4 Resistivity measurement

The bulk and surface resistivity of CMC samples with a size of 14 cm x 9 cm was measured using a four-probe method (SES Instrument Private Ltd., Roorkee). A Keithley 2400 source measurement unit is used to measure the current (I)-voltage (V) characteristics. The four-probe measurement setup is shown in Fig. 3.5. In order to measure the bulk and surface resistivity of the CMC samples, we applied a voltage of 0-5 V. The average of ten readings on each sample was used to calculate the resistivity.

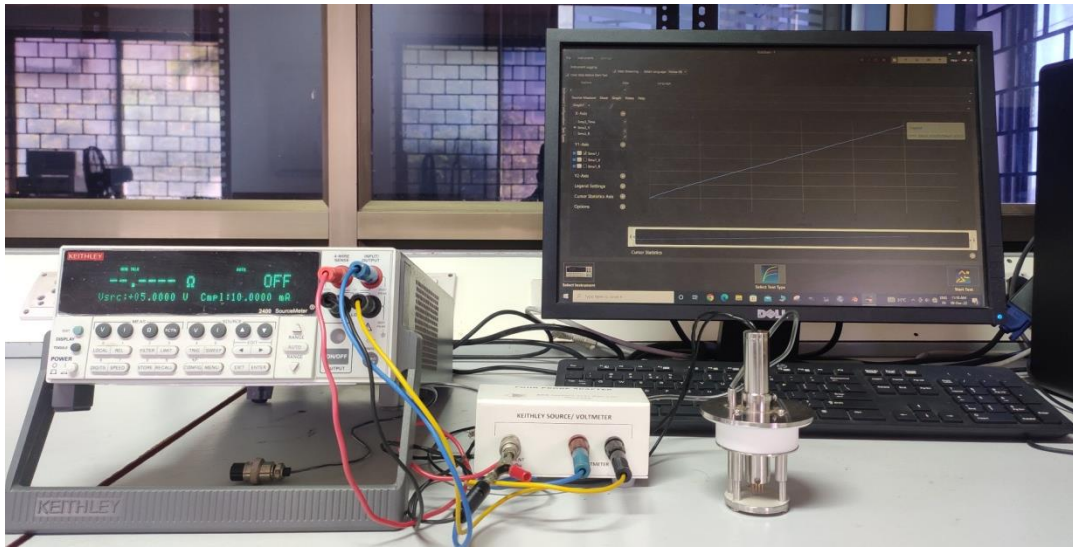


Figure. 3.5: Four-probe measurement setup.

### 3.3.5 Microwave properties measurement

The properties such as permittivity, transmission, reflection, and absorption were measured at the microwave frequency range (X- and Ku- band) by a performance network analyzer (PNA) (Model No. N5224B), and the test sample arrangement is shown in Fig. 3.6. It consists of two antennas (transmitter and receiver) and a waveguide along with the sample holder. The Scattering parameters such as S11 and S21 were measured from the power incident and power received at the horns. Parameter S11 measures the reflecting behavior of the surface, while parameter S21 measures the propagation behavior through the material.

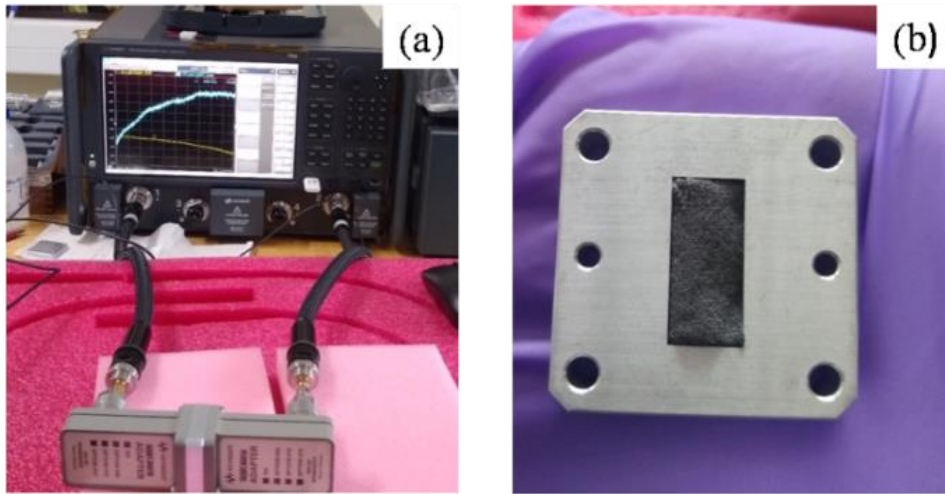


Figure. 3.6: (a) PNA-x flexible network analyzer system (Model No: N5224B), and (b) Waveguide along with the sample holder.

### 3.3.6 Sensing setup and testing of MWCNTs coated cotton fabric gas sensors

The gas sensing setup (SCITRON (IEE), India) as shown in Fig. 3.7 was used to study the gas sensing behavior of all fabricated CMC sensors. A schematic illustration of the gas sensing measurement setup is depicted in Fig. 3.8. The sensing setup consists of a mass flow controller (MFC), an air-sealed glass chamber, a Keithley source measuring unit (model no. 2400), and a USB interfaced with the computer. A mass flow controller (MFC) controls the flow of gases such as air and CO into the gas sensing cell. The gas sensing cell outlet is attached to an exhaust pipe. The sensor was placed inside an air-sealed glass chamber on the sample holder, the silver electrode was deposited on either side of the sensor, and contact was taken using a metallic probe. The metallic probe is connected with the Keithley source measuring unit to measure the electrical signal.

Prior to gas sensing, the gas sensing chamber is purged with an air flow of 5 liters per minute (lpm) for 10-15 minutes in order to stabilize their resistance. The CMC sensor of size 2 cm  $\times$  0.5 cm was exposed to the lowest carbon monoxide (CO) gas concentration at room temperature to study their responding behavior. During an experiment, the CO gas channel is switched ON for 3 minutes once the resistance of the sensor has been stabilized and the total gas flow remains at 5 lpm. Following 3 minutes





Figure. 3.7: Gas sensing setup.

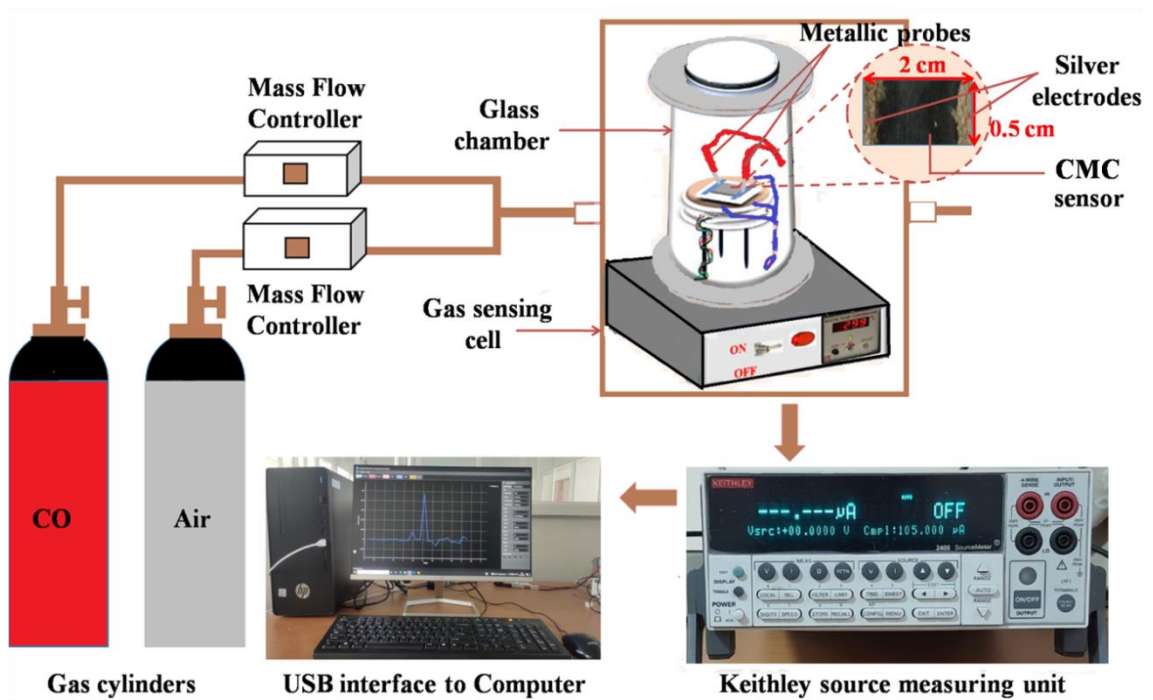


Figure. 3.8: Schematic diagram of gas sensing measurement system and a photograph of CMC sensor placed inside the glass chamber.

of exposure to CO, the CO channel is turned OFF for 5 minutes for the desorption of CO, and for the different CO gas concentrations, the same steps were followed. As part of each testing cycle, CO gas is exposed and released from the test chamber.

### 3.3.7 Testing of electro-thermal heating behavior of CMC wearable heaters

The testing of CMC samples for wearable heating applications using the two-terminal side contact setup is schematically shown in Fig. 3.9(a). We developed the heater to demonstrate the potential of CMC samples for heating applications and the image is shown in Fig. 3.9(b). The heating performance of CMC samples were studied by evaluating the temperature change at the surface of the heater, as a function of time with the help of a thermocouple and a DC power supply (At various voltages, the performance of the electrothermal heating behavior of CMC samples were examined). The CMC samples were tested for their steady-state temperature as well as their faster heating and cooling response for wearable heating applications.

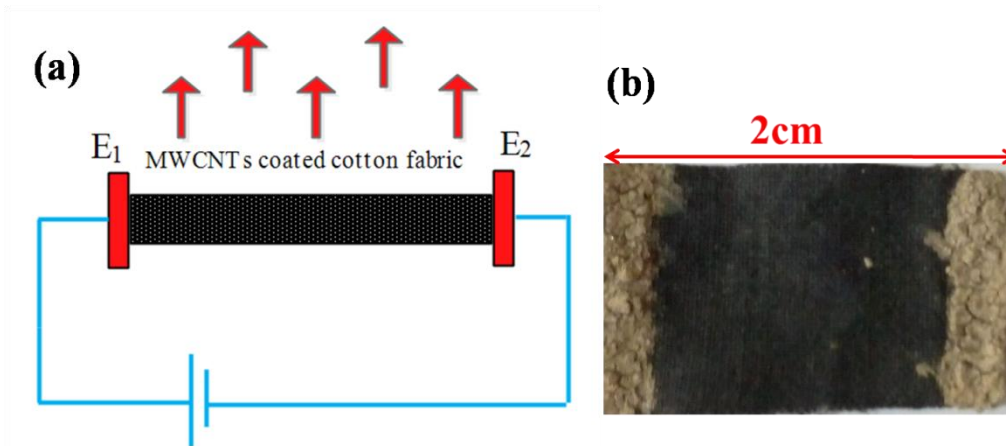


Figure. 3.9: (a) Schematic diagram of the two-terminal side contact setup for testing the electrothermal heating behavior of CMC samples, and (b) image of the heater.

## CHAPTER 4

### RESULTS AND DISCUSSION

This chapter illustrated the characterization studies of fabricated cotton fabric with multi-walled carbon nanotube coating (CMC) samples through FESEM, FTIR, TGA, and resistivity measurement. Moreover, the evaluation of microwave interactive properties and EMI shielding effectiveness of fabricated CMC samples in the frequency range of X- and Ku-band using a performance network analyzer (PNA). Then, the comparison between microwave interactive properties of carbon composites in the literature and CMC samples of this work. Furthermore, testing of CMC sensors for different concentrations of CO gas ranging from 25 to 100 ppm using a gas sensing setup. Finally, testing of electrothermal heating behavior of CMC samples.

#### 4.1 FESEM and FTIR analysis of fabricated CMC samples

The morphology of cotton fabric with multi-walled carbon nanotube coating (CMC) samples were studied using field emission scanning electron microscopy (FESEM). The FESEM micrograph of the cotton fabric shown in Fig. 4.1(a) confirms the interwoven structure of the fabric. The FESEM image of the CMC sample is shown in Fig. 4.1(b), it confirms that MWCNTs are uniformly coated on the cotton fabric surface. Fig. 4.1(c) & (d) shows the MWCNTs coated cotton fabric at low and high magnification respectively. It was observed that there is a well interconnected continuous network of MWCNTs in the CMC sample. The diameter of the MWCNTs was in the range of 140–232 nm. The FESEM images of the CMC confirmed that the surface of the cotton fabric was well covered and coated with MWCNTs. The coating composition is characterized by energy dispersive spectroscopy (EDS) as shown in Fig. 4.1(e). The pi-chart in Fig. 4.1(e) depicts the content of the different elements present in the coating on the CMC surface. It was found that 94.43% carbon (C) was present and the remaining sodium (Na), sulfur (S), and oxygen (O) compounds of total 5.57% deriving from the surfactant sodium dodecyl sulfate (SDS).



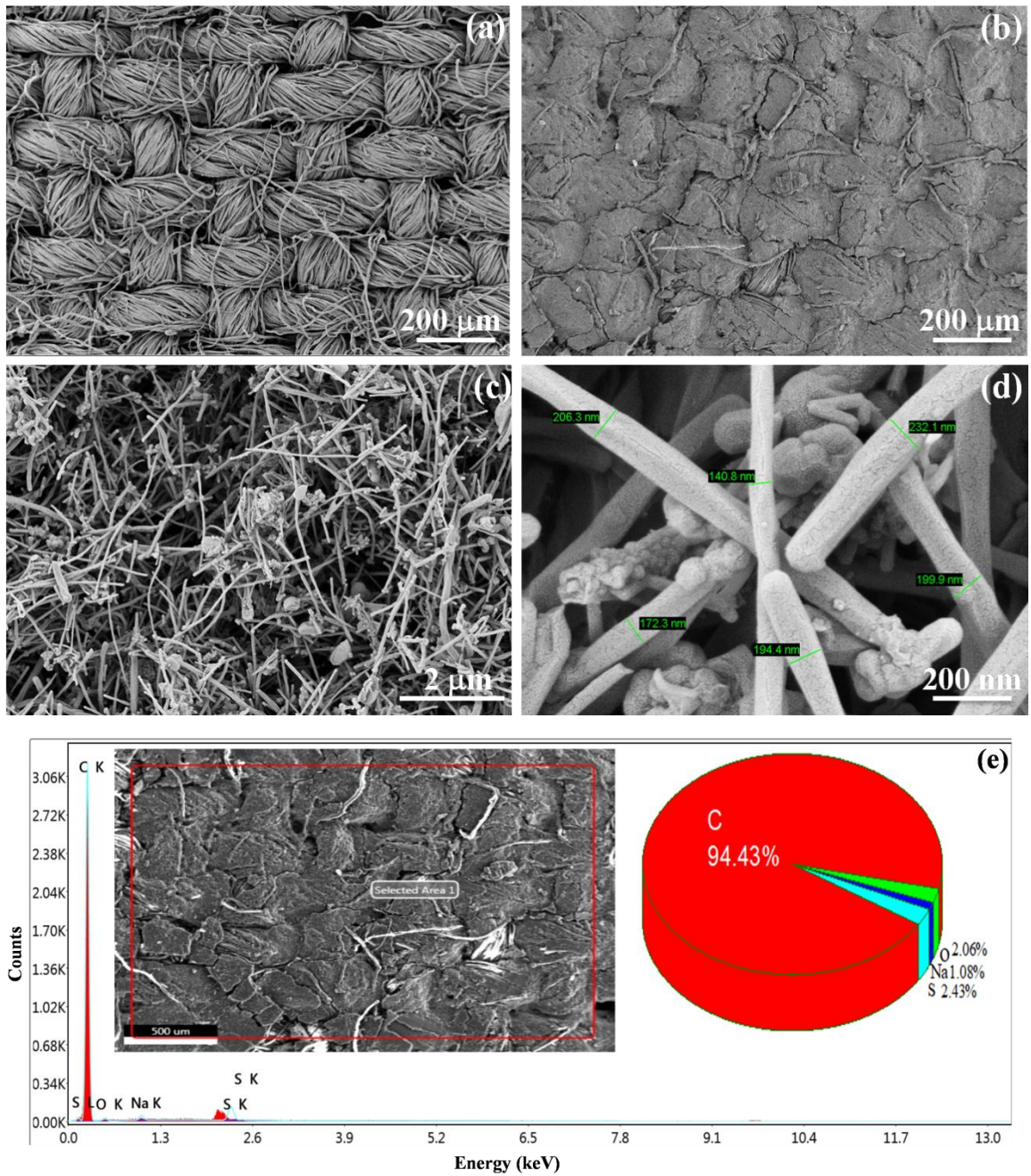


Figure. 4.1: FESEM images: (a) Cotton fabric, (b) Cotton fabric with multi-walled carbon nanotube coating (CMC6 sample), (c) FESEM at low magnification of the MWCNTs coated cotton fabric, (d) FESEM at high magnification of the MWCNTs coated cotton fabric, and (e) EDS spectrum of CMC sample.

The FESEM images of cotton fabric with different concentration of MWCNTs (CMC 1 to CMC 7) are shown in Fig. 4.2(a)-(g). In Fig. 4.2(a) and (b) the density of MWCNTs is poor and MWCNTs is not uniformly coated on the surface of the cotton fabric due to very less concentration of MWCNTs. In Fig. 4.2(c) & (d) the density of MWCNTs is improved compared to Fig. 4.2(a) & (b). Whereas in Fig. 4.2(e) & (f) the network of MWCNTs are more denser, and MWCNTs is uniformly coated on the surface of the cotton fabric compared to Fig. 4.2(a)-(d) due to increased concentration of MWCNTs.

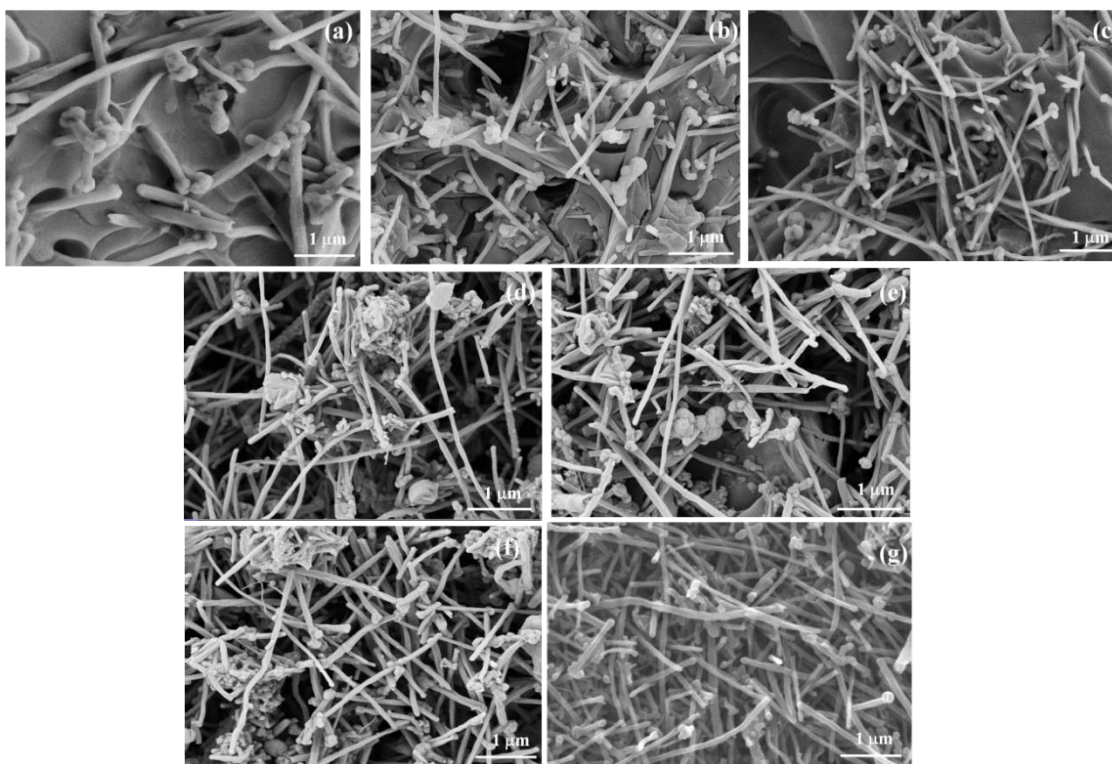


Figure. 4.2: The FESEM images of cotton fabric coated with multi-walled carbon nanotubes: (a) CMC 1 (1 mg/ml), (b) CMC 2 (1.25 mg/ml), (c) CMC 3 (1.5 mg/ml), (d) CMC 4 (1.75 mg/ml), (e) CMC 5 (2 mg/ml), (f) CMC 6 (2.25 mg/ml), and (g) CMC 7 (2.5 mg/ml).

It is observed that the 2D-density of MWCNTs increases as the concentration of MWCNTs dispersed in a solvent increases from 1 mg/ml (CMC 1) to 2.5 mg/ml (CMC 7). In Fig. 4.2(g) the density of MWCNTs is more prominent and the MWCNTs structure

was found to be well interconnected in a continuous and spatially uniform manner over a large area because of the high concentration and proper dispersion of MWCNTs.

Fig. 4.3 shows the Fourier transform infrared (FTIR) spectroscopy of cotton fabric and MWCNTs coated cotton fabric. The FTIR spectra of cotton fabric show vibrational modes in the region of 800 to 1,500  $\text{cm}^{-1}$  associated with C-O stretching and C=O stretching (Krishnamoorthy et al. 2012; Portella et al. 2016). Whereas hydro carboxyl (HO-C=O) peaks are visible in the region of 2900 to 4000  $\text{cm}^{-1}$ . In MWCNT, functional groups like carbonyl and hydroxyl are present, which makes it hydrophilic (Ravindren et al. 2019; Yu et al. 2019). In addition to being hydrophilic, MWCNTs possess a large adsorption surface area, which makes them highly adherent to the surface of the cotton fabric during the dipping process.

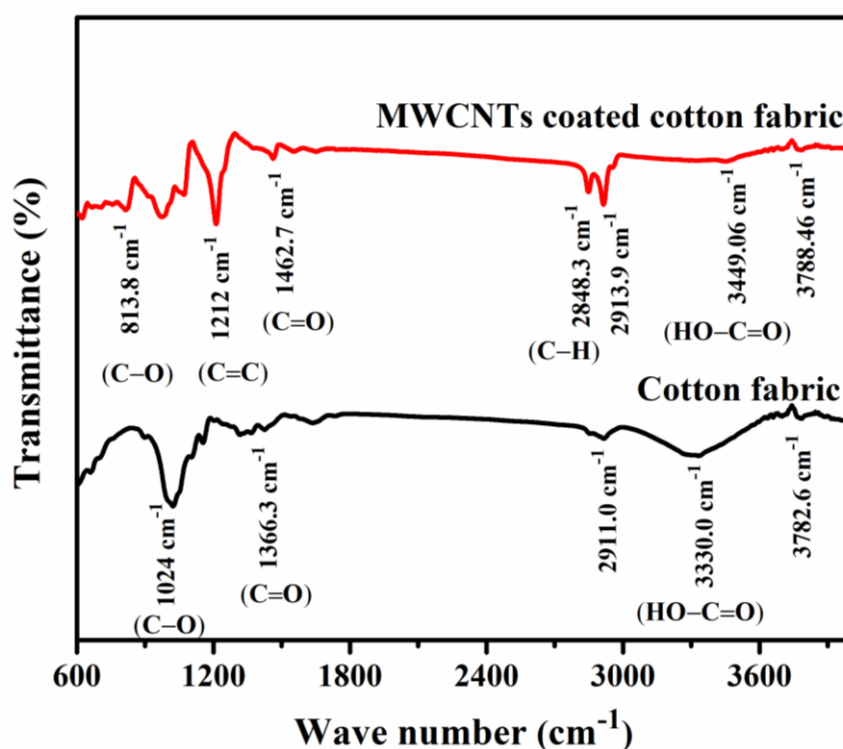


Figure. 4.3: FTIR spectra of cotton fabric and MWCNTs coated cotton fabric.

As in Fig. 4.3 MWCNTs coated cotton fabric shows significant differences in FTIR spectra compared to cotton fabric. FTIR result of the CMC sample shows the bonding of

MWCNT to the cotton fabric, as evidenced by the significant stretching mode of C=C at  $1212\text{ cm}^{-1}$ . This confirms the strong adhesion of MWCNTs to the cotton fabric surface. Due to the MWCNTs being bonded to the cotton fabric, the peak of normal carbonyl (C=O) which appeared in the cotton fabric at  $1366.3\text{ cm}^{-1}$  shifts to the higher wave number at  $1462.7\text{ cm}^{-1}$  in CMC sample (Krishnamoorthy et al. 2012). There is a new peak in the CMC sample at  $2848.3\text{ cm}^{-1}$  due to C-H stretching vibrations that are formed by binding the C-H group from the MWCNT to the cotton fabric (Krishnamoorthy et al. 2012).

#### **4.2 Thermogravimetric analysis**

Thermogravimetric analysis (TGA) was used to find out the MWCNTs wt% in the CMC samples at a heating rate of  $10^{\circ}\text{C}/\text{min}$  under air with a temperature range of up to  $600^{\circ}\text{C}$  (Said et al. 2021; Li et al. 2015; Liu et al. 2013; Rahman and Mieno 2015). The thermograph of the cotton fabric and CMC 6 sample are shown in Fig. 4.4(a). It shows that the thermal degradation of cotton fabric occurs through the multistep process. In the first step, there is only a small loss of weight below  $150^{\circ}\text{C}$  due to the physically adsorbed water being released. The second step occurs between  $300^{\circ}\text{C}$  and  $400^{\circ}\text{C}$ , which is mainly due to the dehydration of cellulose in the cotton fabric, and the third step takes place between  $400^{\circ}\text{C}$  and  $475^{\circ}\text{C}$  due to complete oxidative degradation of the char produced in the first step (Liu et al. 2013; Rahman and Mieno 2015). As observed, the temperature at 5 wt% weight loss ( $T_{5\%}$ ) of plain-woven cotton fabric was  $240^{\circ}\text{C}$  (Liu et al. 2013), and the char residue was found to be 1.84% at  $450^{\circ}\text{C}$  as shown in Fig. 4.4(a). In the CMC 6 sample, the  $T_{5\%}$  was  $200^{\circ}\text{C}$ , and the char residue (Said et al. 2021) increased to 17.63 wt% after the complete decomposition of the cotton fabric at  $400^{\circ}\text{C}$  as shown in Fig. 4.4(a). Therefore, the MWCNTs wt% in the CMC 6 sample is 15.79 wt%. In Fig. 4.4(a), the CMC 6 sample shows 10% more combustion after the first stage and a  $60^{\circ}\text{C}$  lag in the final combustion temperature. This is mainly because of the high thermal conductivity of the MWCNTs, which absorbed heat at a faster rate and transferred it to the cotton fabric (Henry Kuo Feng Cheng, 1, et al. 2011; Zhou et al. 2010; Lin et al. 2018; and Chao et al. 2019). The MWCNTs weight percentage increased from 5.96 wt% to 22.23 wt% with the



increase of MWCNTs concentration from 1 to 2.5 mg/ml in the DI water for samples CMC 1 to CMC 7 as shown in Fig. 4.4(b) and listed in Table 4.1.

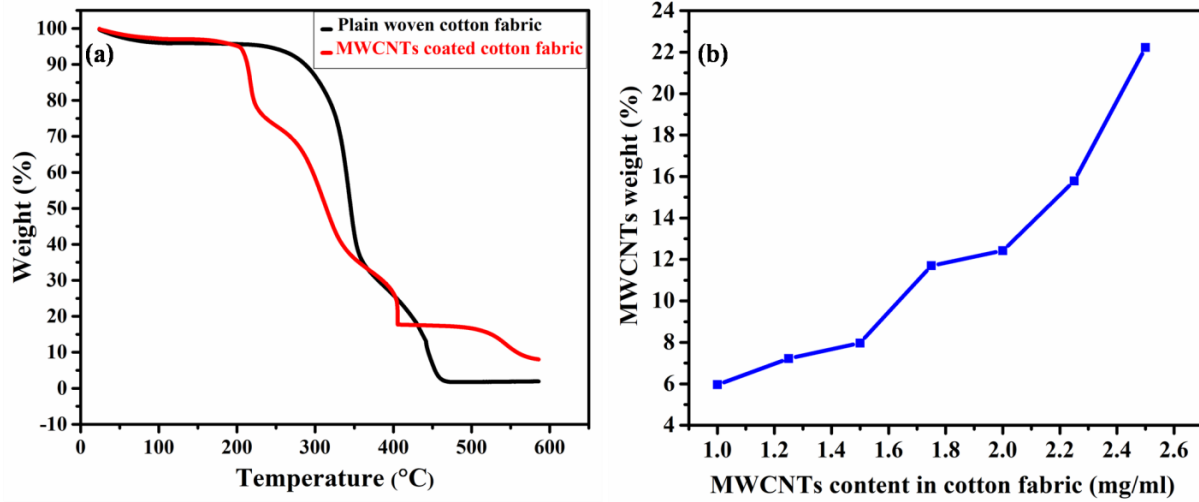


Figure. 4.4: (a) TGA curve of plain-woven cotton fabric and MWCNTs coated cotton fabric (CMC 6 sample), and (b) MWCNTs weight percentage (wt%) in CMC samples.

Table 4.1. MWCNTs wt% in CMC samples

Sample name	CMC 1	CMC 2	CMC 3	CMC 4	CMC 5	CMC 6	CMC 7
MWCNTs concentration (mg/ml)	1	1.25	1.5	1.75	2	2.25	2.5
MWCNTs wt%	5.96	7.22	7.97	11.7	12.42	15.79	22.23

### 4.3. Bulk and surface resistivity of CMC samples

The bulk resistivity ( $\Omega\cdot m$ ) is the product of bulk resistance and the area of the measuring electrode divided by the fabric thickness. Surface resistivity is defined as the ratio of DC voltage (V) drop per unit length on the surface of the CMC sample to surface current ( $I_s$ ) per unit width (D) [ $\rho_s = (V/L) / (I_s/D)$ ] (Ghorbani and Taherian 2018; Gupta et al. 2013). The bulk resistivity and surface resistivity of the CMC samples was measured after each

dip and dry process and it was found that the bulk and surface resistivity decreased with the increase in the number of dip coating in the MWCNTs dispersed solution as shown in Fig. 4.5(a) & (b) for sample CMC 3. This confirms the dip and dry process each time, which makes the continuous network of MWCNTs in the entire fabric area, and as a result, a better interconnection between two conducting MWCNTs is achieved which is also seen in the FESEM image of Fig. 4.2(g). The bulk resistivity and surface resistivity of the CMC sample decreases from 68.44  $\Omega$ -m to 0.042  $\Omega$ -m and 35710  $\Omega$ /sq to 128.5  $\Omega$ /sq respectively, with the increase in MWCNTs wt% as shown in Fig. 4.6(a) & (b). For CMC 1 and CMC 2 samples, the bulk resistivity and surface resistivity decreased moderately from 68.44  $\Omega$ -m to 30.23  $\Omega$ -m and 35710  $\Omega$ /sq to 16069.5  $\Omega$ /sq respectively, due to the low MWCNTs wt% in the CMC sample and poor interconnection between the MWCNTs.

In CMC 3 sample, as the MWCNTs reaches 7.97 wt%, the bulk resistivity and surface resistivity drastically decreased to 0.691  $\Omega$ -m and 2142.6  $\Omega$ /sq, respectively compared to CMC 1 and CMC 2. Since a sufficient amount of MWCNTs is available for the interconnectivity makes the CMC 3 sample has better electrical conducting in terms of good microwave reflecting properties.

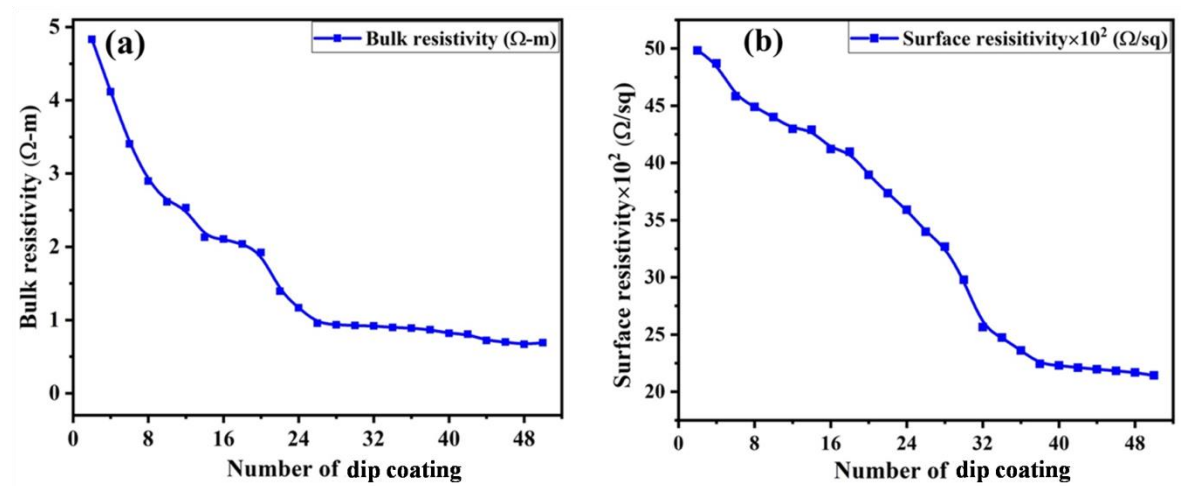


Figure. 4.5: Changes in the resistivity of CMC 3 (7.97 wt%) sample with respect to the number of dip coating: (a) Bulk resistivity, and (b) Surface resistivity.

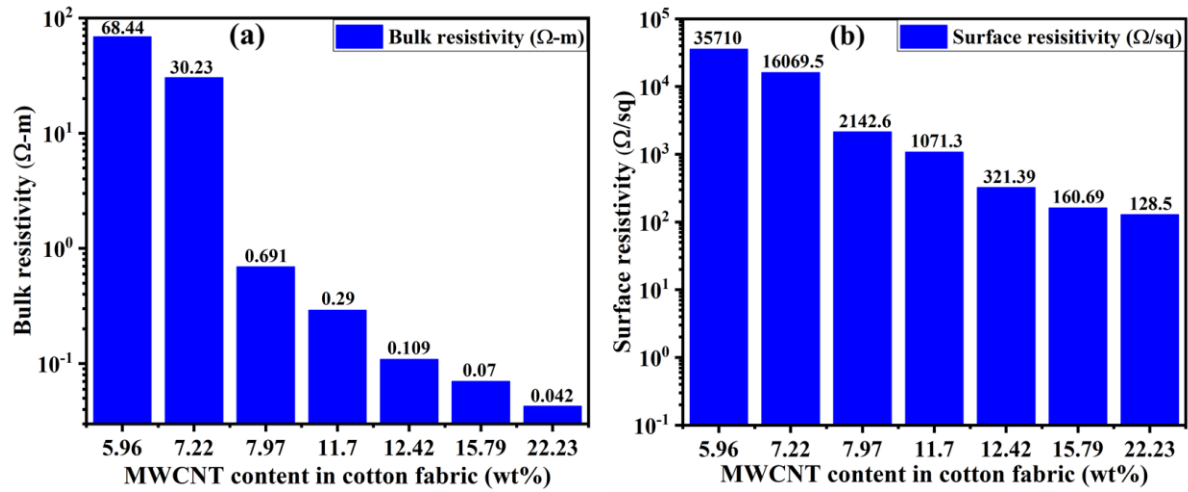


Figure. 4.6: The resistivity of CMC 1 (5.96 wt%) to CMC 7 (22.23 wt%): (a) Bulk resistivity, and (b) Surface resistivity.

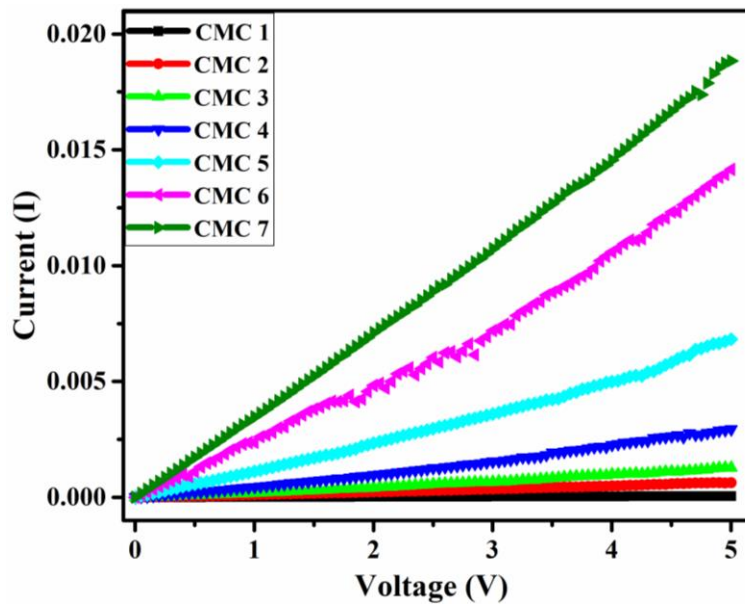


Figure. 4.7: The current(I)-voltage(V) characteristics of CMC samples.

Fig. 4.7 shows the I–V curves of the fabricated MWCNTs coated cotton fabric samples. Throughout the samples, the current increases linearly with voltage for a fixed wt% of MWCNTs. As shown in Fig. 4.7, the current in the CMC samples increases with an increase in the wt% of coated MWCNTs due to a decrease in the resistivity of the CMC

samples. This is because the coated MWCNTs on cotton fabric are well interconnected.

Table 4.2: Electrical conductivity of MWCNT and CMC samples.

<b>Sample name</b>	<b>Electrical conductivity of MWCNT (s/m)</b>	<b>Electrical conductivity of CMC (s/m)</b>
<b>CMC 1</b>	630.80	0.0146
<b>CMC 2</b>	683.52	0.033
<b>CMC 3</b>	709.62	1.445
<b>CMC 4</b>	780.39	3.438
<b>CMC 5</b>	816.99	9.165
<b>CMC 6</b>	894.45	14.27
<b>CMC 7</b>	952.38	23.45

The electrical conductivity of MWCNT and CMC samples were shown in Table 4.2. The electrical conductivity increases from CMC 1 to CMC 7 with respect to the increase in MWCNTs wt%.

#### **4.4. Properties measured at the microwave frequency range**

##### **4.4.1 Permittivity**

Permittivity is the ability of a substance to store electrical energy and measure energy loss ( $\epsilon'$  and  $\epsilon''$ ). Polar materials possess more permittivity than non-polar materials. Due to electric and magnetic dipoles, the wave spreads in the material and its energy is converted into heat (Kim et al. 2003). If the surface resistivity decreases, both permittivity and reflectivity increase, then the material becomes more reflective. The permittivity (real and imaginary) values of the CMC samples are shown in Fig. 4.8. The permittivity was measured using the S-parameters by the in-built algorithm in the performance network analyzer in the frequency range of X- band (8-12 GHz) and Ku-band (12-18 GHz). It has been noted that the permittivity (real and imaginary) values increased as the MWCNTs wt% was increased from 5.96 wt% (CMC 1) to 22.23 wt% (CMC 7) in the X- and Ku- band. The permittivity values of all the CMC samples are reported in Table 4.3. It was evident that when the permittivity increases from sample CMC 1 to CMC 7 in both the X- and Ku- band, indicates that the reflectivity of the CMC



samples increases along with the increase in the MWCNTs wt%. If the  $\tan \delta$  increases, then the absorption increases (Wang et al. 2019). It should be noted that the  $\tan \delta$  is a low value ( $< 0.01$ ) for a lossless perfect dielectric material. For lossy materials, the  $\tan \delta$  should be greater than 0.1. Fig. 4.9 illustrates the CMC samples  $\tan \delta$  values in the X- and Ku-band frequency range. Table 4.3 reports the  $\tan \delta$  values of all the CMC samples. It was observed that the  $\tan \delta$  values of all the CMC samples are greater than 0.1, and the values increase as the MWCNTs wt% increases and it is highest for sample CMC 7, which means that the absorption of the CMC samples will increase as the MWCNTs wt% increases. The absorption of electromagnetic energy is due to the high dissipation factor or  $\tan \delta$  and absorbed energy is converted into heat energy (Wang et al. 2019); (Cao et al. 2018) (Shu et al. 2020).

A conductive network of MWCNTs has been formed across the volume of the CMC sample. This network of MWCNTs is purely due to the high aspect ratio of MWCNTs, and the bond formation between the MWCNTs and cotton fabric as shown in Fig. 4.3. As the electromagnetic wave interacts with the conductive network of the MWCNTs, the conductive electron can hop over one network to another network as a result, the absorption of the electromagnetic wave takes place in the CMC sample. As the MWCNTs wt% increases in the CMC sample, a better network formation occurs across the volume of the CMC sample and better EM absorption was observed in the CMC sample (Cao et al. 2018). The synergy of  $\tan \delta$  allows for precise tuning of EM parameters, impedance matching, and optimizing EM efficiency. Especially, the functional bandwidth is broadened (Shu et al. 2020). The  $\tan \delta$  value will be high for good EMI shielding materials so that the EM energy is converted into the form of heat energy and this contributes to better attenuation of electromagnetic waves. The highest  $\tan \delta$  value of 3.27 is obtained for CMC 7 which is higher than the other epoxy composites with MWCNT and Graphene fillers (shown in Table. 4.3).

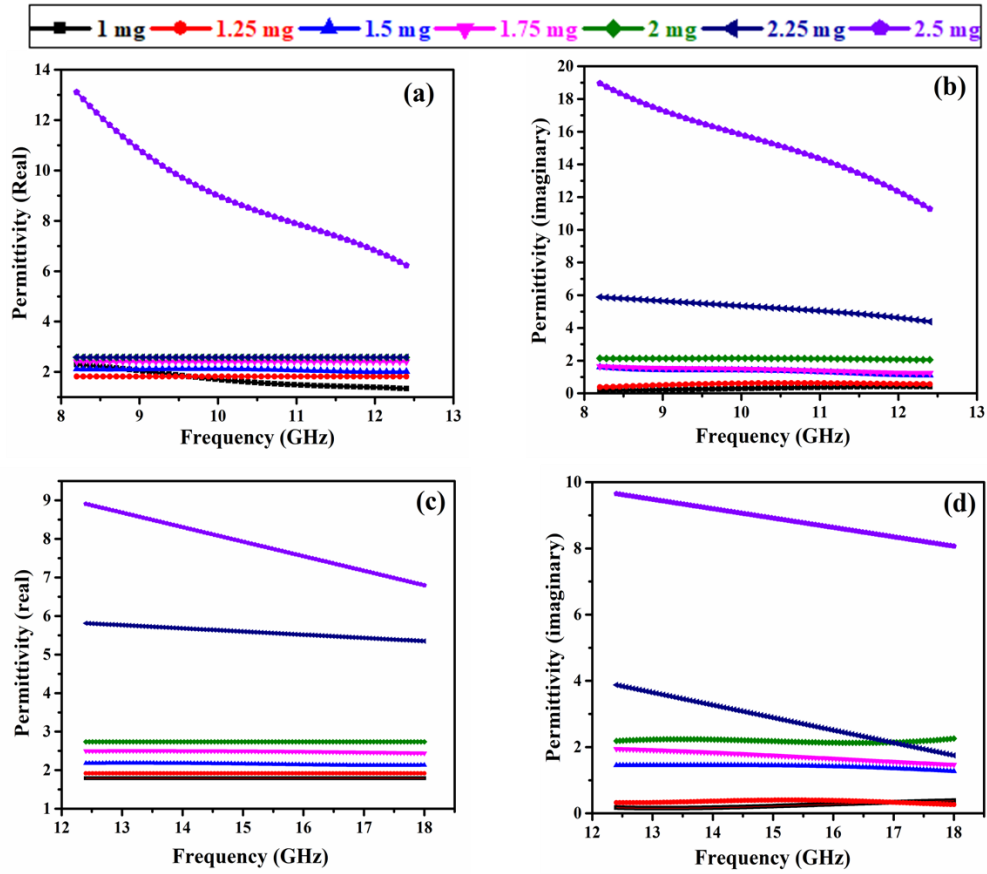


Figure. 4.8: The permittivity v/s frequency for real (a) and imaginary part (b) of CMC samples in the X band, and for real (c) and imaginary part (d) in the Ku band.

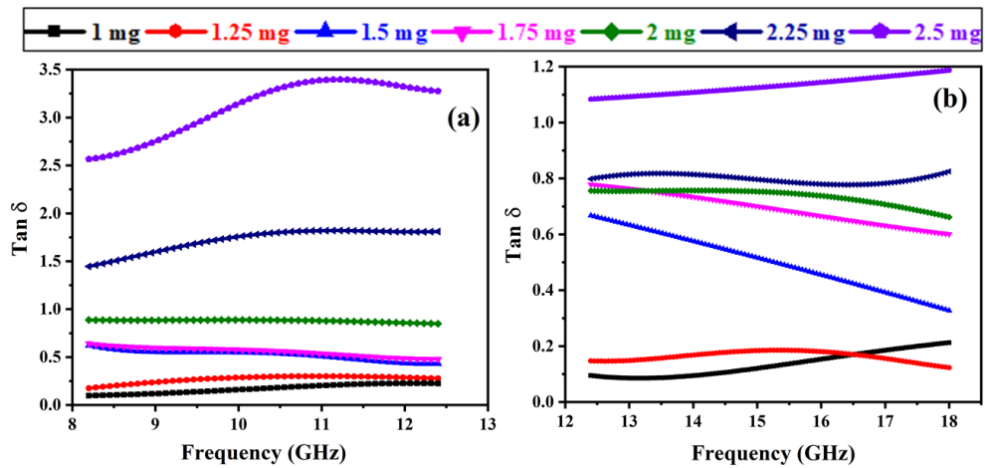


Figure. 4.9:  $\tan \delta$  of CMC samples in the X band (a) and Ku band (b).

#### 4.4.2 Reflection, transmission, and absorption properties

The reflection, transmission, and absorption behavior of the developed samples were studied with the help of the S-parameters in the X- band (8-12 GHz) and Ku- band (12-18 GHz) using the PNA-x microwave measurement system (Fig. 3.6). Fig. 4.10(a)-(e) & Fig. 4.11(a)-(e) represents the S21 parameter, S11 parameter, transmission, reflection, and absorption in X- and Ku- band for all CMC samples respectively. The S21 parameter decreases from sample CMC 1 to CMC 7 and the S11 parameter increases from sample CMC 1 to CMC 7 in both X- and Ku- band respectively. The average S21 and S11 parameter values of all the CMC samples are shown in Table. 4.3. The percentage transmission and reflection were calculated with the help of the S21 and S11 parameters by the following formula: % Transmission =  $10^{(-S21 \text{ parameter} / 10)} \times 100$ , % Reflection =  $10^{(-S11 \text{ parameter} / 10)} \times 100$ , and absorption is calculated as % Absorption =  $100 - (\% \text{ Transmission} + \% \text{ Reflection})$  (Gupta et al. 2016). It was found that as the surface conductivity increases, the S21 parameter decreases, and the S11 parameter increases, i.e., less transmission of the wave and more reflection. The surface reflectivity is found to be dependent on the percentage content of the MWCNTs in the CMC sample. As the MWCNTs wt% rises from 5.96 wt% to 22.23 wt%, the reflection increases from 2.34% to 52.9%, and the absorption increases from 28.53% to 47.05%, while the transmission decreases from 69% to 0.04% for samples CMC 1 to CMC 7, respectively. The change in the reflection was much higher compared with the change in the absorption with an increase in MWCNTs wt% in the developed CMC samples. A comparison of the properties measured at the microwave frequency range of the present work with other works reported in the literature is summarized in Table. 4.3. It can be seen that the thickness of the composite used in the literature for measuring the properties at the microwave frequency range is higher compared to the present study. However, in the present work, 0.04% transmission was observed for the CMC 7 sample of thickness 382 $\mu\text{m}$ . The above transmission value is much superior than the reported work by Mehdipour et al. 2012 in which they obtained 0.26% transmission for a 2 mm thickness of MWCNT-epoxy resin composite.

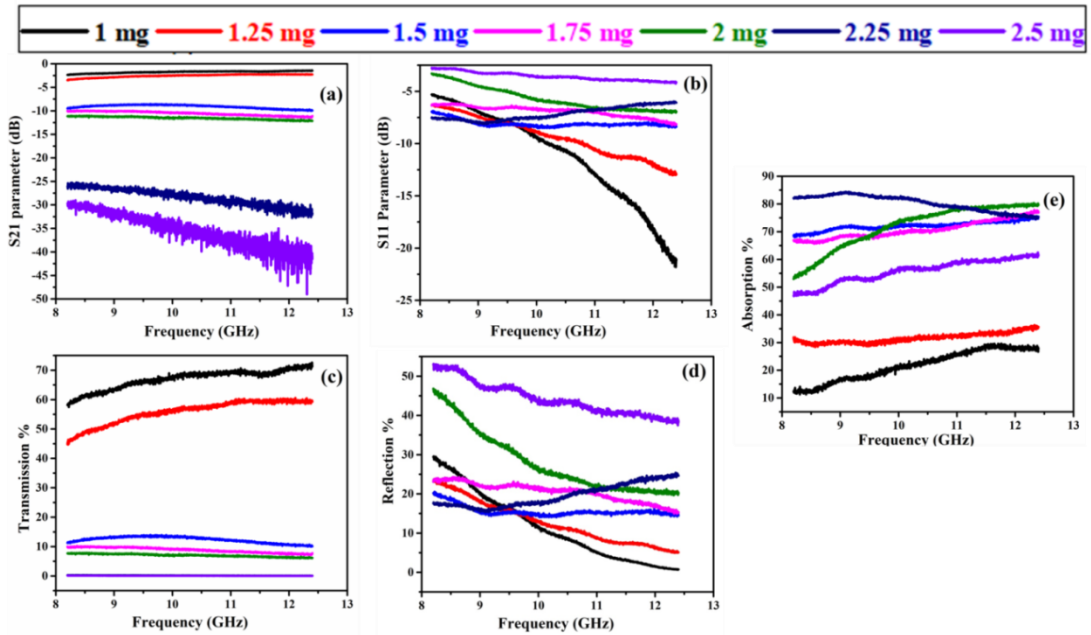


Figure. 4.10: Scattering parameters for CMC fabrics (a) S21 parameter, (b) S11 parameter, (c) Transmission, (d) Reflection, and (e) Absorption in X band.

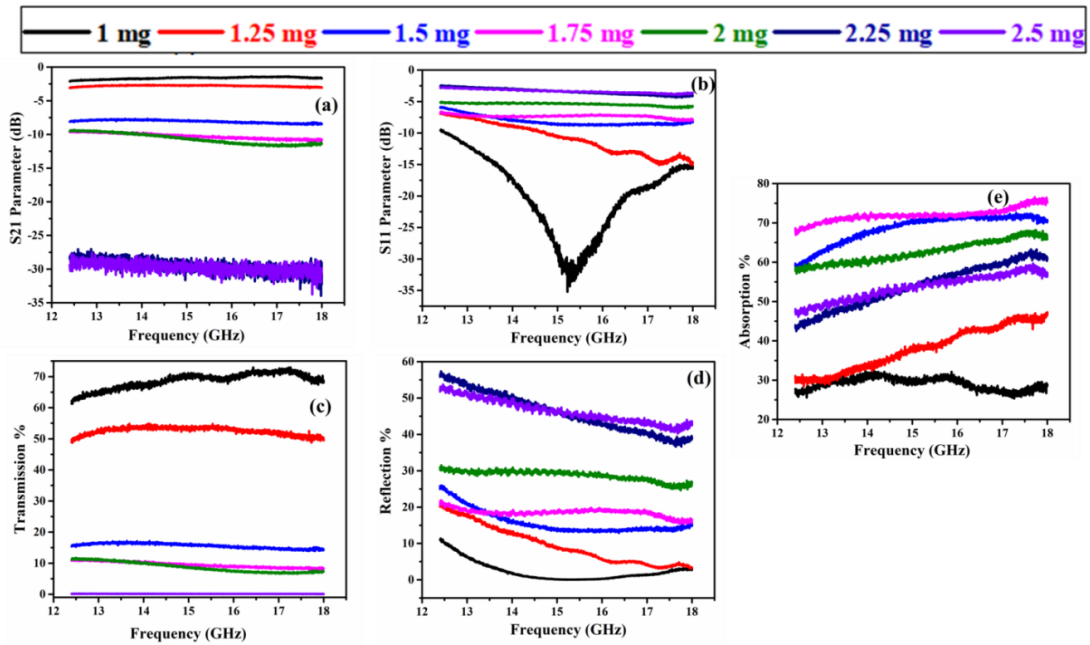


Figure. 4.11: Scattering parameters for CMC fabrics (a) S21 parameter, (b) S11 parameter, (c) Transmission, (d) Reflection, and (e) Absorption in Ku band.

### 4.4.3 EMI shielding property

Shielding effectiveness due to reflection ( $SE_R$ ), shielding effectiveness due to absorption ( $SE_A$ ), and shielding effectiveness due to multiple reflections ( $SE_{MR}$ ) are the three main parameters that can be used to determine EMI shielding. The primary mechanism of EMI shielding is generally a reflection of the electromagnetic wave incident on the shielding material (Cao et al. 2010; Shukla 2019). The shielding material must have mobile charge carriers (electrons or holes) that interfere with the electromagnetic wave in order to reflect the EM waves (Shukla 2019; Yang et al. 2005). Absorption is a secondary mechanism of EMI shielding, which can be described as the energy dissipation of electromagnetic waves within the CMC sample. It happened due to the dissipation factor or  $\tan \delta$  (Cao et al. 2010; Shukla 2019). The sum of shielding efficiency is calculated by  $SE_A$ ,  $SE_R$ , and  $SE_{MR}$ . It is the total shielding effectiveness ( $SE_T$ ), which is represented as  $SE_T = SE_A + SE_R + SE_{MR}$ . Usually, multiple reflections are important only at low frequency (i.e. ~kHz range). The  $SE_{MR}$  can be safely ignored for highly absorbing materials or at very high frequency (~GHz or high) or the shielding effectiveness by absorption is greater than 10dB, i.e.  $SE_{MR} \approx 0$  (Shukla 2019; Saini and Aror 2012). So  $SE_T$  is specified as  $SE_T = SE_R + SE_A$ .

In a PNA, the total EMI SE can be calculated from the S-parameters using the equations below, where  $S_{21}$ ,  $S_{12}$ , and  $S_{11}$  refer to the forward transmission coefficient, reverse transmission coefficient, and forward reflection coefficient, respectively (Sharika et al. 2019).

$$EMI\ SE = 10 \log \frac{1}{|S_{12}|^2} = 10 \log \frac{1}{|S_{21}|^2} \quad (4.1)$$

$$SE_T = SE_R + SE_A \quad (4.2)$$

$$SE_R = 10 \log_{10} \left( \frac{1}{1 - |S_{11}|^2} \right) \quad (4.3)$$

$$SE_A = 10 \log_{10} \left( \frac{1 - |S_{11}|^2}{|S_{21}|^2} \right) \quad (4.4)$$

$$R = |S_{11}|^2 = |S_{22}|^2$$

$$T = |S_{21}|^2 = |S_{12}|^2 \quad (4.5)$$

EMI shielding effectiveness of CMC samples has been evaluated using the above relations and shown in Fig. 4.12. The CMC 1 sample shows the least SE of -2.6 dB (45%) because of MWCNTs poor interconnection and it is seen that improvement in EMI shielding effectiveness (dB) of CMC samples increases when the MWCNTs wt% increases. The sample CMC 7 shows a better SE of -19.7 dB (98.9%) in the X- and Ku-band frequency range due to effective MWCNTs interconnectivity. The SE of CMC samples increases with the increase in MWCNTs wt% as shown in Fig. 4.13.

In this work, the cotton fabric is electrically insulating and does not contribute to shielding. So, the conducting network of MWCNTs makes the cotton fabric electrically conductive. The EMI shielding efficiency is due to both reflection and absorption. The reflection mechanism in CMC samples is due to the conductive nature of the MWCNTs (Shukla 2019). The electrical conductivity of CMC 1 and CMC 2 is very less due to the weak interconnection of MWCNTs network. As a result, the above samples show less reflection. As the MWCNTs reaches 7.97 wt% for sample CMC 3 the electrical conductivity drastically increases up to 1.445 S/m and the electrical conductivity value increases rapidly from sample CMC 3 to CMC 7 due to the good interconnection of MWCNTs network. When the CMC sample is exposed to the microwave, conducting nature of the MWCNTs over the entire surface plays an important role to reflect the electromagnetic waves. In CMC samples, the absorption mechanism is governed by the dissipation factor or  $\tan \delta$  (Shukla 2019).  $\tan \delta$  value increases gradually from sample CMC 1 to CMC 4. Whereas, from CMC 5 to CMC 7 the  $\tan \delta$  value increases rapidly. The rapid increase in  $\tan \delta$  value indicates improved energy dissipation. Moreover in samples, CMC 1 and CMC 2, low electrical conductivity and high  $\tan \delta$  value (absorption property is dominated) result in EMI shielding. However, from sample CMC 3 to CMC 7 the shielding mechanism is due to high electrical conductivity and high  $\tan \delta$  means both reflection and absorption properties are dominated.

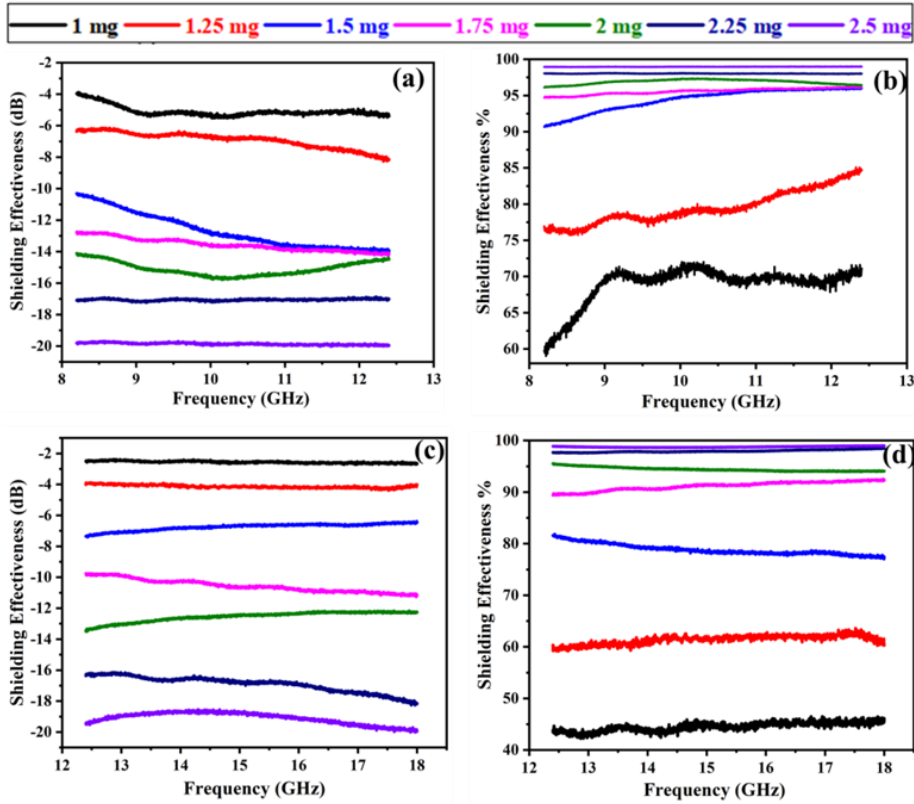


Figure. 4.12: The shielding effectiveness v/s frequency of CMC fabrics (a), (b) in the X band, and (c), (d) in the Ku band.

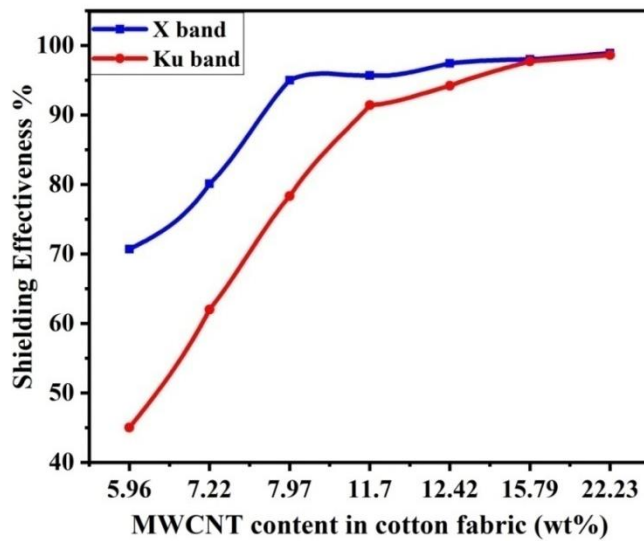


Figure. 4.13: The shielding effectiveness of CMC 1 (5.96 wt%) to CMC 7 (22.23 wt%).

Table 4.3: Comparison between microwave properties of carbon composites in the literature and CMC samples of this work.

Sample name/type	Thic kness (mm)	MW CNTs wt%	Permittivity values			Scattering parameters		EMI SE (dB)	Reflect ion %	Transmi ssion %	Absorp tion %	Ref
			Real ( $\epsilon'$ )	Imagi nary ( $\epsilon''$ )	Tan ( $\delta$ )	S11 (dB)	S21 (dB)					
Micro graphite/ MWCNT composite	7	5	6	0.9	0.15	-16.2	-1.6	-17.6	2.39	69.18	28.43	(Micheli et al. 2011)
NC/MWCNT/ Epoxy composite	1.5	0.1	3.9	0.3	0.07	-26.8	-0.78	-10	0.208	83.56	16.23	(Stergiou et al. 2015)
		0.5	5.8	0.6	0.10	-20	-1.07	-14	1	78.16	20.84	
PVA/SDS/ MWCNT composite Nanofibers	1	10	6.3	1.1	0.17	-15	-1.68	-14.8	3.16	67.92	28.92	(Salimbe ygi et al. 2013)
MWCNT/ epoxy resin composite	9.7	1	3.6	0.3	0.08	-25.9	-0.89	-	0.25	81.47	18.28	(Micheli et al. 2010)
		3	4.1	0.2	0.048	-18.4	-1.21	-	1.44	75.68	22.88	
		5	5.9	0.9	0.152	-16.3	-1.6	-	2.34	69.18	96.06	
MWCNT/ epoxy resin composite	2	8	3.57	2.54	0.71	-3.56	-25.7	-18.8	44.0	0.26	55.74	(Mehdip our et al. 2012)
MWCNT/ polymer composite	3.82 3.75 4.29	0.10	6.34	1.72	0.271	-29	-0.9	-2.1	0.12	81.2	18.68	(Umishit a et al. 2006)
		0.22	9.60	3.53	0.367	-21.8	-1.6	-5.9	0.66	69.18	30.16	
		0.50	16.30	9.09	0.557	-15.1	-1.98	-16.7	3.09	63.38	33.53	
CMC1	0.283	5.96	1.33	0.40	0.22	-16.29	-1.56	-3.9	2.34	69.69	28.53	Present Study
CMC2	0.284	7.22	1.82	0.56	0.27	-11.27	-2.19	-5.1	7.45	60.28	31.91	
CMC3	0.294	7.97	2.01	1.11	0.43	-6.95	-9.75	-10	19.98	10.59	33.84	
CMC4	0.300	11.7	2.41	1.23	0.47	-6.32	-11.1	-12.6	23.32	7.75	36.91	
CMC5	0.302	12.42	2.57	2.04	0.84	-5.31	-11.93	-14.1	29.43	6.39	42.56	
CMC6	0.335	15.79	2.58	4.37	1.81	-3.29	-31.48	-17	46.82	0.07	46.91	
CMC7	0.382	22.23	6.22	11.27	3.27	-2.75	-43.82	-19.7	52.9	0.04	47.05	



#### 4.5 Detection of CO gas by CMC sensors

Carbon nanotubes have a lot of reaction sites, so when carbon monoxide (CO) molecules are adsorbed, they accept electrons from them (Bandi et al. 2018; Choi et al. 2011). Generally, MWCNT acts as a p-type semiconducting material, which means it has a large number of holes and less number of electrons. When CO and MWCNT interact, the carbon monoxide donates electrons to the MWCNT. It ascribes a change in Fermi energy level from the MWCNTs valence band with less hole concentration. Therefore, by reducing the hole concentration, the resistance changes with adsorbed CO gas (Zhao et al. 2002; Jung et al. 2007). Adsorption of CO gas molecules increases with the increase of CO concentration, causing a large change in resistance.

The sensor response ( $S$ ) is calculated using the below equation (Bandi et al. 2018; Debataraja et al. 2017).

$$S(\%) = \left[ \frac{R_a - R_g}{R_a} \right] \times 100 \quad (4.6)$$

Where ' $R_a$ ' indicates the sensor electrical resistance in air and ' $R_g$ ' indicates the electrical resistance in target gas exposure. Fig. 4.14 presents the response of CMC 3 to CMC 7 sensors with the exposure of CO gas at varying concentrations from 25 to 100 ppm at room temperature. In Fig. 4.14(a), sensor CMC 3 shows the lowest response of 2.8% for 25 ppm and 4.3% response for 100 ppm CO gas concentration, the response of the sensor improves as CO concentrations increase from 25 to 100 ppm. Absorption of CO molecules begins when the CO gas channel is switched ON indicating the responding behavior of the CMC sensors. In addition, the desorption of CO molecules starts when the CO channel is turned OFF indicating the recovery of the CMC sensors in the presence of air. Compared to sensor CMC 3, the response is improved in sensor CMC 4 (Fig. 4.14(b)), and it shows more response of 5.4 % for 100 ppm. Whereas in Fig. 4.14(c) & (d), the response of sensors CMC 5 and CMC 6 increases twice compared to sensors CMC 3 & CMC 4 for 25 to 100 ppm concentration of CO gas.

CMC 7 sensor (Fig. 4.14(e)) shows a maximum response compared to all other sensors. It is found that the maximum response of the CMC 7 sensor is 9.11% at 25 ppm and 15.2% at 100 ppm concentration of CO gas respectively due to increased wt% and

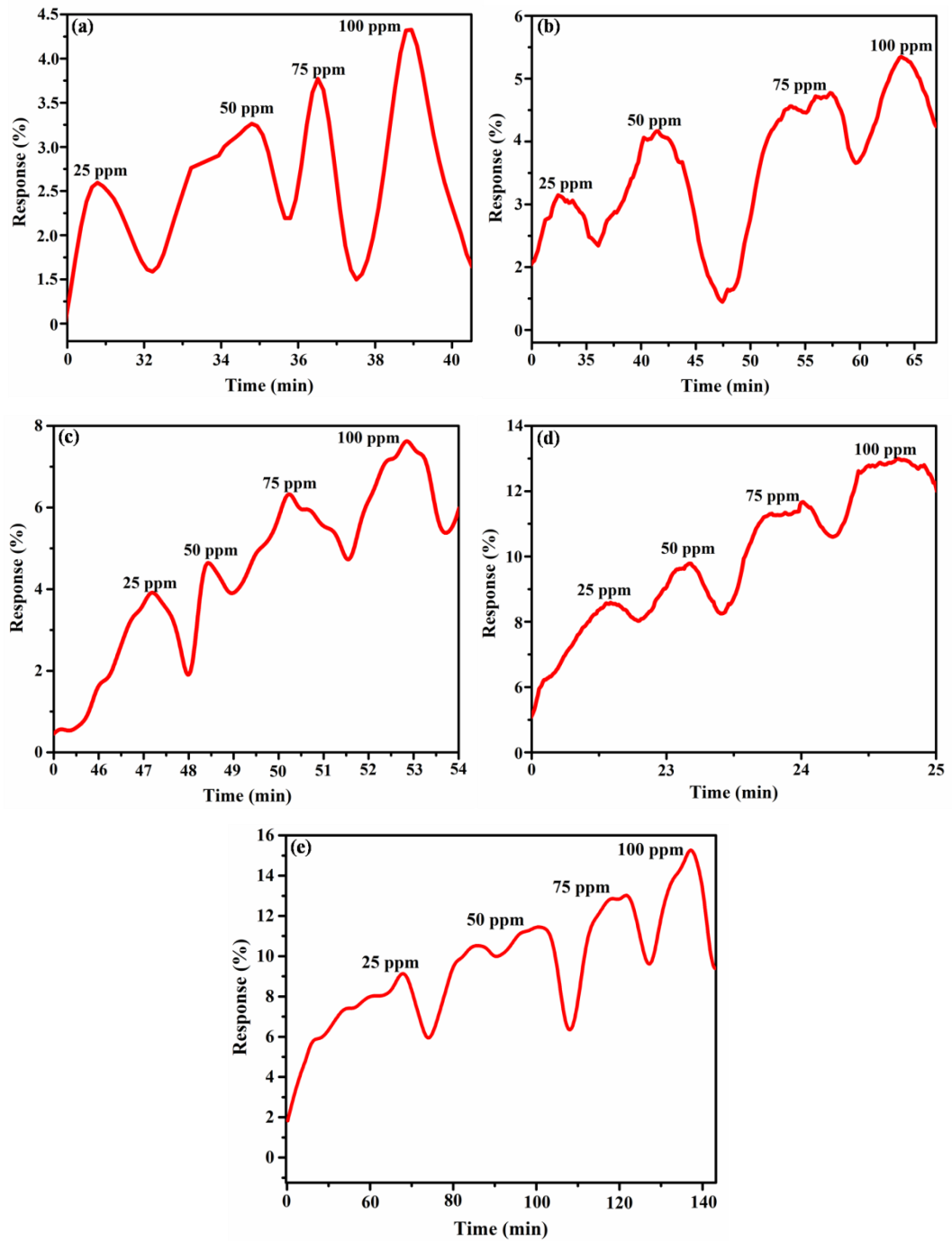


Figure. 4.14: CMC sensor response to a series of carbon monoxide (CO) exposures ranging from 25 to 100 ppm at room temperature: (a) Sensor CMC 3, (b) Sensor CMC 4, (c) Sensor CMC 5, (d) Sensor CMC 6, and (e) Sensor CMC 7.

better interconnection between the MWCNTs. Throughout the entire volume of the CMC 7 sensor, a sufficient amount of MWCNTs are available which have joined together to form a close network of MWCNTs as depicted in the FESEM image (Fig. 4.2(g)). It is observed that the response of the sensors depends on the wt% of MWCNTs in the cotton fabric. In the CMC sensor, a better network forms as the wt% of MWCNTs increases, leading to a better response. As the MWCNTs wt% rises from 7.97 wt% to 22.23 wt% the response increases from 2.8% to 9.11% at 25 ppm of CO, whereas the response increases from 4.3% to 15.2% at 100 ppm, for sensors CMC 3–CMC 7, respectively. It is also observed that the response increases with increasing the CO concentration from 25 to 100 ppm for all five CMC sensors.

During the recovery process, the sensor reacts immediately after the CO is switched OFF in the presence of air. Sensor recovery is observed to be fast within two minutes. Then, recovery has become slow, and even if the sensors were to leave for a full day, they would not be able to completely recover. CO gas molecules self-desorption has a direct correlation with the concentration of CO gas molecules on MWCNTs surfaces. The desorption rate decreases with decreasing concentrations of absorbed analyte molecules, which results in a slow change in the resistance of the sensor with time. In this study, complete recovery is not observed for any fabricated CMC sensor. In comparison to all other CMC sensors, sensor recovery for CMC 7 is improved, as shown in Fig. 4.14(e). Nevertheless, it is also unable to completely recover. The CMC 7 sensor shows better recovery than the other CMC sensors. This is most likely a densely packed and better interconnected network of MWCNTs in the cotton fabric.

Response and recovery time of all CMC sensors towards various concentrations of CO are evaluated through their respective transient sensing curves, as shown in Fig. 4.15(a) & (b), respectively. It is noticed that CMC 6 sensor exhibited a quick response (22–40.1 s) towards the different concentrations of CO gas compared to other sensors. In addition, CMC 6 sensor has recovered its baseline resistance quickly (24.8–48.3 s) upon unloading from 25 to 100 ppm concentration of CO gas compared to other sensors (Fig. 4.15).

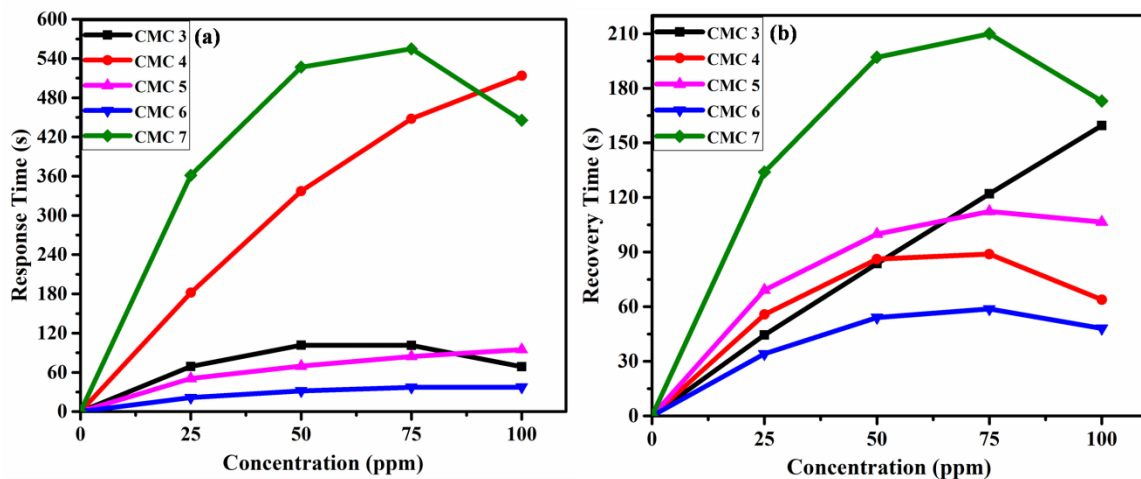


Figure. 4.15: (a) Response time of CMC sensors towards different concentration of CO, and (b) Recovery time of CMC sensors towards different concentration of CO.

CNT-based sensors frequently exhibited a lengthy CO recovery time and a slow sensor recovery has frequently been noted for several gases and vapors (Kauffman et al. 2008; Li et al. 2003). To efficiently enhance molecular desorption, high vacuum procedure (Wongwiriyan et al. 2008), heating (Quang et al. 2006), and UV light illumination (Chauhan et al. 2019) have already been tried. In the present work, all the fabricated CMC sensors are capable of recovering without using high vacuum, heating, and UV light illumination.

CMC samples not recovered completely to their baseline because when we used low wt% of MWCNTs in the cotton fabric the gaseous molecules are free to move beneath the cotton and MWCNTs and it traps there. Once the gas is turned off recovery is happening only from the top surface of the MWCNTs, not from below the MWCNTs and the cotton fabric. As a result, the baseline recovery for the low wt% MWCNTs sample is difficult. However, in the case of the CMC 6 sample, it is observed that optimum porosity is available and a very less amount of MWCNTs molecules trap between the cotton fabric and MWCNTs, therefore, sensor CMC 6 recovers faster than other sensors.

The responses of all five fabricated sensors from 25 to 100 ppm of CO gas at room temperature are compared in Fig. 4.16.

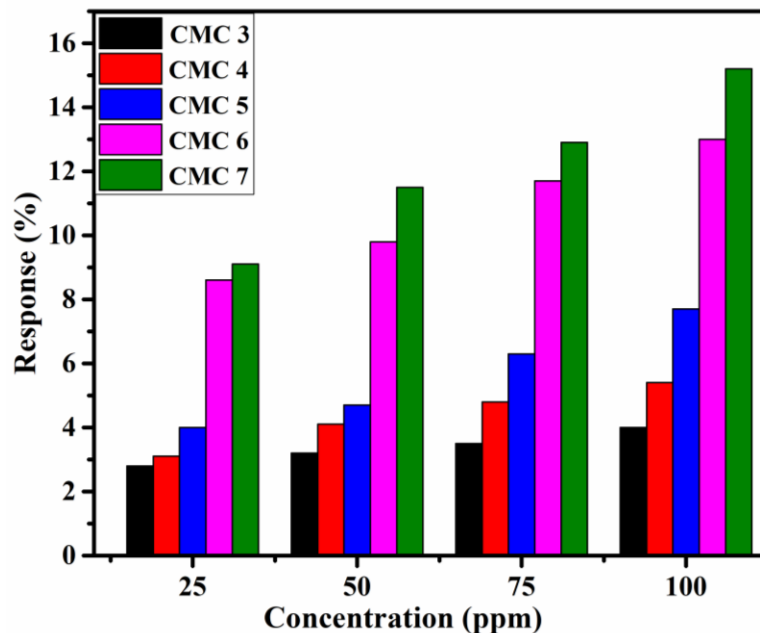


Figure. 4.16: Response comparison of CMC sensors towards different concentrations of carbon monoxide at room temperature.

The sensor CMC 3 showed less response for 25 to 100 ppm of CO gas. As the concentration of CO increases from 25 to 100 ppm, the response of CMC sensors rises. This change in response is due to increased charge transfer occurs between MWCNTs and CO. The CMC 7 sensor showed a better response than all other CMC sensors. In the present work, when the MWCNTs dispersed solution wets the hydrophilic surface of the cotton fabric, the cotton fabric can soak up the MWCNTs by capillary action. Moreover, the van der Waals interaction enhances the bond between MWCNT and cotton fabric. Due to the increased concentration of MWCNTs in the CMC 7 sensor, more individual MWCNTs can be bound tightly along the cotton fabric morphology. Therefore, the CMC 7 sensor shows a better response than all other CMC sensors for varying the concentration of CO gas.

According to Hannon et al., the CO sensor on a printed circuit board uses SWCNT as a sensing element and has a response of less than 5% to 100 ppm CO gas (Hannon et al. 2014). Compared with Hannon et al. (100 ppm), sensor CMC 7 in the

present study shows two time better response as well at low CO concentrations (25 ppm). Fig. 4.17 compares the response of fabricated CMC CO gas sensors with existing literature based on the CO gas sensors.

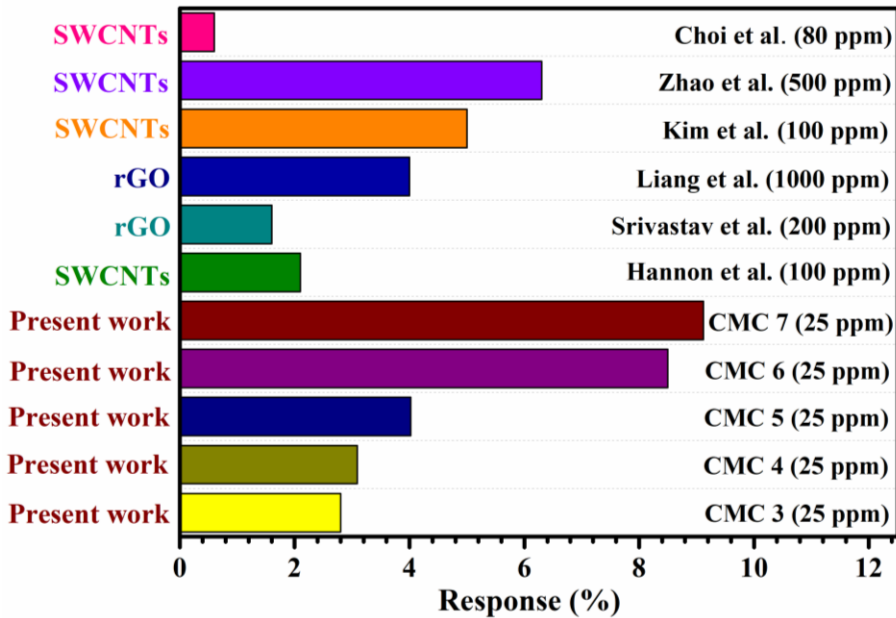


Figure. 4.17: Comparison of the present work and published research on carbon monoxide sensor response.

It is found that the current biodegradable sensor has a better response compared to reported literature based on SWCNT and reduced graphene oxide (rGO) sensors (Hannon et al. 2014; Bandi et al. 2018; Choi et al. 2011) and (Liang et al. 2018; Kim et al. 2011; Zhao et al. 2012). The better response of the CO sensors in this paper refers due to the presence of a hydro carboxyl group of cellulose, homogeneous and dense structures of coated MWCNT network over the cotton fabric.

Moreover, the quantity of MWCNTs needed for the 2 cm × 0.5 cm sensor (sensor CMC 5) was calculated to be 19 µg/ml. An amount of 15 mg silver paste is required for contact electrode coatings. In this work, MWCNTs and Ag paste market prices are ~80 and 15 USD per gram respectively and a 2 cm × 0.5 cm sensor material cost is calculated to be about ~0.3 USD. This evidenced that cotton fabric-based sensors are much cheaper

compared with silicon sensors that spend 90% of production costs on substrates and Au contact electrodes (Abdellah et al. 2013). The cotton fabric sensor had a net weight of 22 mg. As well as enabling a simple fabrication process, the biodegradable sensors are cost-effective, lightweight, fast-responsive, and have low detection limits. These sensors can potentially be used in reaction and environmental monitoring systems.

#### **4.6 Electrothermal heating behavior of CMC samples**

The heating behavior of CMC samples are tested with respect to DC input voltages of 10, 20, 30, and 40 volts. A series of voltages were applied to the heaters, resulting in a linear increase in the steady-state temperature with the applied voltage. Although the voltage was applied, the temperature rise occurred very quickly, in addition, similar heating rates and steady-state temperatures were noted. The heater takes about 40 seconds to achieve steady-state temperature. In Fig. 4.18(a) sample CMC 7 reached a steady-state temperature of 32°C at 10 V, which was enhanced to 80°C for 40V. However, maximum heating rates were found in all CMC samples for 40V. It can be inferred from the results that a higher steady-state temperature is achieved with lower resistance. The CMC samples produce more heat from their entire surface due to the homogeneous distribution of MWCNTs within them. It is also possible that homogeneous temperature distribution would result in faster heating rates (Baughman et al. 2002).

Charge carriers may have initially been moved faster in the system as a result of an external electric potential. As electrons accelerate, they can collide inelastically with phonons, impurities, and defects in MWCNT to release heat (Janas and Koziol 2014; Jiang and Wang 2011). When the applied potentials are increased the MWCNT experience a high scattering rate and as a result mean free path dramatically decreases, which causes the temperature to rise at a faster rate (Rutherglen and Burke 2009). In addition, the MWCNTs are well-bonded into the cotton fabric, so when voltage is applied, the current flows through the conductive layer uniformly, resulting in heat production. As a result, MWCNT coated cotton fabric is an important factor to consider in today's heating applications due to its better thermal and electrical conductivity.

Fig. 4.18(b) compares the steady-state temperatures of CMC samples for various applied voltages. The sample CMC 3 showed the least steady-state temperature for an input voltage of 10-40V. As the input voltage is increased from 10V to 40V, the steady-state temperature of the CMC samples also rises. The CMC 7 sample showed a better electrothermal response than all other CMC samples. Here, a low applied voltage resulted in a higher steady-state temperature and revealing that low voltage is sufficient for CMC samples to achieve superior steady-state temperature (55-80°C). High thermal diffusivity materials generally disperse heat more quickly. In CMC samples the uniform distribution of MWCNTs dispersed the heat uniformly throughout the surface of the sample, even though cotton has poor thermal conductivity. The uniform distribution of MWCNTs in the cotton fabric can help to improve electrothermal response.

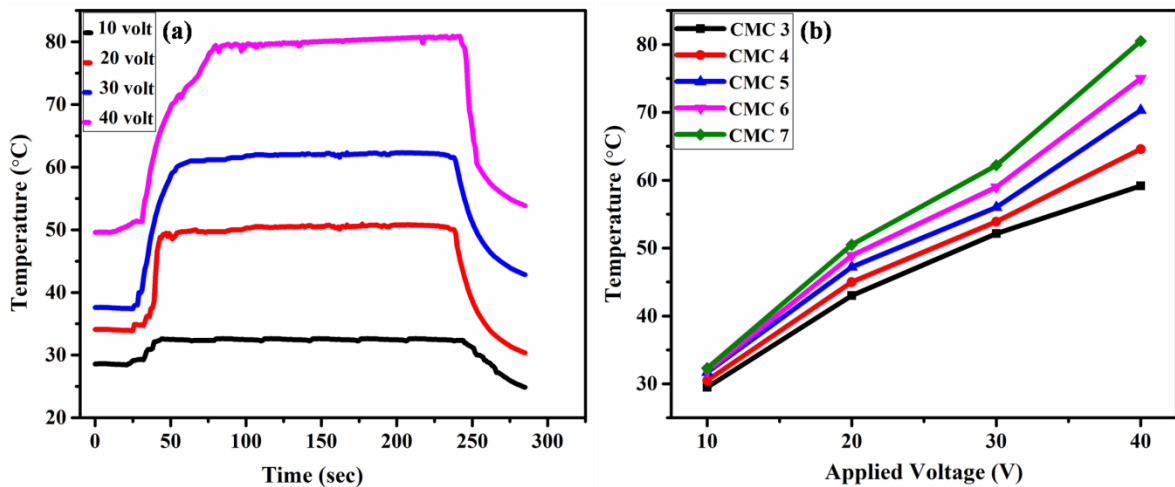


Figure. 4.18: (a) Heating behavior of CMC 7 samples using a thermocouple and DC power supply (turn on and turn off), temperature as a function of time with varying applying voltage, and (b) Steady-state temperature comparison of CMC samples for the different applied voltage.

When voltage is applied to the CMC samples the heat radiate from the CMC sample surface due to the MWCNTs electrothermal behavior which is coated on the cotton fabric. When 40V is applied to CMC 5 sample, the steady-state temperature reaches 70°C and the CMC 5 sample shows two different heating rates as marked in Fig. 4.19(a). From



point 1 to point 2 the heating rate is  $0.8^{\circ}\text{C}/\text{sec}$  is observed and from point 2 to point 3 the heating rate is  $0.21^{\circ}\text{C}/\text{sec}$ . This phenomenon can be explained by the TGA graph shown in Fig. 4.19(b). Fig. 4.19(b) shows the heating of the plain woven cotton fabric and CMC 5 sample. It is very much clear that plain woven cotton fabric releases the moisture present in the fabric at a faster rate than the CMC 5 sample. This is purely due to heat supplied to the CMC sample being first absorbed by the MWCNTs only and then heat transferred to the cotton fabric matrix. However, in the case of an electrothermal heating process, MWCNTs present on the surface of the CMC 5 sample get heated first from point 1 to point 2 and show a faster heating rate of  $0.8^{\circ}\text{C}/\text{sec}$  (up to  $64^{\circ}\text{C}$ ) depicted in Fig. 4.19(a). After that, the surface MWCNTs start transferring heat to the cotton fabric matrix to remove the moisture present in the CMC 5 sample. This is the main reason for observing a low heating rate ( $0.21^{\circ}\text{C}/\text{sec}$ ) from point 2 to point 3 as marked in Fig. 4.19(a).

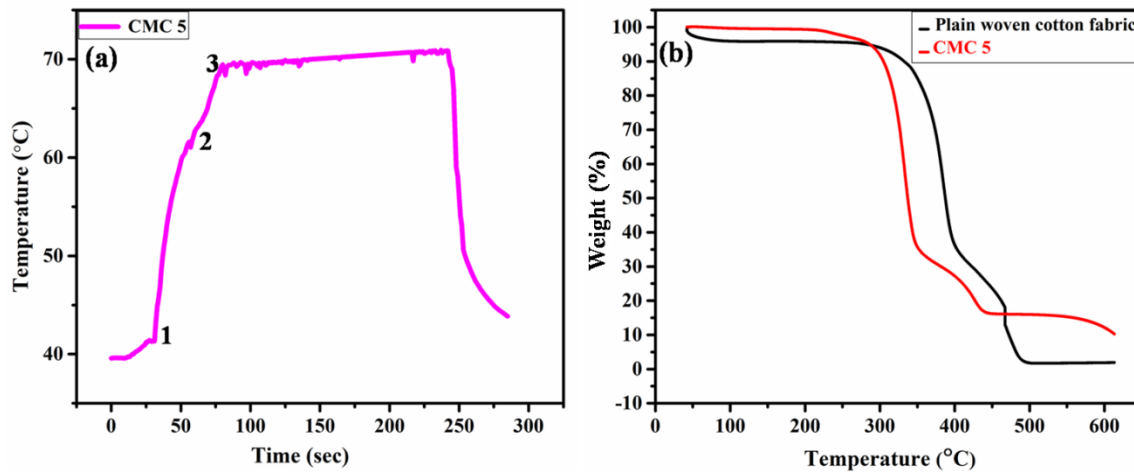


Figure. 4.19: (a) Heating behavior of CMC 5 sample at 40V, and (b) TGA graph of plain-woven cotton fabric and MWCNTs coated cotton fabric (CMC 5 sample).

MWCNT coated fabric heaters were tested to determine their operating stability and reliability over time using the heat cycle test. In Fig. 4.20, we show the temperature response of the sample CMC 7 to a heat cycle at 30V (with an on/off ratio of 130 seconds). The maximum steady-state temperature, as well as better heating and cooling

response, was retained throughout the test. The significant variation in temperature or decrease in heating performance indicates the heaters (CMC) high stability. Furthermore, the present MWCNT coated cotton fabric heaters show good electrical conductivity, are lightweight, and exhibit excellent thermal stability, suggesting that they can be used as wearable heating/electronic devices.

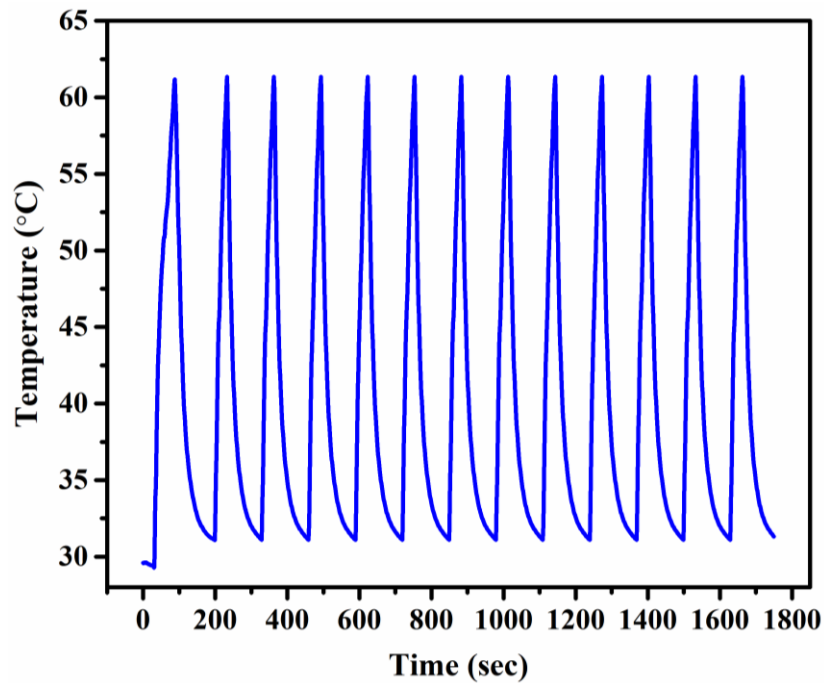


Figure. 4.20: Temperature response of the wearable heater (CMC 7 sample) under a heat cycle.

## CHAPTER 5

### CONCLUSIONS AND SCOPE OF FUTURE WORK

#### 5.1 Conclusions

In the present work, based on the investigations carried out in terms of the fabrication of CNTs coated cotton fabric and their properties of electromagnetic interference (EMI) shielding, CO gas sensing, and electrothermal heating behavior, the following conclusions have been drawn.

- Here, cotton fabric with multi-walled carbon nanotube coating (CMC) samples are successfully fabricated by a dip and dry process.
- The developed coated material with a thickness in the range of hundreds of micron has an excellent EMI shielding ability. The reflection, transmission, absorption, and shielding effectiveness strongly depend on the MWCNTs weight percentage in the CMC sample.
- The CMC sample provides potential applications for EMI shielding compared to conventional materials including other variants of carbon materials like carbon fibers, and exfoliated graphite. The developed CMC sample is cost-effective and easy to process for mass production.
- MWCNT-based CO sensors on cotton fabric were demonstrated and a good response was observed within the tested range of 25-100 ppm. The density of the multi-walled carbon nanotubes network in the cotton fabric depends on the MWCNTs concentration. The sensor with a high concentration of MWCNTs i.e. CMC 7 showed a better response for each CO gas concentration compared to all other CMC sensors.
- The present sensors encompass operating at room temperature, are lightweight, and can be fabricated at a low cost, making them suitable for biodegradable applications. Specific characteristics, such as reasonable response and recovery (without using high vacuum, heating, and UV light illumination) were attained under room temperature. The cotton fabric-based gas sensor could be a key

component in future smart textile applications.

- The electrothermal response of CMC heaters was measured based on response time and input voltage. As MWCNTs have excellent electrical and thermal properties, they may be able to maintain their steady-state temperature at low input power (temperature rise at low voltages).
- The properties shown by MWCNTs coated cotton fabric is an attractive candidate for low-cost wearable heaters because of their better electrothermal behavior.

## **5.2 Scope of future work**

- The research was intended to provide brief and helpful information about the fabrication of nanomaterial coated cotton fabric and its applications. The result of this study not only points out the advantages of polymers with carbon nanomaterials to that of general polymers but also provides a future reference to researchers to develop products out of natural polymers with carbon nanomaterials. The future research that might be done following this study is to test the production of nanomaterials coated polymer products.
- The current cotton fabric with multi-walled carbon nanotube coating (CMC) samples lifetime has not been tested, the future work includes the protection of the coated MWCNTs in order to examine the lifetime performance of CMC samples for applications such as EMI shielding, gas sensing, and wearable heating.
- Further study includes increasing the detection limit of CO gas while maintaining the response of the sensors, as well as MWCNTs has to modify with other nanomaterials such as SWCNTs, graphene, and metal nanoparticles to improve sensor performance.
- Future studies will focus on the durability of the CO sensor. In addition, needed to address several practical issues including the effects of humidity and other interfering or similar analytes.

## LIST OF PUBLICATIONS

1. **Arun Kumar D.S**, Puneeth Kumar T.R, **Krishnamoorthy K**, *Member, IEEE*, Devadas Bhat P, and **M.R. Rahman** (2022). “Flexible Electromagnetic Shielding Material Using Multi-Walled Carbon Nanotube Coated Cotton Fabric”. *IEEE Transactions on Components, Packaging and Manufacturing Technology, IEEE 10.1109/TCPMT.2022.3154226 (SCI)*.
2. **Arun Kumar D.S**, Sandeep Singh Chauhan, **Krishnamoorthy K**, Devadas Bhat P, K. Divya Bharathi, Abhilash Ravikumar, and **M.R. Rahman** (2023). “Flexible and cost effective CNT coated cotton fabric for CO gas sensing application”. *Sensors and Actuators: A. Physical, 362 (2023) 114640, Elsevier, Impact Factor - 4.6 (SCI)*.
3. **Arun Kumar D.S**, **Krishnamoorthy K**, and **M.R. Rahman**. “Multi-walled carbon nanotube coated cotton fabric for wearable heating application” *Journal of Materials Science: Materials in Electronics, Springer* (Submitted), *Impact Factor - 2.8 (SCIE)*.

## REFERENCES

Abdellah, A., Abdelhalim, A., Horn, M., Scarpa, G., and Lugli, P. (2013). “Scalable spray deposition process for high-performance carbon nanotube gas sensors.” *IEEE Trans. Nanotechnol.*, 12(2), 174–181.

Afzal, A., Cioffi, N., Sabbatini, L., and Torsi, L. (2012). “NO<sub>x</sub> sensors based on semiconducting metal oxide nanostructures: Progress and perspectives.” *Sensors Actuators, B Chem.*, 171–172(2012), 25–42.

Ahamed, V. I. T., Karthick, N. G., and Joseph, P. K. (2008). “Effect of mobile phone radiation on heart rate variability.” *Comput. Biol. Med.*, 38(6), 709–712.

Akash, Sreenivasa Rao, K. V, Venkatesha Gupta, N. S., and Arun kumar, D. S. (2016). “Mechanical Properties of Sisal/Coir Fiber Reinforced Hybrid Composites Fabricated by Cold Pressing Method.” *IOP Conf. Ser. Mater. Sci. Eng.*, 149, 012092.

American Society for Testing & Mater. (1985). “Standard test methods for mass per unit area (weight) of woven fabric.” 7–11.

Andretta, A., Terranova, M. L., Lavecchia, T., Gay, S., Picano, A., Mascioletti, A., Stirpe, D., Cucchiella, C., Pascucci, E., Dugnani, G., Gatti, D., Laria, G., Codenotti, B., Maldini, G., Roth, S., Passeri, D., Rossi, M., and Tamburri, E. (2014). “Nanotechnology and textiles engineered by carbon nanotubes for the realization of advanced personal protective equipments.” *AIP Conf. Proc.*, 1603(December 2015), 71–77.

Arun Kumar, D. S., Puneeth Kumar, T. R., Krishnamoorthy, K., Devadas Bhat, P., and Rahman, M. R. (2022). “Flexible Electromagnetic Shielding Material Using Multi-Walled Carbon Nanotube Coated Cotton Fabric.” *IEEE Trans. Components, Packag. Manuf. Technol.*, 12(3), 479–488.

Balberg I. (1987). “Tunneling and nonuniversal conductivity in composite materials.” *Phys. Rev. Lett.*, 59(12), 1305–1308.

- Bandi, S., Hastak, V., Peshwe, D. R., and Srivastav, A. K. (2018). “In-situ TiO<sub>2</sub>-rGO nanocomposites for CO gas sensing.” *Bull. Mater. Sci.*, 41(5), 115.
- Baughman, R. H., Zakhidov, A. A., and Heer, W. A. De. (2002). “Carbon nanotubes - The route toward applications.” *Science* (80-. ), 297(5582), 787–792.
- Bhattacharjee, Y., Arief, I., and Bose, S. (2017). “Recent trends in multi-layered architectures towards screening electromagnetic radiation: Challenges and perspectives.” *J. Mater. Chem. C*, 5(30), 7390–7403.
- Bhattacharya, P., Sahoo, S., and Das, C. K. (2012). “Microwave absorption behavior of MWCNT based nanocomposites in X-band region.” *Express Polym. Lett.*, 7(3), 212–223.
- Bower, C., Rosen, R., Jin, L., Han, J., and Zhou, O. (1999). “Deformation of carbon nanotubes in nanotube-polymer composites.” *Appl. Phys. Lett.*, 74(22), 3317–3319.
- Budtova, T., and Navard, P. (2016). “Cellulose in NaOH–water based solvents: a review.” *Cellulose*, 23(1), 5–55.
- Cao, H. Z., Yao, Y., Halada, G., Jung, H. J., and Kim, T. (2021). “Impact of naoh concentration on deweaving of cotton fabric in aqueous solutions.” *Sustain.*, 13(4), 1–10.
- Cao, M. S., Song, W. L., Hou, Z. L., Wen, B., and Yuan, J. (2010). “The effects of temperature and frequency on the dielectric properties, electromagnetic interference shielding and microwave-absorption of short carbon fiber/silica composites.” *Carbon N. Y.*, 48(3), 788–796.
- Cao, M., Wang, X., Cao, W., Fang, X., Wen, B., and Yuan, J. (2018). “Thermally Driven Transport and Relaxation Switching Self-Powered Electromagnetic Energy Conversion.” *Small*, 14(29), 1–8.
- Centers for Disease Control and Prevention. (2006). “Carbon monoxide poisonings after two major hurricanes.” *Morbidity and Mortality Weekly Report.*, 55, 236–239.

Centers for Disease Control and Prevention. (2007). “Carbon monoxide–related deaths—United States.” *Morbidity and Mortality Weekly Report.*, 56, 1309–1312.

Chao, M., Li, Y., Wu, G., Zhou, Z., and Yan, L. (2019). “Functionalized multiwalled carbon nanotube-reinforced polyimide composite films with enhanced mechanical and thermal properties.” *Int. J. Polym. Sci.*, 2019.

Chauhan, S. S., Kumar, D., Chaturvedi, P., and Rahman, M. R. (2019). “Highly Sensitive and Stable NO<sub>2</sub> Gas Sensors Based on SWNTs with Exceptional Recovery Time.” *IEEE Sens. J.*, 19(24), 11775–11783.

Chen, Z., Xu, C., Ma, C., Ren, W., and Cheng, H. M. (2013). “Lightweight and flexible graphene foam composites for high-performance electromagnetic interference shielding.” *Adv. Mater.*, 25(9), 1296–1300.

Cheng, T., Reynolds, Bitter, J. L., and Howard Fairbrother, D. (2012). “Chemical and structural characterization of carbon nanotube surfaces.” *Carbon N. Y.*, 1(10), 3919–3945.

Choi, H. H., Lee, J., Dong, K. Y., Ju, B. K., and Lee, W. (2011). “Noxious gas detection using carbon nanotubes with Pd nanoparticles.” *Nanoscale Res. Lett.*, 6, 1–6.

Chu, K., Kim, D., Sohn, Y., Lee, S., Moon, C., and Park, S. (2013). “Electrical and thermal properties of carbon-nanotube composite for flexible electric heating-unit applications.” *IEEE Electron Device Lett.*, 34(5), 668–670.

Damon, S. A., Poehlman, J. A., Rupert, D. J., and Williams, P. N. (2013). “Storm-related carbon monoxide poisoning: An investigation of target audience knowledge and risk behaviors.” *Soc. Mar. Q.*, 19(3), 188–199.

Debataraja, A., Muchtar, A. R., Septiani, N. L. W., Yulianto, B., Nugrahaauth, and Sunendar, B. (2017). “High Performance Carbon Monoxide Sensor Based on Nano Composite of SnO<sub>2</sub>-Graphene.” *IEEE Sens. J.*, 17(24), 8297–8305.



Dinesh, P., Renukappa, N. M., Siddaramaiah, and Rajan, J. S. (2012). “Electrical properties and EMI shielding characteristics of multiwalled carbon nanotubes filled carbon black-high density polyethylene nanocomposites.” *Compos. Interfaces*, 19(2), 121–133.

Dong, K. Y., Choi, J., Lee, Y. D., Kang, B. H., Yu, Y. Y., Choi, H. H., and Ju, B. K. (2013). “Detection of a CO and NH<sub>3</sub> gas mixture using carboxylic acid-functionalized single-walled carbon nanotubes.” *Nanoscale Res. Lett.*, 8(1), 1–6.

Dowling, a, Clift, R., Grobert, N., Hutton, D., Oliver, R., O’neill, O., Pethica, J., Pidgeon, N., Porritt, J., Ryan, J., and Et Al. (2004). “Nanoscience and nanotechnologies : opportunities and uncertainties.” *London R. Soc. R. Acad. Eng. Rep.*, 46(July), 618–618.

Geetha, S., Satheesh Kumar, K. K., Rao, C. R. K., Vijayan, M., and Trivedi, D. C. (2009). “EMI shielding: Methods and materials-A review.” *J. Appl. Polym. Sci.*, 112(4), 2073–2086.

Ghasemi, A., Sepelak, V., Liu, X., and Morisako, A. (2012). “Structural, microwave, and magnetic properties of self-assembled substituted strontium ferrite dot array on multiwalled carbon nanotubes.” *IEEE Trans. Magn.*, 48(11), 3474–3477.

Ghorbani, M. M., and Taherian, R. (2018). Methods of measuring electrical properties of material. *Electr. Conduct. Polym. Compos. Exp. Model. Appl.*, Elsevier Inc.

Gorpinchenko, I., Nikitin, O., Banyra, O., and Shulyak, A. (2014). “The influence of direct mobile phone radiation on sperm quality.” *Cent Eur. J Urol.*, 67(January), 65–71.

Grossiord, N., Loos, J., Regev, O., and Koning, C. E. (2006). “Toolbox for dispersing carbon nanotubes into polymers to get conductive nanocomposites.” *Chem. Mater.*, 18(5), 1089–1099.

Gupta, K. K., Abbas, S. M., and Abhyankar, A. C. (2016). “Carbon black/ polyurethane

nanocomposite-coated fabric for microwave attenuation in X & Ku-band (8–18 GHz) frequency range.” *J. Ind. Text.*, 46(2), 510–529.

Gupta, K. K., Abbas, S. M., Srivastava, A., Nasim, M., Saxena, A. K., and Abhyankar, A. (2013). “Microwave interactive properties of cotton fabrics coated with carbon nanotubes/polyurethane composite.” *Indian J. Fibre Text. Res.*, 38(4), 357–365.

Guzman, J. A. (2012). “Carbon Monoxide Poisoning.” *Crit. Care Clin.*, 28(4), 537–548.

Håkansson, E., Amiet, A., and Kaynak, A. (2006). “Electromagnetic shielding properties of polypyrrole/polyester composites in the 1-18 GHz frequency range.” *Synth. Met.*, 156(14–15), 917–925.

Han, J. W., Kim, B., Li, J., and Meyyappan, M. (2014). “A carbon nanotube based ammonia sensor on cellulose paper.” *RSC Adv.*, 4(2), 549–553.

Han, M., Kim, J. K., Lee, G. S., Kang, S. W., and Jung, D. (2019). “A CO gas sensor based on Pt-loaded carbon nanotube sheets.” *Jpn. J. Appl. Phys.*, 58(SD).

Hannon, A., Lu, Y., Li, J., and Meyyappan, M. (2014). “Room temperature carbon nanotube based sensor for carbon monoxide detection.” *J. Sensors Sens. Syst.*, 3(2), 349–354.

Harris, P. J. F. (2004). “Carbon nanotube composites.” *Int. Mater. Rev.*, 49(1), 31–43.

Henry Kuo Feng Cheng, 1, 2 Yongzheng Pan, 1 Nanda Gopal Sahoo, 1 Kahwei Chong, 1 Lin Li, 1 Siew Hwa Chan, 1 Jianhong Zhao. (2011). “Improvement in Properties of Multiwalled Carbon Nanotube/Polypropylene Nanocomposites Through Homogeneous Dispersion with the Aid of Surfactants Henry.” *J. Appl. Polym. Sci.*, 124(5), 1117–1127.

Hsieh, Y. lo. (1995). “Liquid Transport in Fabric Structures.” *Text. Res. J.*, 65(5), 299–307.

Hu, B., Chen, W., and Zhou, J. (2013). “High performance flexible sensor based on

inorganic nanomaterials.” *Sensors Actuators, B Chem.*, 176, 522–533.

Hu, S., Han, J., Shi, Z., Chen, K., Xu, N., and Wang, Y. (2022). “Biodegradable , Super - Strong , and Conductive Cellulose Macrofibers for Fabric - Based Triboelectric Nanogenerator.” *Nano-Micro Lett.*, (0123456789), 1–20.

Hussain, F., Hojjati, M., Okamoto, M., and Gorga, R. E. (2006). “Review article: Polymer-matrix nanocomposites, processing, manufacturing, and application: An overview.” *J. Compos. Mater.*, 40(17), 1511–1575.

Iijima, S. a. o. (1991). "Helical Microtubules of Graphitic Carbon." *Nature.*, 354(6348), 56-58.

Ichihashi, T. (1993). "Single-Shell Carbon Nanotubes of 1-nm Diameter." *Nature.*, 363, 603-605.

Ilanchezhiyan, P., Zakirov, A. S., Kumar, G. M., Yuldashev, S. U., Cho, H. D., Kang, T. W., and Mamadalimov, A. T. (2015). “Highly efficient CNT functionalized cotton fabrics for flexible/wearable heating applications.” *RSC Adv.*, 5(14), 10697–10702.

Iqbal, S., Khatoon, H., Hussain Pandit, A., and Ahmad, S. (2019). “Recent development of carbon based materials for energy storage devices.” *Mater. Sci. Energy Technol.*, 2(3), 417–428.

Janas, D., and Koziol, K. K. (2014). “A review of production methods of carbon nanotube and graphene thin films for electrothermal applications.” *Nanoscale*, 6(6), 3037–3045.

Jiang, J. W., and Wang, J. S. (2011). “Joule heating and thermoelectric properties in short single-walled carbon nanotubes: Electron-phonon interaction effect.” *J. Appl. Phys.*, 110(12).

Journet, C., Maser, W. K., Bernier, P., Loiseau, A., Lamy de la Chapelle, M., Lefrant, S.,

Deniard, P., Lee, R., and Fischer, J. E. (1997). "Large-scale production of single-walled carbon nanotubes by the electric-arc technique." *Nature*, 388(6644), 756–758.

Jung, D., Han, M., and Lee, G. S. (2014). "Flexible transparent conductive heater using multiwalled carbon nanotube sheet." *J. Vac. Sci. Technol. B, Nanotechnol. Microelectron. Mater. Process. Meas. Phenom.*, 32(4), 04E105.

Jung, H. Y., Jung, S. M., Kim, J., and Suh, J. S. (2007). "Chemical sensors for sensing gas adsorbed on the inner surface of carbon nanotube channels." *Appl. Phys. Lett.*, 90(15).

Kang, J., Kim, H., Kim, K. S., Lee, S. K., Bae, S., Ahn, J. H., Kim, Y. J., Choi, J. B., and Hong, B. H. (2011). "High-performance graphene-based transparent flexible heaters." *Nano Lett.*, 11(12), 5154–5158.

Kauffman, D. R., and Star, A. (2008). "Carbon nanotube gas and vapor sensors." *Angew. Chemie - Int. Ed.*, 47(35), 6550–6570.

Kaushik, B. K., and Majumder, M. K. (2015). "Carbon nanotube based VLSI interconnects: Analysis and design." *SpringerBriefs Appl. Sci. Technol.*, (9788132220466), i–iv.

Kim, B., Lee, J., and Yu, I. (2003). "Electrical properties of single-wall carbon nanotube and epoxy composites." *J. Appl. Phys.*, 94(10), 6724–6728.

Kim, D., Pikhitsa, P. V., Yang, H., and Choi, M. (2011). "Room temperature CO and H<sub>2</sub> sensing with carbon nanoparticles." *Nanotechnology*, 22(48).

Kong, J., Franklin, N. R., Zhou, C., Chapline, M. G., Peng, S., Cho, K., and Dai, H. (2000). "Nanotube molecular wires as chemical sensors." *Science (80-. )*, 287(5453), 622–625.

Krishnamoorthy, K., Navaneethaiyer, U., Mohan, R., Lee, J., and Kim, S. J. (2012).

“Graphene oxide nanostructures modified multifunctional cotton fabrics.” *Appl. Nanosci.*, 2(2), 119–126.

Kumar, M., and Ando, Y. (2010). “Chemical vapor deposition of carbon nanotubes: A review on growth mechanism and mass production.” *J. Nanosci. Nanotechnol.*, 10(6), 3739–3758.

Kumar, N., and Kumar, G. (2009). “Biological Effects of Cell Tower Radiation on Human Body.” *Ismot*, dec 16-19(318), 1365–1368.

Lee, Y., Le, V. T., Kim, J. G., Kim, E. S., Ahn, S. E., and Suh, D. (2018). “Versatile, High-Power, Flexible, Stretchable Carbon Nanotube Sheet Heating Elements Tolerant to Mechanical Damage and Severe Deformation.” *Adv. Funct. Mater.*, 28(8), 1–8.

Lei, T., Deng, Q., Zhang, S., Cai, S., and Xie, C. (2016). “Fast identification of CO by using single Pt-modified WO<sub>3</sub> sensing film based on optical modulation.” *Sensors Actuators, B Chem.*, 232, 506–513.

Lewandowski, C. M., Co-investigator, N., and Lewandowski, C. M. (2015). *Carbon Nanotube and Graphene Device Physics*. Cambridge.

Li, J., Lu, Y., Ye, Q., Cinke, M., Han, J., and Meyyappan, M. (2003). “Carbon nanotube sensors for gas and organic vapor detection.” *Nano Lett.*, 3(7), 929–933.

Li, R., He, M., Li, T., and Zhang, L. (2015). “Preparation and properties of cellulose / silver nanocomposite fibers.” *Carbohydr. Polym.*, 115, 269–275.

Liang, F., Chen, S., Xie, W., and Zou, C. (2018). “The decoration of Nb-doped TiO<sub>2</sub> microspheres by reduced graphene oxide for enhanced CO gas sensing.” *J. Phys. Chem. Solids*, 114(September 2017), 195–200.

Lin, D., Zeng, X., Li, H., and Lai, X. (2018). “Facile fabrication of superhydrophobic and flame-retardant coatings on cotton fabrics via layer-by-layer assembly.” *Cellulose*.

- Liu, H., Lee, Y., and Norsten, T. B. (2013). "In situ formation of nanoparticles on cotton textiles."
- Liu, K., Sun, Y., Lin, X., Zhou, R., Wang, J., Fan, S., and Jiang, K. (2010). "Scratch-Resistant, Highly Conductive, and High-Strength Carbon Nanotube- Based Composite Yarns." 4(10), 5827–5834.
- Liu, Y., Wang, X., Qi, K., and Xin, J. H. (2008). "Functionalization of cotton with carbon nanotubes." *J. Mater. Chem.*, 18(29), 3454.
- Liu, Z., Bai, G., Huang, Y., Li, F., Ma, Y., Guo, T., He, X., Lin, X., Gao, H., and Chen, Y. (2007). "Microwave absorption of single-walled carbon nanotubes/soluble cross-linked polyurethane composites." *J. Phys. Chem. C*, 111(37), 13696–13700.
- Majumdar, A., Mukhopadhyay, S., and Yadav, R. (2010). "Thermal properties of knitted fabrics made from cotton and regenerated bamboo cellulosic fibres." *Int. J. Therm. Sci.*, 49(10), 2042–2048.
- Mao, N., and Russell, S. J. (2015). *Fibre to Fabric: Nonwoven Fabrics. Text. Fash. Mater. Des. Technol.*, Elsevier Ltd.
- Marinkovic, S. N. (2008). "Carbon nanotubes." *J. Serbian Chem. Soc.*, 73(8–9), 891–913.
- Markevicius, T., Furferi, R., Olsson, N., Meyer, H., Governi, L., Carfagni, M., Volpe, Y., and Hegelbach, R. (2014). "Towards the development of a novel CNTs-based flexible mild heater for art conservation." *Nanomater. Nanotechnol.*, 4(1), 1–13.
- Mathur, P., and Raman, S. (2020). "Electromagnetic Interference (EMI): Measurement and Reduction Techniques." *J. Electron. Mater.*, 49(5), 2975–2998.
- Mehdipour, A., Rosca, I. D., Trueman, C. W., Sebak, A. R., and Hoa, S. Van. (2012). "Multiwall carbon nanotube-epoxy composites with high shielding effectiveness for aeronautic applications." *IEEE Trans. Electromagn. Compat.*, 54(1), 28–36.

Micheli, D., Apollo, C., Pastore, R., and Marchetti, M. (2010). “X-Band microwave characterization of carbon-based nanocomposite material, absorption capability comparison and RAS design simulation.” *Compos. Sci. Technol.*, 70(2), 400–409.

Micheli, D., Pastore, R., Apollo, C., Marchetti, M., Gradoni, G., Primiani, V. M., and Moglie, F. (2011). “Broadband electromagnetic absorbers using carbon nanostructure-based composites.” *IEEE Trans. Microw. Theory Tech.*, 59(10), 2633–26646.

Nam, I. W., Lee, H. K., and Jang, J. H. (2011). “Electromagnetic interference shielding/absorbing characteristics of CNT-embedded epoxy composites.” *Compos. Part A Appl. Sci. Manuf.*, 42(9), 1110–1118.

Nandy, T., Coutu, R. A., and Ababei, C. (2018). “Carbon monoxide sensing technologies for next-generation cyber-physical systems.” *Sensors (Switzerland)*, 18(10).

Negru, D., Buda, C. T., and Avram, D. (2012). “Electrical conductivity of woven fabrics coated with carbon black particles.” *Fibres Text. East. Eur.*, 90(1), 53–56.

Nilsson, M., and Strømme, M. (2005). “Electrodynamic investigations of conduction processes in humid microcrystalline cellulose tablets.” *J. Phys. Chem. B*, 109(12), 5450–5455.

Ogunkunle, O., and Ahmed, N. A. (2021). “Overview of biodiesel combustion in mitigating the adverse impacts of engine emissions on the sustainable human–environment scenario.” *Sustain.*, 13(10).

Orlando, A., Mushtaq, A., D., Lugli, P., and Petti, L. (2023). “The Influence of Surfactants on the Deposition and Performance of Single-Walled Carbon Nanotube-Based Gas Sensors for NO<sub>2</sub> and NH<sub>3</sub> Detection.” *Chemosensors*, 11(2), 1–20.

Oriakhi, C.O. (1998). “Nano Sandwiches.” *Chem. Br.*, 34, 59–62.

Özbek, C., Okur, S., Mermer, Ö., Kurt, M., Sayin, S., and Yilmaz, M. (2015). “Effect of

Fe doping on the CO gas sensing of functional calixarene molecules measured with quartz crystal microbalance technique.” *Sensors Actuators, B Chem.*, 215, 464–470.

Panda, D., Nandi, A., Datta, S. K., Saha, H., and Majumdar, S. (2016). “Selective detection of carbon monoxide (CO) gas by reduced graphene oxide (rGO) at room temperature.” *RSC Adv.*, 6(53), 47337–47348.

Pang, H., Xu, L., Yan, D. X., and Li, Z. M. (2014). “Conductive polymer composites with segregated structures.” *Prog. Polym. Sci.*, 39(11), 1908–1933.

Portella, E. H., Romanzini, D., Angrizani, C. C., Amico, S. C., and Zattera, A. J. (2016). “Influence of stacking sequence on the mechanical and dynamic mechanical properties of cotton/glass fiber reinforced polyester composites.” *Mater. Res.*, 19(3), 542–547.

Quang, N. H., Trinh, M. Van, Lee, B. H., and Huh, J. S. (2006). “Effect of NH<sub>3</sub> gas on the electrical properties of single-walled carbon nanotube bundles.” *Sensors Actuators, B Chem.*, 113(1), 341–346.

Rahman, M. J., and Mieno, T. (2015). “Conductive Cotton Textile from Safely Functionalized Carbon Nanotubes.” *J. Nanomater.*, 2015.

Raton, B., Lauderdale, F., Davie, Beach, D., Jupiter, and Lucie, P. St. (2006). “Preventing Carbon Monoxide Poisoning After an Emergency.” 6348(561), 6348

Ravindren, R., Mondal, S., Nath, K., and Das, N. C. (2019). “Investigation of electrical conductivity and electromagnetic interference shielding effectiveness of preferentially distributed conductive filler in highly flexible polymer blends nanocomposites.” *Compos. Part A Appl. Sci. Manuf.*, 118(December 2018), 75–89.

Rizvi, R. (2014). “Piezoresistance in Polymer Nanocomposites.”

Rutherglen, C., and Burke, P. (2009). “Nanoelectromagnetics: Circuit and electromagnetic properties of carbon nanotubes.” *Small*, 5(8), 884–906.



Said, M. M., Rehan, M., El-sheikh, S. M., Zahran, M. K., and Abdel-aziz, M. S. (2021). “Multifunctional Hydroxyapatite / Silver Nanoparticles / Cotton Gauze for Antimicrobial and Biomedical Applications.” 1–22.

Saini, P., and Aror, M. (2012). “Microwave Absorption and EMI Shielding Behavior of Nanocomposites Based on Intrinsically Conducting Polymers, Graphene and Carbon Nanotubes.” *New Polym. Spec. Appl.*

Salimbeygi, G., Nasouri, K., Shoushtari, A. M., Malek, R., and Mazaheri, F. (2013). “Fabrication of polyvinyl alcohol/multi-walled carbon nanotubes composite electrospun nanofibres and their application as microwave absorbing material.” *Micro Nano Lett.*, 8(8), 455–459.

Sandilands, E. A., and Bateman, D. N. (2016). “Carbon monoxide.” *Med. (United Kingdom)*, 44(3), 151–152.

Santini, L., Forleo, G. B., and Santini, M. (2013). “Implantable devices in the electromagnetic environment.” *J. Arrhythmia*, 29(6), 325–333.

Seesaard, T., Lorwongtragool, P., and Kerdcharoen, T. (2015). “Development of fabric-based chemical gas sensors for use as wearable electronic noses.” *Sensors (Switzerland)*, 15(1), 1885–1902.

Senthil Kumar, P., and Gunasundari, E. (2018). “Nanocomposites: Recent Trends and Engineering Applications.” *Nano Hybrids Compos.*, 20, 65–80.

Sharika, T., Abraham, J., Arif P, M., George, S. C., Kalarikkal, N., and Thomas, S. (2019). “Excellent electromagnetic shield derived from MWCNT reinforced NR/PP blend nanocomposites with tailored microstructural properties.” *Compos. Part B Eng.*, 173(May), 106798.

Shenthar, J., Bohra, S., Jetley, V., Vora, A., Lokhandwala, Y., Nabar, A., Naik, A., Calambur, N., and Gupta, S. B. (2016). “A survey of cardiac implantable electronic

device implantation in India: By Indian Society of Electrocardiology and Indian Heart Rhythm Society.” *Indian Heart J.*, 68(1), 68–71.

Shobin, L. R., and Manivannan, S. (2015). “Carbon nanotubes on paper: Flexible and disposable chemiresistors.” *Sensors Actuators, B Chem.*, 220(March), 1178–1185.

Shu, J. C., Cao, M. S., Zhang, M., Wang, X. X., Cao, W. Q., Fang, X. Y., and Cao, M. Q. (2020). “Molecular Patching Engineering to Drive Energy Conversion as Efficient and Environment-Friendly Cell toward Wireless Power Transmission.” *Adv. Funct. Mater.*, 30(10), 1–10.

Shukla, V. (2019). “Nanoscale Advances Review of electromagnetic interference shielding.” *Nanoscale Adv.*, 1, 1640–1671.

Singh, B. P., Prabha, Saini, P., Gupta, T., Garg, P., Kumar, G., Pande, I., Pande, S., Seth, R. K., Dhawan, S. K., and Mathur, R. B. (2011). “Designing of multiwalled carbon nanotubes reinforced low density polyethylene nanocomposites for suppression of electromagnetic radiation.” *J. Nanoparticle Res.*, 13(12), 7065–7074.

Stanković, S. B., Popović, D., and Poparić, G. B. (2008). “Thermal properties of textile fabrics made of natural and regenerated cellulose fibers.” *Polym. Test.*, 27(1), 41–48.

Stankovic, S. B., Popovic, D., Poparic, G. B., and Bizjak, M. (2009). “Ultraviolet Protection Factor of Gray-state Plain Cotton Knitted Fabrics.” *Text. Res. J.*, 79(11), 1034–1042.

Stergiou, C. A., Stimoniaris, A. Z., and Delides, C. G. (2015). “Hybrid Nanocomposites With Organoclay and Carbon-Based Fillers for EMI Suppression.” *IEEE Trans. Electromagn. Compat.*, 57(3), 470–476.

Terrones, M. (2003). “Science and Technology of the Twenty-First Century: Synthesis, Properties, and Applications of Carbon Nanotubes.” *Annu. Rev. Mater. Res.*, 33, 419–501.

Treacy, M. M. J., Ebbesen, T. W., and Gibson, J. M. (1996). “Exceptionally high Young’s modulus observed for individual carbon nanotubes.pdf.”

Umishita, K., Okubo, T., Takuya, N., and Hashimoto, O. (2006). “Absorption and shielding effect of electromagnetic wave at GHz frequency by multi-walled carbon nanotube/polymer composites.” *Proc. 9th Eur. Conf. Wirel. Technol. ECWT 2006*, 2(September), 291–294.

Venkatesha Gupta, N. S., Akash, Sreenivasa Rao, K. V, and Arun kumar, D. S. (2016). “Fabrication and evaluation of mechanical properties of alkaline treated sisal/hemp fiber reinforced hybrid composite.” *IOP Conf. Ser. Mater. Sci. Eng.*, 149, 012093.

Wanasinghe, D., Aslani, F., Ma, G., and Habibi, D. (2020). “Review of polymer composites with diverse nanofillers for electromagnetic interference shielding.” *Nanomaterials*, 10(3).

Wang, C., Yin, L., Zhang, L., Xiang, D., and Gao, R. (2010). “Metal oxide gas sensors: Sensitivity and influencing factors.” *Sensors*, 10(3), 2088–2106.

Wang, X. X., Shu, J. C., Cao, W. Q., Zhang, M., Yuan, J., and Cao, M. S. (2019). “Eco-mimetic nanoarchitecture for green EMI shielding.” *Chem. Eng. J.*, 369(March), 1068–1077.

Wanna, Y., Srisukhumbowornchai, N., Tuantranont, A., Wisitsoraat, A., Thavarungkul, N., and Singjai, P. (2006). “The effect of carbon nanotube dispersion on CO gas sensing characteristics of polyaniline gas sensor.” *J. Nanosci. Nanotechnol.*, 6(12), 3893–3896.

Wen, B., Cao, M., Lu, M., Cao, W., Shi, H., Liu, J., Wang, X., Jin, H., Fang, X., Wang, W., and Yuan, J. (2014). “Reduced graphene oxides: Light-weight and high-efficiency electromagnetic interference shielding at elevated temperatures.” *Adv. Mater.*, 26(21), 3484–3489.

Wongwiriyapan, W., Inoue, S., Honda, S. ichi, and Katayama, M. (2008). “Adsorption

- kinetics of NO<sub>2</sub> on single-walled carbon nanotube thin-film sensor.” *Jpn. J. Appl. Phys.*, 47(10 PART 1), 8145–8147.
- Yamazoe, N. (2005). “Toward innovations of gas sensor technology.” *Sensors Actuators, B Chem.*, 108(1-2 SPEC. ISS.), 2–14.
- Yang, S., Lozano, K., Lomeli, A., Foltz, H. D., and Jones, R. (2005a). “Electromagnetic interference shielding effectiveness of carbon nanofiber/LCP composites.” *Compos. Part A Appl. Sci. Manuf.*, 36(5), 691–697.
- Yang, Y., Gupta, M. C., Dudley, K. L., and Lawrence, R. W. (2005b). “A comparative study of EMI shielding properties of carbon nanofiber and multi-walled carbon nanotube filled polymer composites.” *J. Nanosci. Nanotechnol.*, 5(6), 927–931.
- Yong, C. Y., Rahman, T. A., and Chew, K. M. (2015). “Wireless industry emission: Electromagnetic field monitoring and analysis.” *ARPJ. Eng. Appl. Sci.*, 10(20), 9800–9807.
- Yu, Q., Weng, P., Han, L., Yin, X., Chen, Z., Hu, X., Wang, L., and Wang, H. (2019). “Enhanced thermal conductivity of flexible cotton fabrics coated with reactive MWCNT nanofluid for potential application in thermal conductivity coatings and fire warning.” *Cellulose*, 26(12), 7523–7535.
- Zhang, T., Mubeen, S., Myung, N. V., and Deshusses, M. A. (2008). “Recent progress in carbon nanotube-based gas sensors.” *Nanotechnology*, 19(33).
- Zhang, Y., Jia, G., and Wang, P. (2017). “Nondestructive rubbing fabrication of flexible graphene film for precise temperature controlling.” *AIP Adv.*, 7(4).
- Zhao, J., Buldum, A., Han, J., and Lu, J. P. (2002). “Gas molecule adsorption in carbon nanotubes and nanotube bundles.” *Nanotechnology*, 13(2), 195–200.
- Zhao, W., Fam, D. W. H., Yin, Z., Sun, T., Tan, H. T., Liu, W., Tok, A. I. Y., Boey, Y.

C. F., Zhang, H., Hng, H. H., and Yan, Q. (2012). “A carbon monoxide gas sensor using oxygen plasma modified carbon nanotubes.” *Nanotechnology*, 23(42).

Zhou, T., Wang, X., Liu, X. H., and Lai, J. Z. (2010). “Effect of silane treatment of carboxylic-functionalized multi-walled carbon nanotubes on the thermal properties of epoxy nanocomposites.” *Express Polym. Lett.*, 4(4), 217–226.

## BIO-DATA

**Name:** ArunKumar.D.S  
**Father's Name:** Shivappa D  
**Mother's Name:** Lalithamma  
**Date of Birth:** 31-12-1992  
**Nationality:** Indian  
**Marital Status:** Single



### **Permanent Address:**

Ambedkar Nagara, Shikaripura Taluk, Shimoga District, Karnataka, India-577427.

### **Contact Details:**

Mobile Number: +91-9901752537

E-mail: [arunshi71@gmail.com](mailto:arunshi71@gmail.com)

### **Academic Qualification:**

Master of Technology in Manufacturing Science and Engineering from Siddaganga Institute of Technology (Affiliated to Visvesvaraya Technological University, Belgaum), Tumkur, Karnataka, India (2016).

Bachelor of Engineering in Mechanical Engineering from Malnad College of Engineering (Affiliated to Visvesvaraya Technological University, Belgaum), Hassan, Karnataka, India (2014).

### **Research Publications:**

Articles in International Journals: 03

Articles in Conference Proceedings: 04